UNIVERSITY OF SOUTHAMPTON

School of Electronics and Computer Science

Molecular Transceiver Design and Performance Study in Diffusive Molecular Communications

by

Lu Shi

BEng

A doctoral thesis submitted in partial fulfilment of the requirements for the award of Doctor Philosophy at the University of Southampton

May 2020

SUPERVISOR: Professor Lie-Liang Yang

BEng MEng PhD, FIEEE, FIET

Professor of Communications, Southampton Next Generation Wireless group

School of Electronics and Computer Science University of Southampton

Southampton SO17 1BJ

United Kingdom

Dedicated to my family

UNIVERSITY OF SOUTHAMPTON

ABSTRACT

School of Electronics and Computer Science
Faculty of Physical Science and Engineering

Molecular Transceiver Design and Performance Study in Diffusive Molecular Communications

by Lu Shi

Molecular communication (MC) is inspired by the nature, where chemical or biological molecules are used to transmit information instead of electronic or electromagnetic signals in the traditional wireless communications. Due to non toxic material and possible energy-efficient signal propagation, MC has been recognised to be the naturally fitting methods to provide communication inside the living bodies and other biological environments, including the applications in biomedical, industrial and consumer goods, military, environmental, etc. In this thesis, we focus on the diffusion-based molecular communication (DMC), where information molecules are only driven by the Brownian motion.

In this thesis, we first provide an introduction for the research and development of DMC, as well as address the background in the research and development of DMC, including channel model, modulation schemes, receiver design, detection algorithm and multiple access technique. Based on the background, we realize that there is strong inter-symbol interference (ISI) in DMC systems due to the slow propagation speed and random movements of information molecules. Furthermore, it can be shown that on-off keying (OOK) modulation is lack of the capability to reduce ISI effect and is also hard to implement in practice. On the other hand, binary molecule shift keying (BMoSK) is a promising modulation technique, which employs some embedded capability to reduce ISI. Therefore, in this thesis we first propose a low-complexity ISI cancellation (ISIC) to improve the performance of DMC systems with either OOK or BMoSK modulation. In order to investigate the achievable performance of the DMC systems with OOK and BMoSK modulation and with/without ISIC, we then analyse the bit-error rate (BER) performance of DMC systems by introducing different analytical approaches. Specifically, we first consider the Poisson modelling of the DMC systems as the exact approach to analyse the BER of the DMC systems with OOK or BMoSK modulation. Then, the Gaussian and Gamma approximation approaches are introduced to reduce the computation complexity. Moreover, the simplified Poisson, simplified Gaussian and Monte-Carlo approaches are proposed to further reduce the computation burden for BER. We demonstrate that all the approximation and simplified approaches can provide near-accurate estimation of the BER performance of DMC systems.

As ISI is a main factor affecting the performance of DMC systems, following the above studies, a range of linear equalisers, including matched-filter (MF), zero-forcing (ZF) and minimum mean-

square error(MMSE) equalisers, are introduced to the BMoSK-modulated DMC systems, in order to mitigate the effect of ISI. Our studies show that ZF and MMSE equalisers can significantly reduce the effect of ISI.

Furthermore, we propose and study a molecular code-division multiple access (MoCDMA) systems with BMoSK modulation, in order to allow multiple nano-machines to simultaneously communicate with an access-point receiver. We mirror the proposed MoCDMA to the conventional radio-based CDMA with binary phase-shift keying (BPSK) modulation, based on which we derive the various expressions for received signals, so that the information conveyed by different nano-users can be flexibly detected on either symbol-by-symbol or block-by-block basis. For signal detection in MoCDMA systems, a range of detectors are proposed, which include the symbol-based, block-based and frequency-domain detectors that are operated in the principles of MF, ZF, and MMSE. Furthermore, the performance of the MoCDMA systems with various detection schemes is studied and compared, showing that the MoCDMA with these detection schemes are capable of providing required communications in multiple user environments. Finally, we conclude the thesis and propose some possible future research issues.

Declaration of Authorship

I, **Lu Shi**, declare that the thesis entitled **Molecular Transceiver Design and Performance Study in Diffusive Molecular Communications** and the work presented in it are my own and has been generated by me as the result of my own original research. I confirm that:

- This work was done wholly or mainly while in candidature for a research degree at this University;
- Where any part of this thesis has previously been submitted for a degree or any other qualification at this University or any other institution, this has been clearly stated;
- Where I have consulted the published work of others, this is always clearly attributed;
- Where I have quoted from the work of others, the source is always given. With the exception of such quotations, this thesis is entirely my own work;
- I have acknowledged all main sources of help;
- Where the thesis is based on work done by myself jointly with others, I have made clear exactly what was done by others and what I have contributed myself;
- Parts of this work have been published.

Signed: ..... Date: .....

Acknowledgements

First of all, I would like to give my sincere gratitude to my supervisor Prof. Lie-Liang Yang for his excellent and careful supervision and support. His guidance and inspiration helped me at the research and writing of this thesis. Secondly, I would like thank my colleagues in NGW group, and university staffs for their help. I also thank to all my friends. In particular, I would like to expressly mention Yichuan Li, Fayong Liu and Shufeng Chen for their invaluable help and advice on every occasion needed and making my stay more enjoyable. Last but not the least, I would like thank my family and especially my parents, for their constant love and support during study. Their endless support was a key factor for me in completing this degree.

List of Publications

Journal Papaers

1. **Lu Shi**, Lie-liang Yang, "Error Performance Analysis of Diffusive Molecular Communication Systems With On-Off Keying Modulation", ***IEEE Transactions on Molecular, Biological and Multi-Scale Communications***, vol.3, no.4, pp. 224-238, Dec. 2017.

2. **Lu Shi**, Lie-liang Yang, "Performance of Binary Molecular Shift Keying Modulated Diffusive Molecular Communication Systems without/with Inter-Symbol Interference Compression", ***IET Communications***, Volume: 14, Issue: 2, Page(s): 262 - 273, January 2020.

3. **Lu Shi**, Lie-liang Yang, "Equalization and Performance of Diffusive Molecular Communication Systems with Binary Molecular-Shift Keying Modulation", ***IET Communications***, Volume: 14, Issue: 4, Page(s): 549 - 555, February 2020.

4. **Lu Shi**, Lie-liang Yang, Chen Kwang-Cheng, "Molecular Code-Division Multiple-Access: Signaling, Signal Detection and Performance", submitted to ***IEEE Transactions on NanoBioscience***.

Conference Papers

1. **Lu Shi**, Lie-liang Yang, "Diffusion-based molecular communications: Inter-symbol interference cancellation and system performance", ***2016 IEEE/CIC International Conference on Communications in China (ICCC)***, (**ICCC 2016**), pp. 1-6., 2016.

Contents

Glossary

3D: 3-dimensional

ASK: amplitude shifting keying

BCSK: binary concentration shifting keying

BER: bit error ratio

BMoSK: binary molecular shift keying

BPSK: binary phase-shift keying

CDF: cumulative density function

CDMA: code-division multiple-access

CSK: concentration shifting keying

DFE: decision-feedback equalizer

DMC: diffusion-based molecular communication

DMCs: diffusion-based molecular communications

EGC: equal-gain combining

FDE: F-domain equalization

FDMA: frequency-division multiple-access

FFT: fast Fourier transform

FSK: frequency shift keying

ICI: inter-chip interference

ISI: inter-symbol interference

ISIC: ISI cancellation

LEQ: linear equalizer

MAI: multiple-access interference

MAP: maximum a-posterio

MCSK: molecular concentration shift keying

MDMA: molecular division multiple-access

MF: matched-filtering

MFSK: molecular frequency shift keying

MIMO: multiple-input multiple-output

ML: maximum likelihood

MLS: maximum length sequence

MMSE: minimum mean-square error

MoCDMA: molecular code-division multiple-access

MoSDMA: molecular space-division multiple-access

MoSK: molecular shifting keying

MoTDMA: molecular time-division multiple-access

MPPM: molecular pulse position modulation

MRC: maximal ratio combining

MSE: mean-square error

NUs: nano-users

OFDM: orthogonal frequency-division multiplexing

OOK: on-off keying

PDF: probability density function

PMF: probability mass function

PPM: pulse position modulation

PSK: phase-shift keying

RdCDMA: radio-based CDMA

RHS: righthand side

SNR: signal-to-noise ratio

SINR: signal to interference-plus-noise ratio

TDMA: time-division multiple-access

ZF: zero-forcing

List of Symbols

$\lvert \cdot \rvert$:	Absolute value.
$\lVert \cdot \rVert^2$:	Euclidean norm operation.
$(\cdot)^H$:	Hermitian transpose of a matrix.
$(\cdot)^+$:	Hermitian transpose of a matrix.
$(\cdot)^T$:	Transpose of a matrix.
$(\cdot)^*$:	Conjugate of a complex symbol/vector/matrix.
$\sum$:	Summation operation.
$\prod$:	Product operation.
$\int$:	Integration.
$E[\cdot]$:	Expectation operation.
$\exp(\cdot)$:	Exponential function.
$\log(\cdot)$:	Logarithm function.
$\ln(\cdot)$:	Natural logarithm function.
$\max(\cdot)$:	Maximum function.
$\min(\cdot)$:	Minimum function.
$\mathrm{tr}(\cdot)$:	Trace of a matrix.
$\mathbf{Var}(\cdot)$:	Variance of a random variable.
$\mathrm{diag}(\cdot)$:	Diagonalizing operation.
∇^2:	Laplace operator
$\triangleq$:	Equal by definition

Chapter 1

Introduction

1.1 Motivation

Nanotechnology in these days can design and build devices at nano-scale for completing basic tasks like sensing and simple computation. A nano-scale device composed of several molecules that can perform basic functions is called a nano-machine [1, 2]. Communication between nano-machines is essential when complicated tasks require collaboration among them. In this case, the nano-machines require communication channels to exchange data among them and with outside device. On the other hand, medical or health systems are interested in efficient drug delivery to improve the efficiency of drug [3]. In order to transport or deliver medicine to target the right place within the body, nano-machines must be able to recognise tumours and navigate through the body, which also require the basic communication functions.

Obviously, reducing the size of traditional communication devices to let them be directly employed by nano-machines is the most straightforward way to implement communications between nano-scale devices. However, traditional communication technologies are usually not suitable for nano-scale environments due to their high power consumption, complexity and size [4]. In order to overcome these problems, many new designs and materials have been proposed to improve the efficiency and reliability of traditional communication designs, in order to make them fit the environments at nano-scale. However, there are still a lot of challenges to meet.

On the other side, molecular communication is inspired by the communication schemes naturally occurring between living cells, which convey information between nano-machines with the aid of molecules [5]. In addition, biological cells may be modified to act as the basic function unit, which is already at nano-scale and is hence suitable for surrounding environments. Moreover, the existing communication schemes on bio-nanomachines are usually more energy efficient than the current man-made design. Therefore, high-efficiency communication schemes may be designed by reviewing and improving these existing schemes. Hence, this thesis focuses on the molecular

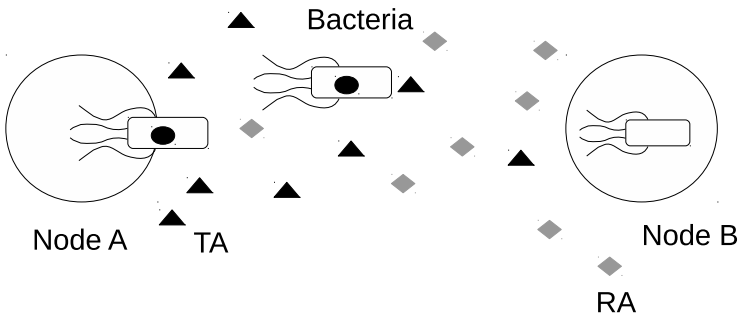

Figure 1.1: A model of bacteria-based molecular communication.

communications for providing information exchange at nano-scale.

1.2 Outline of Molecular Communication

The principle of molecular communication is encoding the message according to the properties of information molecules, e.g. structure, quantity, identity or timing [6–8]. Then, these information molecules carrying message are released and propagated through the channel which is filled with various medium. Finally, these molecules are detected by the receiver and their carried information is recovery. In biological system, molecular communication has extremely slow propagation speed ($\mu m/s - cm/s$) and short transmission range ($nm - \mu m$), in contrast to the traditional wireless communication. According to the propagation patterns of molecules, various types of molecular communication schemes can be divided into two categories: passive transport and active transport [9]. In the passive transport molecular communication systems [9], information molecules are driven by the external force e.g, collisions from fluid medium, where the random movements of information molecules can usually be described by the Brownian motion. For example, calcium ions are widely used in the cellular process, where information is encoded into the concentration of calcium ions [8]. By contrast, in the active transport molecular communication systems [9], due to the self-contained guide and power module, information molecules have the ability to push themselves toward the receiver or destination. Bacteria-Based molecular communication and vesicular trafficking are examples of active transport model [8]. In these two cases, information is encoded into biochemical structure and encapsulated into a vesicle or bacteria. Then the motor proteins attached on container push the container to the destination according to the guide module in the bacteria case or microtubules in vesicular trafficking case. In the following two subsections, we describe the bacteria-based molecular communication as an example of active transport model and take free diffusion-based molecular communication (DMC) as an example of passive transport model.

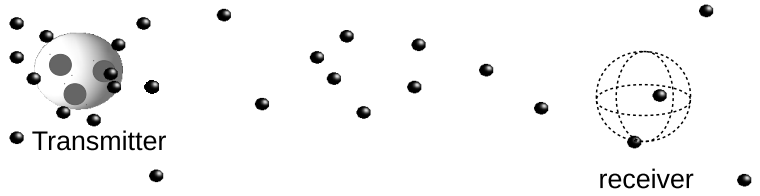

Figure 1.2: A model of diffusion-based molecular communication.

1.2.1 Bacteria-Based Molecular Communication

Fig. 1.1 demonstrates a model of bacteria-based molecular communication with two nodes. During transmission, information molecules are contained by the bacteria, which protect the information molecules from chemical reaction or other dangerous environment [10, 11]. In this system, bacteria have the ability to sense the concentration of the attractants released by the nearby nodes. When transmission is required, the transmission attractant (TA) is released by the transmit node to attract empty bacteria. Then, the information molecule is encapsulated inside a bacterium by the node. At the same time, the reception attractant (RA) is released by the target node to guide the bacterium to pass through the fluid medium. After the bacterium achieves at the destination node, the information molecule is extracted from the bacterium and message is recovered by the receive node. During this processing, the energy of bacteria is obtained from the external environment, e,g, light or chemical reaction. Since the transmitted molecule is protected by the bacteria, more information can be encoded in the structure of the molecule, which can provide higher information transmission throughout than diffusion-based molecular communication.

1.2.2 Diffusion-Based Molecular Communication

Fig. 1.2 demonstrates a model of diffusion-based molecular communication (DMC) with a transmitter and a receiver. In DMC, information molecules are created or stored inside the transmitter and are released at specific time through gate around transmitter surface [12]. Then, theses information molecules move randomly in the fluid medium due to Brownian motion. Some of them may chemically react with other components and many of them may move in the wrong directions and disappear in the channel. In DMC, the receiver can be designed to have the ability to count the number of information molecules presenting in the detection range around itself. For example, ligand-receptor [13, 14] can blind with molecules under certain blinding rate. Due to the uncertain movement of a specific transmitted molecule, in DMC, information is normally encoded by the number of molecule or the type of molecule. In some environments, there may be a constant strong flow in the medium, e.g., blood vessels. Correspondingly, this model is termed as the diffusion-based molecular communication with drift.

Because of the random movements of information molecules in passive transport MC [9], where

transmitter may have to release a lot of molecules at one time to ensure that a sufficient number of them can reach the destination. Moreover, the transmitted distance is limited by the random movement. By contrast, longer transmission distance can be achieved by the active transport MC [9]. In this case, only a small number of information molecule is required by the transmission. However, more complex architecture of information molecules is needed in order to adjust the power and employ guide module. Furthermore, a challenge of employing active transport MC is the management of the energy required during the transmission.

In this thesis, we focus on the DMC instead of active transport MC. This is because in DMC, there is no need to design complex transmitter, information molecules and receiver. Moreover, there is no energy harvesting problem and the design of guild module in DMC. Hence, DMC has many advantages for nano-scale communication, especially, when low-rate communication is considered. However, there still remain many problems need to be solved before the application of DMC in the reality.

1.3 Background for Research

In DMC, both signals and devices are biological type instead of electrical or electromagnetic based in the tradition wireless communication. Therefore, we have to deal with a range of problem that can not be sloved using the existing approaches in wirless communication. In the following subsections, we list some problems that have been studied in the literature.

1.3.1 Channel Modelling

The first problem for studying the diffusing-based communication system is modelling the physical channel. The models of transmitter, propagation process and receiver are required for system design and performance analysis. Moreover, the noise during transmission and ISI created by the remaining information molecules need to be considered as well. In [15, 16], authors have proposed a physical end-to-end model for the DMC and noise analysis is carried out based on this model. In more detail, this model consists of particle emission, particle diffusion and particle reception. The corresponding numerical results are provided in terms of normalized gain and delay as the functions of the input frequency and of the transmission range. The particle sampling noise at transmitter and the particle counting noise at receiver were also analyzed based on this model. In [17–19], an inexpressive molecular communication tabletop platform has been built to verify the proposed theoretical model in [15, 16]. Due to the imperfect nature of transmitter, receiver and turbulent flow, the results show that the platform resembles a nonlinear system rather than a linear system described in [15]. Authors in [18, 19] have proposed a corrected channel impulse response model for the platform and the nonlinearity of the system can be formulated and simplified as Gaussian noise.

Except from the physical end-to-end model for DMC, many researchers have investigated the

receiver modelling [13, 14, 20–29]. The passive receiver is the simplest one and the ideal receiver model has been investigated in [20–22]. In the ideal receiving scenario, the receiver only senses the concentration of information molecules and does not execute any reaction on them. However, chemical reaction occurs in reality, when ligand-receptor is employed for counting the number of information molecules. Then, partially or fully absorptive receivers have been proposed for modelling the receivers. For absorptive receivers, information molecules binding to the receptor may be irreversible [13, 25, 29] or reversible [14, 23, 24, 26–28]. In [14, 24], the noise from ligand binding process has been studied and the close-form expression has been proposed based on the ligand-receptor kinetics model. The effect of the density and size of ligand receptor has been investigated in [25], showing that a comparable signal energy to a perfectly absorbing sphere can be achieved by covering as little as 1% of the surface area of the receiver. The impact and analytical expression of reaction receivers have been studied in [23, 26, 28], where the bit error probability is studied to demonstrate the effect of the absorbing and desorption rate [26]. In addition, a framework has been proposed to investigate the degradation, reversible reaction inside a bound medium [28].

In DMC, channel impulse response is affected by the information degradation during molecular transmission. Hence, the degradation phenomenon has been studied [27, 29–31]. Specifically, the Michaelis-Menten reaction mechanism for information molecules reacting with enzyme molecules has been considered in [30]. Correspondingly, the channel impulse response and received signal are derived based on this modeling. Furthermore, an optimal sequence detector and a weighted sum detector have been proposed for the signal detection. It can be shown that the weighted sum detector performs very close to the optimal sequence detector in low ISI situation, and that the presence of enzymes degradation or moderate steady flow can improve the system performance. In [29], the effect of degradation on the performance of the systems with absorbing receiver has been studied, showing that the detection performance can be improved when a right level of degradation is indtroduced to the system. Additionally, in [27, 31], the authors have investigated the effect of degradation on the systems utilizing reactive receiver, and the close-form expressions for the expected received signal at the receiver have been derived, which are also verified by simulation results.

1.3.2 Time-Varying DMC Channels

Most channel models discussed in the previous subsection are assumed to be fixed channels. In reality, transmission distance and propagation speed vary over time. Hence, a range of researches have studied the DMC in mobile environments. First, in DMC, the propagation speed of information molecules is depended on the diffusion coefficient of the medium. When the temperature and pressure of medium change, the propagation speed increases or decreases according to the varying of diffusion coefficient. In [32], the effect of the temporal variation on the system performance has been studied, showing that the temperature variation follows a Gaussian distribution, and the

channel gain has the closed-form expressions for the cumulative distribution function (CDF) and probability density function (PDF). Furthermore, the joint distribution of the channel gain and noise with considering the effect of temporal variation on ISI has been derived in [32]. Second, the positions of both transmitter and receiver may be on move over time. This dynamic change of positions causes the channel response to change [33]. It can be shown that the effect of the distance variant during transmission on the received signal follows a Poisson-Lognormal distribution, which can also be approximated by a Poisson distribution. Furthermore, considering both ISI and noise, the probability of error has been evaluated based on Gaussian approximation. Based on the transmission distance varying model, the authors in [34] have proposed an adaptive ISI mitigation method for the DMC systems. In this paper, the distance is estimated and based on which the corresponding channel impulse response is reconstructed for signal detection. Furthermore, both the concentration-based and peak-time-based adaptive threshold detection schemes have been proposed and investigated, showing that these detection schemes are reliable for operation in mobile environments. Moreover, in [35], both distance varying and molecules degradation have been considered in the contex with DMC. It is shown that the channel impulse response of the mobile DMC system can be obtained by appropriately modifying the diffusion coefficient of the molecules. Correspondingly, the error performance for the DMC systems has been analyzed and the expression for the error probability has been obtained.

1.3.3 Noise in DMC Channel

In the channel modelling section of 1.3.1, we have introduced several noise sources studied in the literature, including particle sampling noise, particle counting noise and the noise due to the imperfect nature of transceiver [15, 16, 18, 19]. In our proposed system model, we consider only the particle counting noise, which is because of the Brownian motion of particles and the observation uncertainty, when the number of particles is measured in the detection space at receiver. In more details, due to the random movement of particles, the measured number of particles presented in the detection space at receiver differs from the number of particles predicted by the system model based on diffusion process, such as Fick's second law of diffusion [16]. Therefore, the particle counting noise is caused by the measuring process, yielding the difference between the actually measured number of particles and the expected number of particles, rather than by the property of receivers or the particles used in the system. Hence, the particle counting noise is dependent on the number of particles emitted at transmitter and that retain in the communication environment. In other words, particle counting noise is related to both the particles emitted for transmitting the current data symbol, and the particles emitted for transmitting the previous data symbols, which impose ISI on the current data symbol.

1.3.4 Modulation and Detection

In DMC, amplitude detection and energy detection are two widely studied detection methods. Specifically, with the amplitude detection method, the measured signal at receiver is the concentration of information molecules. When the concentration is higher than a given threshold, the receiver interprets the detected information as '1', otherwise as '0'. On the other hand, in the energy detection, the energy is obtained as the integral of the concentration over a period of time. This measured energy is compared to a given threshold to decide whether a received bit is '1' or '0' [36–38]. The studies show that the energy detection method usually achieves more reliable transmission but lower transmission rate than the amplitude detection method.

In order to improve the performance of DMC systems, various modulation schemes have been proposed based on the properties of DMC. Specifically in DMC, message can be encoded in the form of molecule concentration, which is the principle of concentration shift keying (CSK) modulation scheme. In literature, the CSK modulation scheme has been investigated in [21, 36–41] with amplitude detection or energy detection. More specifically, in [41], the performance of the DMC systems with on-off keying (OOK) modulation supported by pulses of finite width or impulse has been studied and compared. It is shown that with full duty cycle, the OOK with pulses of finite width yields worse performance than the OOK with impulse. However, impulse biological signal is impossible in reality, hence we may expect the performance of the DMC systems based on impulse signals underperforms in practice. In the context of DMC, another widely studied modulation scheme is the molecule shift keying (MoSK), where the types of molecule are used to carry information. The performance of the DMC system with MoSK modulation have been investigated and compared to that with CSK modulation in [39, 40]. It is shown that the MoSK modulation outperforms the CSK modulation but at the cost of more complicated transmitter and receiver.

Besides the concentration and type based modulation schemes, molecule's releasing time can also be an alternative way to convey information in DMC. As we know, the propagation speed of molecules in DMC is extremely slow. This limits the modulation scheme based on molecule's releasing time from achieving high transmission date rate. However, the modulation schemes based on molecule's releasing time is suitable for asynchronous channels or the channels with drift [42, 43]. In this category, the pulse-position modulation (PPM) scheme proposed in [42] encodes information to the releasing time of molecules at the transmitter. In [43], two modulation schemes based on releasing time of molecules have been proposed for asynchronous DMC systems. In the first modulation scheme, information is encoded to the time between two consecutive releases of indistinguishable information molecule. By contrast, in the second modulation scheme, two consecutive releases of distinguishable information molecule are used for information encoding. The performance of both modulation schemes have been studied and compared with the synchronous systems, which shows that the synchronous system achieves better performance and the modulation scheme utilizing distinguishable molecules is capable of obtaining similar performance

as the synchronous system.

In addition to the above mentioned schemes, modulation schemes have been designed based on the change of molecule or property have been proposed in [44, 45]. Specifically, in [44], the chemical reaction occurred between information molecules and other molecules in the environment has been exploited to design the reaction shift keying (RSK) modulation scheme. Due to the chemical reaction occurred during the transmission, information may be encoded according to the change of concentration of received molecules or of the period of signal. Moreover, hybrid modulation schemes may be designed [46, 47], where information is jointly encoded to concentration and type of molecules. In this way, more information may be transmitted with lower error rate, but usually at the cost of more complex transmitter or receiver.

1.3.5 Multiple Access Communication

Research efforts have been made to investigate the molecular communication nanonetwork or relay systems [48–55], where multiple access techniques are the foundation to implement the networks with multiple users. In [1, 55–61] different multiple access techniques have been promoted and studied. In [1], molecular division multiple-access (MDMA) has been proposed, where each user in the system is assigned an unique type of molecules for communicating with a common receiver. Although the principle of MDMA is straightforward, the design of its receiver is challenging, as a complex receiver is required to observe the concentrations of all the different types of molecules. Molecular time-division multiple-access (MoTDMA) is an alternative technique for system to provide multiple access capability [57, 60]. In MoTDMA, information of different users is encoded in the time domain and only one type of molecules is required. For operation of MoTDMA, the time axis is divided into frames, each of which consists of multiple time slots. In order to distinguish different users, each user is only allowed to transmit its message at the corresponding time slot assigned to it. MoTDMA has the advantages that the design of both transmitter and receiver is simple, and only one type of molecules is used in transmission. However, the whole transmission requires good synchronization in order to reduce inter-user-interference. As we discussed in subsection considering channel models, the positions of transmitter and receiver might be on the move, and there is also possible dynamic change due to chemical reaction between information molecules and the molecules in the environment. All those make it hard to keep a DMC system to be in a good state of synchronization in reality. In addition to MDMA and MoTDMA, molecular code-division multiple-access (MoCDMA) can also be an option for supporting multiple users in DMC [56, 61]. In MoCDMA, the unique code is assigned to each of the users in the DMC system, where both encoding and decoding of information make use of the code assigned to the user. The advantages of this multiple access technique are that it does not require strict synchronization and many type of molecules. However, both the transmitter and receiver in MoCDMA require the relatively complex modules to implement the encoding and decoding functions.

1.3.6 Performance Analysis

Performance analysis and evaluation is always important in any communication system design. In the context of DMC, performance studies have been conducted from different perspectives, based on different channel models, as well as considering different modulation and detection schemes. Specifically, in [46], the authors have compared the performance of the DMC system with MoSK, CSK and proposed MCSK modulation schemes, based on the Poisson modeling and the assumption that ISI is only from one previously transmitted bit. The studies show that the proposed MCSK achieves better performance than the other two modulation schemes. The error probability, false-alarm probability and detection probability of the DMC systems with binary and M-ary CSK modulation schemes have been studied in [21, 62], when both the counting noise and ISI are model as Gaussian noise. In [63], the error performance of the DMC system with energy and amplitude detection has been analyzed by assuming presence of both the counting noise and ISI present in the system. Additionally, in [64, 65], assuming that information molecule arrived receiver follows the binomial distributions, the authors have studied the performance of the DMC system with M-ary CSk and MoSK modulations.

1.4 Summary of Research Issues

In this thesis, our focus is on the transceiver design and performance study of DMC systems. Our motivation is to study the approaches that are facilitate to the performance evaluation of DMC systems, as well as the signalling and signal detection schemes, so that high-efficiency DMC is possible for different purposes. In more details, the research issues concerned in this thesis are summarized as follows.

First, in Chapter 2, we analyze the bit error rate (BER) performance of the diffusive molecular communication (DMC) systems employing OOK modulation. We also analyze the BER of the OOK-modulated DMC systems with ISIC. Our main motivation in thesis and next chapter is to introduce alternative tools for analyzing and efficiently computing the BER of the DMC systems without or with ISIC. Specifically, in this chapter, for the OOK-modulated DMC systems without ISIC, we first derive an exact BER expression based on the Poisson modeling of DMC systems. Then, the Gaussian- and Gamma-approximation approaches are introduced to approximate the discrete Poisson distribution, and based on the approximation approaches, the corresponding BER expressions are derived. Furthermore, in order to reduce the computation complexity imposed by long ISI, we propose the Monte-Carlo, simplified Poisson, simplified Gaussian and the simplified Gamma approaches for BER computation. In the context of the OOK-modulated DMC systems with ISIC, we consider both the Poisson and Gaussian-approximation approaches for BER analysis. Again, exact and approximate BER expressions are derived under the Poisson, Gaussian-approximation, simplified Poisson and simplified Gaussian approaches. Finally, the considered

approaches are compared and validated by a range of performance results obtained from evaluation of the derived expressions or by simulations. Our studies show that the alternative approaches are in general effective for providing near-accurate BER estimation.

Following Chapter 3 concerning the DMC systems with OOK modulation, we analyze and investigate the BER performance of the DMC systems employing BMoSK modulation. Again, DMC systems both without and with ISIC are considered. Specifically, by modelling the number of molecules of one type presenting in a 3-dimensional (3D) detection space as a Poisson, or Gaussian distributed random variable, we derive the BER expressions of the BMoSK-modulated DMC systems without/with ISIC. However, the strong ISI presenting in DMC systems makes the computation of the above-mentioned BER formulas highly involved or even impossible. Therefore, we introduce some simplified approaches, namely the Monte-Carlo and the simplified Poisson (or simplified Gaussian) approaches, to reduce the computation complexity in the cases of long ISI. Furthermore, based on the statistics of decision variables, we analyze the effect of decision threshold on the BER performance. Finally, the BER performance of the BMoSK-modulated DMC systems without/with ISIC is investigated with considering the impact from different aspects, while the different analytical approaches are compared in terms of the accuracy of the BER evaluated based on these approaches.

The above studies show that ISI contributies to the significant performance degradation of DMC systems. In order to mitigate the effect of ISI, in Chapter 4, we investigate the equalization techniques for the DMC systems with BMoSK modulation, referred to as the BMoSK-DMC systems. We first show that in terms of receiving equalization, a BMoSK-DMC system is in fact equivalent to a conventional binary phase-shift keying (BPSK) modulated radio communication system encountering ISI. Hence, a wealth of equalization techniques developed with the conventional radio communication systems may be introduced for equalization of BMoSK-DMC signals. However, considering the limited capability of molecular transceivers on computation and storage, in this chapter, we investigate only the linear equalizers (LEQ) in the principles of matched-filtering (MF), zero-forcing (ZF) and minimum mean-square error (MMSE). We characterize the effects of the different aspects related to DMC signaling and propagation on the achievable performance of the BMoSK-DMC systems with these linear equalizers. Our studies and performance results demonstrate that both the ZF- and MMSE-LEQ are capable of efficiently suppressing the ISI and attaining promising performance, while still have low-complexity to facilitate implementation.

In Chapter 5, we address the multiuser communication in DMC. Specifically, relying on two types of molecules, we design a molecular code-division multiple-access (MoCDMA) scheme to enable multiple nano-users (NUs) to share a common molecular communication media, and to simultaneously communicate with a receiver. We mirror the proposed MoCDMA to the conventional radio-based CDMA (RdCDMA) with binary phase-shift keying (BPSK) modulation, based on which we derive the various expressions for received signals, so that the information conveyed by different NUs can be flexibly detected on either symbol-by-symbol or block-by-block basis.

Correspondingly, we introduce a range of relatively low-complexity detectors in the principles of MF, ZF and MMSE, which are operated at either symbol or block level. Furthermore, at block level, we derive the frequency (F)-domain detectors operated also in the principles of MF, ZF or MMSE. We analyze the noise characteristics in MoCDMA systems, and the complexity of the various detection schemes. Moreover, we investigate and compare the error performance of the MoCDMA systems with various detection schemes based on numerical simulations. Our studies and performance results demonstrate that the MoCDMA constitutes a promising scheme for supporting multiple-access in molecular communications, and that the various detection schemes may be implemented to attain a required complexity-reliability trade-off.

Finally, in Chapter 6, we summarize the main conclusions and observations obtained from the research. Furthermore, some optional future research issues related to the thesis are conceived.

Chapter 2

Error Performance Analysis of Diffusive Molecular Communication Systems with On-Off Keying Modulation

In this chapter, we analyze the bit error rate (BER) of the diffusive molecular communication (DMC) systems employing on-off keying (OOK) modulation. We also analyze the BER of the OOK-modulated DMC systems with inter-symbol interference cancellation (ISIC). Our main motivation is to introduce alternative tools for analyzing and efficiently computing the BER of the DMC systems without or with ISIC. Specifically, for the OOK-modulated DMC systems without ISIC, we first derive an exact BER expression based on the Poisson modeling of DMC systems. Then, the Gaussian- and Gamma-approximation approaches are introduced to approximate the discrete Poisson distribution, and based on the approximation approaches, the corresponding BER expressions are derived. Furthermore, in order to reduce the computation complexity imposed by long ISI, we propose the Monte-Carlo, simplified Poisson, simplified Gaussian and the simplified Gamma approaches for BER computation. In the context of the OOK-modulated DMC systems with ISIC, we consider both the Poisson and Gaussian-approximation approaches for BER analysis. Again, exact and approximate BER expressions are derived under the Poisson, Gaussian-approximation, simplified Poisson and simplified Gaussian approaches. Finally, the considered approaches are compared and validated by a range of performance results obtained from evaluation of the derived expressions or by simulations. Our studies show that the alternative approaches are in general effective for providing near-accurate BER estimation.

2.1 Introduction

In molecular communications (MC), information is conveyed between nano-machines with the aid of molecules [1, 7]. Recently, MC has been drawing an increasing attention in terms of its research and implementation, as witnessed, e.g., by the references [5–7, 66–68] and the references therein. In MC, the diffusion-based molecular communications (DMC) has been recognized as one of the most practical information transmission methods, which relies on the law of diffusion for molecule propagation from (nano-)transmitters to (nano-)receivers [7, 66, 69].

As in any existing communication systems, information in DMC is delivered via the data modulation operated at transmitters and the signal demodulation (detection) carried out at receivers, and both of which are critical for achieving high-efficiency and high-reliability. Hence in literature, there are many references dedicated to the design of DMC data modulation, signal detection and transceiver optimization schemes, based on the proposed channel models and noise statistics in DMC. To be more specific, for data modulation, there are typically three basic types. The first type relies on the molecule concentration, referred to as the concentration shift keying (CSK) [21, 36–41, 70, 71], which divides the molecule concentration into some levels for information configuration. The second type belongs to the pulse position modulation (PPM) [42], which delivers information by the positions of the pulses of molecule concentration. In the above two types, one type of molecules is usually used. By contrast, the third type uses multiple types of molecules, forming the so-called molecule shift keying (MoSK) [1, 39, 40, 72]. Based on these basic modulation schemes, hybrid and improved modulation schemes [46, 47, 73] may be designed for different purposes, e.g., for achieving higher data rate, interference control, etc. In DMC, a typical phenomenon severely affecting communication is the inter-symbol interference (ISI) generated by the long delay spread of molecular diffusion in liquid medium [19, 68]. Hence in literature, a range of advanced detection algorithms have been proposed to mitigate the effect of ISI [20, 22, 74–77].

Regardless of which data modulation scheme and detection scheme are employed, it is always important to predict the achievable performance of DMC systems. Hence, in this chapter, we motivate to provide some approaches for analysis and evaluation of the error performance of DMC systems. More importantly, we motivate the approaches that are feasible for computation and are capable of providing accurate or near-accurate estimation of the error performance of the DMC systems experiencing strong ISI.

In literature, there are a number of references dedicated specifically to the error rate analysis of the DMC systems with different modulation and detection schemes. Specifically, in [46], the error performance of the DMC systems with respectively three modulation schemes, namely, CSK, MoSK and the proposed so-called molecule concentration shift-keying (MCSK), all in binary forms, has been analyzed based on Poisson modeling. In its analysis for CSK and MoSK, a current symbol is assumed only to experience ISI from one previously sent symbol, while for MCSK it is assumed that there is no ISI. Poisson modeling has also been introduced in [20, 78] for deriving the

probability density function (PDF) and cumulative density function (CDF) of the DMC systems with CSK modulation. In [21, 62], the authors have analyzed the false-alarm probability, detection probability, and ultimately the error probability of the DMC systems with binary and M-ary CSK modulations, when the counting noise and ISI are both modeled as Gaussian noise. In [63], the authors have analyzed the error performance of the DMC systems with pulse-based modulation, and energy or amplitude detection, and some closed-form expressions have been derived also by approximating both the counting noise and ISI as Gaussian noise. In [64], the authors have analyzed the error performance (also capacity) of the DMC systems employing an M-ary amplitude modulation or an extended modulation scheme. In their analysis, molecules transmitted associated with different symbols are assumed to arrive at the receiver according to the binomial distributions, which are then approximated by the Gaussian distributions for deriving the error probability. Very recently, the authors of [65] have carried out the analysis for the DMC systems with both CSK and MoSK modulations, when modeling the number of molecules hitting the receiver at any time as the binomial distribution.

Against the background, in this chapter, we focus on the bit error rate (BER) analysis of the DMC systems with binary CSK modulation, which we refer to as the on-off keying (OOK) modulation. According to the results established in [16] as well as the analysis and theory in [20, 79], when the number of molecules appearing in a DMC environment is large, the number of molecules within an observation space can be accurately modelled by the Poisson distribution. Hence, based on the Poisson modeling, we first derive an exact BER expression under the Poisson modeling. In our analysis, both counting noise and ISI are considered, and furthermore, we assume that the length of ISI is arbitrary, and varies according to the transmission distance, data rate, etc. However, it shows that the BER expression derived from the Poisson modeling in some cases may be too complicated to evaluate, which is mainly the responsibility of two aspects. The first one is due to the discrete Poisson distribution, while the second one is resulted from the long ISI. In order to cope with the first aspect, we consider two continuous distributions for approximating the Poisson distribution, which are the Gaussian- and Gamma-approximation. Based on these two approximation approaches, we then derive the corresponding closed-form BER expressions. In order to mitigate the computational complexity resulted from long ISI, we also propose two approaches. The first one is the Monte-Carlo approach, which computes the BER by randomly generating a sufficient number of binary bits imposing ISI, instead of considering all the possible sequences that may be extreme in practice. In the second approach, we divide the ISI into two components. The first ISI component is generated by a number of bits sent in the front of the reference bit being detected, and all the possible combinations of these bits are considered in the BER computation. By contrast, the second ISI component consists of all the bits other than those included in the first component. The ISI imposed by these bits is approximated as a Poisson (or Gaussian, etc.) random variable that is independent of the specific bit sequence. Both the above approaches are then integrated with the Poisson, Gaussian- and Gamma-approximation approaches, and correspondingly, the formulas

for BER evaluation are provided. Following the BER analysis of the DMC systems with OOK modulation, we then analyze the BER of the OOK-modulated DMC systems with ISI cancellation (ISIC) [74, 77]. In our analysis, the Poisson modeling, Gaussian-approximation, and the two approaches for ISI handling are considered. Correspondingly, the closed-form BER expressions are derived. Finally, our analytical approaches are compared and validated by a range of numerical and simulation results. The BER performance of the OOK-modulated DMC systems without/with ISIC is studied and compared by considering the impact of different system parameters. The accuracy of various approximation approaches is demonstrated via comparison of the BER evaluated from the analytical expressions and/or obtained by simulations. Our studies and performance results demonstrate that all the BER expressions derived are valid for predicting the BER of the OOK-modulated DMC systems without/with ISIC. Furthermore, in some communication scenarios, employing the low-complexity ISIC scheme is capable of improving the error performance of DMC systems.

We should note that, although in this chapter we consider only the OOK modulation, the analytical approaches considered in Sections 2.3 and 2.4 may be extended straightforwardly to the DMC systems with other types of modulation schemes, including M-ary CSK [21, 36–41, 70, 71], MoSK [1, 39, 40, 72], etc.

The rest of the chapter is organized as follows. In section 2.2, we describe the DMC system model and state the main assumptions. Section 2.3 analyzes the BER of the DMC systems employing OOK modulation, while Section 2.4 deals with the BER of the OOK-modulated DMC systems with ISIC. In Section 2.5, we demonstrate the BER performance results obtained from numerical computation and particle-based as well as Monte-Carlo simulations. Finally, in Section 2.6, we summarize the main observations obtained from the studies.

2.2 System Model and Assumptions

We consider a typical DMC system [20, 22, 38, 74], which consists of a transmitter, a molecular diffusion channel and a receiver. At the transmitter, information is emitted via molecular release patterns, which propagate over a molecular diffusion channel. The receiver is a passive observer [78], which recovers information according to the time-varying molecule concentration measured within a detection space. For convenience of study, some typical assumptions generally used in references, such as, [38, 74], are applied. In detail, the transmitter is assumed to be a point molecule source with released molecules not interacting with the transmitter. The receiver is assumed to be able to ideally measure the molecule concentration within a spherical detection space with a radius of ρ. We assume that ρ is small with respect to the communication distance, yielding a near-uniform concentration within the detection space. In other words, the receiver is idealized as a point receiver. During a transmission, the positions of both transmitter and receiver are assumed at fixed locations. Furthermore, we assume that molecules at transmitter are released as impulses of molecules. Based on these assumptions, then, according to the Fick's law of diffusion [38], when an impulse of Q

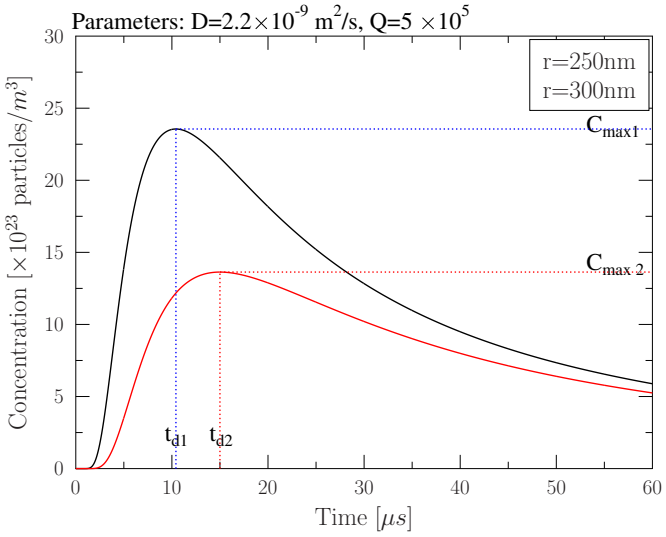

Figure 2.1: Pulse functions of molecule concentration with respect time and distance.

molecules are released by a transmitter at $t = 0$, the molecule concentration measured at a point having a distance r from the transmitter can be expressed as [38, 74]

$$c(t) = \frac{Q}{(4\pi Dt)^{\frac{3}{2}}} \exp\left(-\frac{r^2}{4Dt}\right), t > 0 \tag{2.1}$$

where D is medium's diffusion coefficient, and $t > 0$ is the observation time at receiver.

The molecule concentration $c(t)$ is a time-domain pulse function, having a shape as shown in Fig. 2.1, when assuming that an impulse of molecules is released at $t = 0$. It can be shown [38] that the concentration at a point having a fixed distance r from the transmitter reaches its maximum at the instant $t_d = \frac{r^2}{6D}$, and the peak value of $c(t)$ is $c_{\max} = c_{\max}(r) = \left(\frac{3}{2\pi e}\right)^{\frac{3}{2}} \frac{Q}{r^3}$.

2.2.1 DMC Employing On-Off Keying Modulation

DMC with OOK modulation has been investigated in many references, such as in [20,22,38,40,74]. Its principle can be briefly described as follows. Let $\{b_j\} = \{b_0, b_1, \ldots, b_j, \ldots\}$ be a binary information sequence, where $b_j \in \{0, 1\}$. When the OOK modulation is employed, the transmitter emits an impulse of molecules to send $b_j = 1$, but releases no molecules for sending $b_j = 0$. Therefore, after sending the uth bit, the molecule concentration measured by the receiver within its detection space can be expressed as [22]

$$z(t) = \sum_{j=0}^{u} b_j[c(t - jT) + n_j(t)],\ uT \le t < (u+1)T \tag{2.2}$$

where T represents the symbol interval, which is also the bit interval when binary OOK modulation is considered. Hence, the information rate is $R = 1/T$ bits per second (bps). In (2.2), $u = \lceil t/T \rceil$ is the largest integer not exceeding t/T, with $(u+1)$ representing the total number of bits transmitted

within $[0, t)$. Finally, $n_j(t)$ in (2.2) is due to the particle counting noise associated with the process of sending b_j. According to [16], counting noise is the result of the (random) Brownian motions of molecules, which cause an unwanted perturbation to the concentration predicted by the Fick's diffusion law.

As shown in Fig. 2.1, when an impulse of molecules is sent at $t = 0$, it would be desirable for the receiver to sample at $t = t_d$ for the maximum molecule concentration, in order to make most reliable detection. Therefore, in order to detect the uth bit, we assume that the receiver samples for the molecule concentration at $t = uT + \hat{t}_d$, where $\hat{t}_d$ represents the estimate to t_d. This gives the decision variable for detection of the uth bit as

$$\begin{aligned} Z_u =& z(t = uT + \hat{t}_d) \\ =& \sum_{j=0}^{u} b_j \left[c([u-j]T + \hat{t}_d) + n_j(uT + \hat{t}_d) \right], \ u = 0, 1, \ldots \end{aligned} \tag{2.3}$$

Let us define $c_{u-j} = c([u-j]T + \hat{t}_d)$ and $n_{ju} = n_j(uT + \hat{t}_d)$. Then, the above equation can be rewritten as

$$Z_u = \sum_{j=0}^{u} b_j \left[c_{u-j} + n_{ju} \right], \ u = 0, 1, \ldots \tag{2.4}$$

Explicitly, the detection of bit u experiences ISI. Let us assume that the maximum length of ISI is L bits. Then, upon applying the variable transform of $i = u - j$, we can express Z_u of (2.4) in the form of

$$\begin{aligned} Z_u =& \sum_{j=\max\{0,u-L\}}^{u} b_j \left[c_{u-j} + n_{ju} \right] \\ =& \sum_{i=0}^{\min\{L,u\}} b_{u-i} \left[c_i + n_{(u-i)u} \right], \ u = 0, 1, \ldots \end{aligned} \tag{2.5}$$

where $c_i = c(iT + \hat{t}_d)$. Furthermore, for convenience, we may also write (2.5) as

$$Z_u = \sum_{i=0}^{\min\{L,u\}} b_{u-i} c_i + n_u, \ u = 0, 1, \ldots \tag{2.6}$$

where $n_u = \sum_{i=0}^{\min\{L,u\}} b_{u-i} n_{(u-i)u}$.

Let $V_R = \frac{4}{3}\pi\rho^3$ be the volume of the spherical detection space. Then, as given in [16, 20, 22], $Y_u = V_R Z_u$ can be accurately modeled as a Poisson distributed random variable with both the mean and variance given by $\mu_Y = V_R \sum_{i=0}^{\min\{L,u\}} b_{u-i} c_i$, which is expressed as $Y_u \sim \mathcal{P}(\mu_Y)$. Furthermore, when μ_Y is sufficiently large, making the Gaussian approximation applicable, Y_u can be approximated as a Gaussian random variable with both the mean and the variance given by μ_Y, which is expressed as $Y_u \sim \mathcal{N}(\mu_Y, \mu_Y)$. Correspondingly, Z_u in (2.6) obeys the Gaussian distribution of $Z_u \sim \mathcal{N}(\mu_Z, \sigma_Z^2)$ [74], where the mean and variance are given by $\mu_Z = \sum_{i=0}^{\min\{L,u\}} b_{u-i} c_i$ and $\sigma_Z^2 = V_R^{-1} \sum_{i=0}^{\min\{L,u\}} b_{u-i} c_i$. Hence, the PDF of the noise samples $\{n_u\}$ seen in (2.6) is $n_u \sim \mathcal{N}(0, \sigma_Z^2)$.

Let C_T be a threshold used by the OOK modulation for decision making. Considering that the concentration presenting at the receiver has a function as shown in Fig. 2.1, it is sometimes convenient to set the threshold relative to the peak $c_{\max}$ as

$$C_T = \alpha c_{\max} \tag{2.7}$$

where $0 \leq \alpha \leq 1$ can be referred to as the normalized threshold. Consequently, the receiver makes the decision for a bit by comparing the measured concentration with the threshold according to the rules of

$$\hat{b}_u = \begin{cases} 1, & \text{when } Y_u > V_R C_T,\ Z_u > C_T, \text{ or } \frac{Z_u}{C_{max}} > \alpha \\ 0, & \text{when } Y_u \leq V_R C_T,\ Z_u \leq C_T, \text{ or } \frac{Z_u}{C_{max}} \leq \alpha \end{cases} \tag{2.8}$$

Here we should note that Y_u represents the number of molecules counted within the detection space with a volume of V_R, hence it is an integer.

As seen, e.g., in (2.5), the detection of b_u experiences ISI, which becomes severer as the data rate becomes higher, resulting in a reduced symbol duration. Without ISI mitigation, the performance of DMC may be severely degraded. Below we consider the ISI mitigation in the OOK-modulated DMC systems.

2.2.2 Inter-Symbol Interference Cancellation

In [74], a simple ISIC method has been proposed, when the DMC with OOK modulation is assumed. In this method, the receiver forms decision variables as

$$\begin{aligned} Z_u =& z(t = uT + \hat{t}_d) - z(t = uT) \qquad (2.9) \\ =& \sum_{j=0}^{u} b_j \left[c([u-j]T + \hat{t}_d) + n_j(uT + \hat{t}_d) \right] \\ & - \sum_{j=0}^{u} b_j \left[c([u-j]T) + n_j(uT) \right], \ u = 0, 1, \ldots \qquad (2.10) \end{aligned}$$

which is the difference between the two observations, $z(t = uT + \hat{t}_d)$ and $z(t = uT)$, obtained at $t = uT + \hat{t}_d$ and $t = uT$, respectively. With the aid of Fig. 2.1, we can know that the first observation measures the molecule concentration peak after sending bit b_u. By contrast, the second observation obtained at the start of sending b_u provides a reference for the ISI imposed on b_u at $t = uT + \hat{t}_d$. Therefore, after the subtraction operation as seen in (2.9) and (2.10), most of the ISI will be cancelled. From Fig. 2.1 we can be implied that this approach is in particular effective, when the transmission rate $R = 1/T$ is relatively low, resulting in that the ISI measured at $t = uT$ is nearly the same as that measured at $t = uT + \hat{t}_d$.

However, when the transmission rate becomes high, the ISI obtained at $t = uT$ may be very different from that at $t = uT + \hat{t}_d$, as implied by Fig. 2.1. This becomes even severer, when

$b_{u-1} = +1$ is sent before b_u. Let us rearrange (2.10) to express the decision variable as

$$\begin{aligned} Z_u =& b_u c(\hat{t}_d) + \sum_{j=0}^{u-1} b_j \left[c([u-j]T + \hat{t}_d) - c([u-j]T) \right] \\ &+ \sum_{j=0}^{u} b_j \left[n_j(uT + \hat{t}_d) - n_j(uT) \right], \quad u = 0, 1, \ldots \end{aligned} \tag{2.11}$$

where $c(0) = 0$ is assumed. Furthermore, we also have $n_u(uT) = 0$, as it is the counting noise contributed by the uth bit that has not yet sent at $t = uT$. At the righthand side (RHS) of (2.11), the first term is the desired observation, the second term is the residue ISI due to non-ideal ISIC, while the last term is the counting noise presenting at $t = uT + \hat{t}_d$ and at $t = uT$. Assume that the transmission rate is high, resulting in that the symbol duration T is only slightly larger than t_d. Then, with the aid of Fig. 2.1, we can be implied that the ISI at $t = uT$ can be much larger than the ISI at $t = uT + \hat{t}_d$, due to the fast decrease of molecule concentration resulted from the impulses of molecules sent most recently. In this case, the ISIC based on (2.9) results in over cancellation, yielding a large residue ISI given by the second term at the RHS of (2.11). Furthermore, as seen in (2.11), the counting noise after the ISIC is contributed by both the counting noise presenting at $t = uT$ and that at $t = uT + \hat{t}_d$. According to [16], provided that $\hat{t}_d > \rho^2/D$, two adjacent samples of the counting noise process can be regarded as statistically independent. In this case, the ISIC operation of (2.9) enhances the noise, which may further degrade the achievable performance of DMC.

In order to improve the performance of the ISIC, a more accurate estimate to the ISI at $t = uT + \hat{t}_d$ is desirable, while simultaneously mitigating the impact from noise enhancement. With this motivation, in [77], we have proposed an improved ISIC scheme, which forms the decision variable according to the formula

$$Z_u = z(t = uT + \hat{t}_d) - \lambda_u z(t = uT) \tag{2.12}$$

where $0 \leq \lambda_u \leq 1$ is used to scale the ISI measured at $t = uT$. Following (2.11), we can express (2.12) in detail as

$$\begin{aligned} Z_u =& b_u c(\hat{t}_d) + \sum_{j=0}^{u-1} b_j \left[c([u-j]T + \hat{t}_d) - \lambda_u c([u-j]T) \right] \\ &+ \sum_{j=0}^{u} b_j \left[n_j(uT + \hat{t}_d) - \lambda_u n_j(uT) \right], \quad u = 0, 1, \ldots \end{aligned} \tag{2.13}$$

Explicitly, at the RHS of (2.13), the desired term is not affected by the ISIC, while the noise enhancement in the third term is mitigated due to $\lambda_u < 1$.

Furthermore, in [77], we have proposed the approaches for estimating the scaling factor in (2.12). For completeness, these approaches are also detailed below. First, the optimum value of λ_u for given transmission rate and pulse shape may be obtained via numerical/simulation approaches. Second, we may estimate the scaling factor with the motivation to fully cancel the ISI presenting

at $t = uT + \hat{t}_d$ as follows. Let the average ISI at t be expressed as $I_{SI}(t)$. Then, we can find an estimate to λ_u by solving the equation of

$$\lambda_u I_{SI}(uT) = I_{SI}(uT + \hat{t}_d) \tag{2.14}$$

where both $I_{SI}(uT)$ and $I_{SI}(uT + \hat{t}_d)$ can be calculated, once we know the correct estimates of $\hat{b}_0, \hat{b}_1, \ldots, \hat{b}_{u-1}$ for the transmitted bits $b_0, b_1, \ldots, b_{u-1}$. However, considering all the past symbols results in high complexity and possibly degraded performance due to error propagation and noise enhancement, as above-mentioned. Furthermore, in practice, it may not be necessary to consider all the past symbols, as the ISI contributed by a pulse becomes nearly flat after some time, as shown in Fig. 2.1. When taking all these into account, we may estimate λ_u as follows. Let us consider J $(J < u)$ most recent bits. Then, we can compute J coefficients corresponding to the most recent J bits as

$$\beta_{u-1} = \frac{c(T + \hat{t}_d)}{c(T)}, \ldots, \ \beta_{u-J} = \frac{c(JT + \hat{t}_d)}{c(JT)} \tag{2.15}$$

if the pulse $c(t)$ presenting at the receiver is known. The value of J can be chosen, so that the remaining ISI at uT and that at $uT + \hat{t}_d$ satisfy

$$C_J(u) = \sum_{j=0}^{J-1} b_j c([u-j]T + \hat{t}_d) \approx \sum_{j=0}^{J-1} b_j c([u-j]T) \tag{2.16}$$

which can be evaluated as

$$C_J(u) = z(t = uT) - \sum_{l=1}^{J} \hat{b}_{u-l} c(lt) \tag{2.17}$$

Alternatively, we may simply use the average value of $C_J(u)$, which can be estimated as

$$\bar{C}_J = \frac{1}{N} \sum_{u=J+1}^{J+N} C_J(u) \tag{2.18}$$

Finally, with the aid of (2.15) and (2.16), as well as the estimated bit values, (2.14) can be expressed as

$$\hat{\lambda}_u \left(\sum_{j=1}^{J} \hat{b}_{u-j} c(jT) + C_J(u) \right) = \sum_{j=1}^{J} \hat{b}_{u-j} \beta_{u-j} c(jT) + C_J(u) \tag{2.19}$$

from which λ_u can be expressed as

$$\hat{\lambda}_u = \frac{\sum_{j=1}^{J} \hat{b}_{u-j} \beta_{u-j} c(jT) + C_J(u)}{\left(\sum_{j=1}^{J} \hat{b}_{u-j} c(jT) + C_J(u) \right)} \tag{2.20}$$

In the above equation, if $C_J(u) \approx 0$, we have

$$\hat{\lambda}_u = \frac{\sum_{j=1}^{J} \hat{b}_{u-j} \beta_{u-j} c(jT)}{\sum_{j=1}^{J} \hat{b}_{u-j} c(jT)} \tag{2.21}$$

According to above analysis, if detection is highly reliable, we may expect that the ISIC seen in (2.12) (and (2.13)) is fully removed or significantly reduced. If the detection becomes less reliable, the ISIC results in error propagation. As seen in (2.21), $\hat{\lambda}_u$ is dependent on the J bits received before the uth bit. If a bit is detected in error, it will affect the detection of its following J bits. In order to mitigate the error propagation, in practice, the value of λ_u in (2.12) may be adjusted according to the detection reliability. When the detection reliability is low, a λ_u smaller than $\hat{\lambda}_u$ of (2.21) may be employed, in order to mitigate the effect of error propagation. By contrast, when the detection reliability increases, the value of λ_u can be gradually increased towards the value of $\hat{\lambda}_u$ estimated by (2.21), in order to further enhance the detection reliability. However, we should note that the ISIC results in additional noise, which increases as λ_u increases. Therefore, for a given λ_u, there exists a trade-off between ISIC and noise enhancement.

In the following two sections, we will analyze the bit error rate (BER) of the DMC systems employing or without employing the ISIC. Specifically in Section 2.3, we address the BER performance of the DMC systems employing OOK modulation, while in Section 2.4, the BER performance of the OOK-modulated DMC systems with ISIC is analyzed.

2.3 BER Analysis of DMC Systems Employing OOK Modulation

We analyze the BER of the DMC systems employing the OOK modulation based on the decision variable given by (2.5). In our analysis, we assume that the DMC process is in its static state, meaning that $u >> L$, here L is the maximum length of ISI. Correspondingly, the decision variable of (2.5) can be written as

$$Z_u = \sum_{i=0}^{L} b_{u-i} \left[c_i + n_{(u-i)u} \right] \tag{2.22}$$

Furthermore, we assume that the sampling duration, which is the bit duration T, satisfies the condition of $T > \rho^2/D$ [16]. Hence, adjacent noise samples are independent. Additionally, we assume that the transmitted binary bits obey the distribution of $P(1) = P(0) = 0.5$.

2.3.1 Poisson Approach: Exact BER Analysis

Let us first analyze the exact BER of the DMC systems employing OOK modulation based on the Poisson distribution of $Y_u = V_R Z_u$, which for convenience is referred to as the *Poisson approach*. Note that in literature, the Poisson approach has been employed by a number of references, e.g., [20, 46, 78], for performance studies, as detailed in the literature review in Section 2.1. As shown in Section 2.2.1, the decision variable Y_u obeys the Poisson distribution with the probability mass function (PMF) given by $\mathcal{P}(\mu_Y)$, where $\mu_Y = V_R \sum_{i=0}^{L} b_{u-i} c_i$. Explicitly, μ_Y is dependent on the transmitted data sequence. Let us define a vector $\boldsymbol{b}_L = [b_{u-L}, \ldots, b_{u-1}]^T$ containing the L bits

imposing ISI on b_u. Then, when $b_u = 1$, we express the Poisson PMF as [79]

$$f_{Y_u}(n|\boldsymbol{b}_L, b_u = 1) = \frac{\mu_{Y_1}^n e^{-\mu_{Y_1}}}{n!}, n = 0, 1, 2, \ldots \tag{2.23}$$

where $\mu_{Y_1} = V_R \left(c_0 + \sum_{i=1}^{L} b_{u-i} c_i\right)$. When $b_u = 0$, the Poisson PMF can be expressed as

$$f_{Y_u}(n|\boldsymbol{b}_L, b_u = 0) = \frac{\mu_{Y_0}^n e^{-\mu_{Y_0}}}{n!}, n = 0, 1, 2, \ldots \tag{2.24}$$

associated with $\mu_{Y_0} = V_R \sum_{i=1}^{L} b_{u-i} c_i$. The BER of the DMC systems employing the OOK modulation is given by

$$\begin{aligned} P_b =& \frac{1}{2} P(\hat{b}_u = 0|b_u = 1) + \frac{1}{2} P(\hat{b}_u = 1|b_u = 0) \\ =& \frac{1}{2} \left(P_M + P_{FA}\right) \end{aligned} \tag{2.25}$$

where $P_M = P(\hat{b}_u = 0|b_u = 1)$ is the probability of detecting $\hat{b}_u = 0$ for an actually transmitted $b_u = 1$, which is usually referred to as the miss-probability, while $P_{FA} = P(\hat{b}_u = 1|b_u = 0)$ is the probability of detecting $\hat{b}_u = 1$ for an actually transmitted $b_u = 0$, which is called as the false-alarm probability. Let us below derive these probabilities in detail.

First, given a detection threshold C_T with respect to the molecule concentration, the miss-probability can be expressed as

$$\begin{aligned} P_M =& P(\hat{b}_u = 0|b_u = 1) \\ =& P(Y_u \leq V_R C_T|b_u = 1) \\ =& \sum_{\boldsymbol{b}_L \in \mathcal{B}^L} P(\boldsymbol{b}_L) P(Y_u \leq V_R C_T|\boldsymbol{b}_L, b_u = 1) \end{aligned} \tag{2.26}$$

where $\mathcal{B} = \{1, 0\}$, $P(\boldsymbol{b}_L)$ is the probability of the occurrence of a specific sequence of $\boldsymbol{b}_L$. When assuming that $P(1) = P(0) = 0.5$, we have $P(\boldsymbol{b}_L) = 1/2^L$. Finally, $P(Y_u \leq V_R C_T|\boldsymbol{b}_L, b_u = 1)$ is the probability conditioned on a given data sequence of $\boldsymbol{b}_L$ and $b_u = 1$. With the aid of the PMF given by (2.23), we have [79]

$$P(Y_u \leq V_R C_T|\boldsymbol{b}_L, b_u = 1) = \sum_{n=0}^{\lceil V_R C_T \rceil} \frac{\mu_{Y_1}^n e^{-\mu_{Y_1}}}{n!} \tag{2.27}$$

Upon substituting this result into (2.26), we obtain the miss-probability of

$$P_M = \frac{1}{2^L} \sum_{\boldsymbol{b}_L \in \mathcal{B}^L} \sum_{n=0}^{\lceil V_R C_T \rceil} \frac{\mu_{Y_1}^n e^{-\mu_{Y_1}}}{n!} \tag{2.28}$$

For the false-alarm probability, we have the relationships of

$$\begin{aligned} P_{FA} =& P(\hat{b}_u = 1|b_u = 0) \\ =& P(Y_u > V_R C_T|b_u = 0) \\ =& 1 - P(Y_u \leq V_R C_T|b_u = 0) \\ =& 1 - \sum_{\boldsymbol{b}_L \in \mathcal{B}^L} P(\boldsymbol{b}_L) P(Y_u \leq V_R C_T|\boldsymbol{b}_L, b_u = 0) \end{aligned} \tag{2.29}$$

Similar to (2.27), we can obtain

$$P_{FA} = 1 - \frac{1}{2^L} \sum_{\boldsymbol{b}_L \in \mathcal{B}^L} \sum_{n=0}^{\lceil V_R C_T \rceil} \frac{\mu_{Y_0}^n e^{-\mu_{Y_0}}}{n!} \tag{2.30}$$

Finally, applying both (2.28) and (2.30) into (2.25), the BER of the DMC systems employing OOK modulation can be expressed as

$$P_b = \frac{1}{2} + \frac{1}{2^{L+1}} \sum_{\boldsymbol{b}_L \in \mathcal{B}^L} \left(\sum_{n=0}^{\lceil V_R C_T \rceil} \frac{\mu_{Y_1}^n e^{-\mu_{Y_1}} - \mu_{Y_0}^n e^{-\mu_{Y_0}}}{n!} \right) \tag{2.31}$$

2.3.2 Gaussian-Approximation

From (2.31), we can see that evaluating the BER has the complexity of $\mathcal{O}\left(\lceil V_R C_T \rceil 2^L\right)$ contributed by the two sum in the formula, where 2^L is due to the L-length binary data sequence imposing ISI, while $\lceil V_R C_T \rceil$ is the result of the discrete Poisson distribution. If the discrete Poisson distribution can be approximated by a continuous distribution, the second sum in (2.31) can be replaced by an integration, which may be simplified to obtain a closed-form convenient for evaluation.

It is well-known that the Poisson distribution has the property [79] that it can be approximated by a Gaussian distribution, if the Poisson parameter (μ) is sufficiently large, e.g., $\mu > 20$. Therefore, in literature, the performance of some DMC systems has been studied under the Gaussian modeling of counting noise [20, 21, 62, 63]. In our case, if μ_{Y_1} in (2.23) and μ_{Y_0} in (2.24) are sufficiently large, then both $f_{Y_u}(n|\boldsymbol{b}_L, b_u = 1)$ and $f_{Y_u}(n|\boldsymbol{b}_L, b_u = 1)$ can be approximated by the Gaussian distributions. In this case, we can derive the BER directly from the concentration-based decision variable Z_u given by (2.22). Therefore, when assuming $u >> L$, the PDFs of Z_u conditioned on $\boldsymbol{b}_L$, $b_u = 1$ or 0 can be expressed as [79]

$$\begin{aligned} f_{Z_u}(y|\boldsymbol{b}_L, b_u = 1) &= \frac{1}{\sqrt{2\pi}\sigma_{Z_1}} \exp\left(-\frac{[y - \mu_{Z_1}]^2}{2\sigma_{Z_1}^2} \right), \\ f_{Z_u}(y|\boldsymbol{b}_L, b_u = 0) &= \frac{1}{\sqrt{2\pi}\sigma_{Z_0}} \exp\left(-\frac{[y - \mu_{Z_0}]^2}{2\sigma_{Z_0}^2} \right) \end{aligned} \tag{2.32}$$

where $-\infty < y < \infty$, by definition, we have

$$\begin{aligned} \mu_{Z_1} &= c_0 + \sum_{i=1}^{L} b_{u-i} c_i; \;\; \sigma_{Z_1}^2 = \frac{c_0}{V_R} + \frac{1}{V_R} \sum_{i=1}^{L} b_{u-i} c_i \\ \mu_{Z_0} &= \sum_{i=1}^{L} b_{u-i} c_i; \;\; \sigma_{Z_0}^2 = \frac{1}{V_R} \sum_{i=1}^{L} b_{u-i} c_i \end{aligned} \tag{2.33}$$

which are all functions of $\boldsymbol{b}_L$. Therefore, following the analysis in (2.26), the miss-probability P_M

can be expressed as

$$\begin{aligned} P_M =& \frac{1}{2^L} \sum_{\boldsymbol{b}_L \in \mathcal{B}^L} P(Z_u \leq C_T | \boldsymbol{b}_L, b_u = 1) \\ =& 1 - \frac{1}{2^L} \sum_{\boldsymbol{b}_L \in \mathcal{B}^L} P(Z_u > C_T | \boldsymbol{b}_L, b_u = 1) \\ =& 1 - \frac{1}{2^L} \sum_{\boldsymbol{b}_L \in \mathcal{B}^L} \frac{1}{\sqrt{2\pi}\sigma_{Z_1}} \int_{C_T}^{\infty} \exp\left(-\frac{[y - \mu_{Z_1}]^2}{2\sigma_{Z_1}^2} \right) dy \\ =& 1 - \frac{1}{2^L} \sum_{\boldsymbol{b}_L \in \mathcal{B}^L} Q\left(\frac{C_T - \mu_{Z_1}}{\sigma_{Z_1}} \right) \end{aligned} \tag{2.34}$$

where $Q(x)$ is the Gaussian Q-function [80] defined as $Q(x) = (2\pi)^{-1/2} \int_x^{\infty} e^{-t^2/2} dt$, which is the built-in function of many software packages, e.g., Matlab, for numerical computation.

Similarly, the false-alarm probability P_{FA} can be derived as

$$\begin{aligned} P_{FA} =& \frac{1}{2^L} \sum_{\boldsymbol{b}_L \in \mathcal{B}^L} P(Z_u > C_T | \boldsymbol{b}_L, b_u = 0) \\ =& \frac{1}{2^L} \sum_{\boldsymbol{b}_L \in \mathcal{B}^L} \frac{1}{\sqrt{2\pi}\sigma_{Z_0}} \int_{C_T}^{\infty} \exp\left(-\frac{[y - \mu_{Z_0}]^2}{2\sigma_{Z_0}^2} \right) dy \\ =& \frac{1}{2^L} \sum_{\boldsymbol{b}_L \in \mathcal{B}^L} Q\left(\frac{C_T - \mu_{Z_0}}{\sigma_{Z_0}} \right) \end{aligned} \tag{2.35}$$

Finally, when substituting both (2.34) and (2.35) into (2.25), the BER of the OOK modulated DMC systems under the Gaussian-approximation can be obtained.

2.3.3 Gamma-Approximation

In comparison to (2.31), the BER expression obtained from the Gaussian-approximation may be slightly advantageous for evaluation. However, in order to apply the Gaussian-approximation, the mean $\mu_{Y_1} = V_R \left(c_0 + \sum_{i=1}^{L} b_{u-i} c_i \right)$ and $\mu_{Y_0} = V_R \left(\sum_{i=1}^{L} b_{u-i} c_i \right)$ need to be relatively large, typically, exceed 20. Since V_R is usually a very small value in comparison to the diffusion space of molecules, the above conditions may not be satisfied, unless the number of molecules Q per transmission impulse is very big. This situation often means that the signal-to-noise ratio (SNR) for DMC is high. In a nutshell, the Gaussian-approximation is only suitable for high SNR scenarios. Furthermore, as seen in (2.32), the Gaussian distributions are defined in the range of $(-\infty, \infty)$, which makes the Gaussian-approximation for the Poisson distribution defined in $(0, \infty)$ insensible, especially when the mean of μ_{Y_1} or μ_{Y_0} is relatively small. Considering the above issues, in this section, we propose the Gamma-approximation [81] to approximate the Poisson distribution as a Gamma-distribution with the PDF in the form of [82]

$$f_Y(y) = \frac{1}{\Gamma(m)\Omega^m} y^{m-1} \exp\left(-\frac{y}{\Omega} \right), \ 0 \leq y < \infty \tag{2.36}$$

where m is the *shape* parameter and Ω is the *scale* parameter, while $\Gamma(x)$ is the gamma function. It can be shown that the Gamma distributed variable Y has the mean and variance given by [82]

$$E[Y] = m\Omega, \quad \text{Var}[Y] = m\Omega^2 \tag{2.37}$$

From these relationship, we can readily know that

$$m = \frac{E^2[Y]}{\text{Var}[Y]}, \quad \Omega = \frac{\text{Var}[Y]}{E[Y]} \tag{2.38}$$

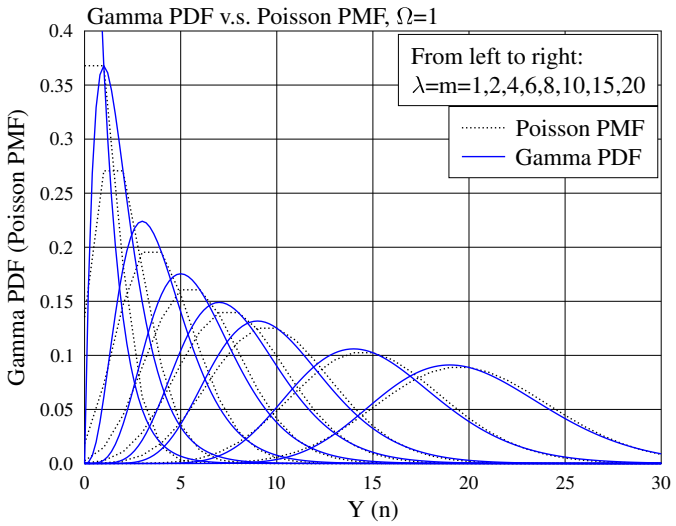

Figure 2.2: Comparison between the Poisson PMF and the corresponding Gamma PDF.

Assume a Poisson PMF of $f(n|\lambda) = \lambda^n e^{-\lambda}/n!$. Then, it can be shown that for the corresponding Gamma PDF of (2.36), we have $m = \lambda$ and $\Omega = 1$. The comparison between the Poisson PMF and Gamma PDF are shown in Figs. 2.2 for some λ, m values and $\Omega = 1$. Explicitly, the Gamma distribution is capable of providing a good approximation for the Poisson distribution for all the considered λ values, and more closer approximation presents, as the value of λ increases. In fact, from the research of radio communication channel modeling [83–86], the Gamma distribution (or the Nakagami distribution for the square-roots of Gamma distributed random variables) usually fits well the measurement data in terms of SNR (or magnitude) from practical experiments. This might imply that the Nakagami and Gamma distributions are also the good tools for describing the statistical properties of DMC channels, especially in the case when continuous distribution functions are required.

Let us now return to derive the BER of the OOK-modulated DMC systems under the Gamma-approximation. In this case, we can express the Gamma PDFs conditioned on $b_u = 1$ and $b_u = 0$

respectively as

$$f_{Z_u}(y|\boldsymbol{b}_L, b_u = 1) = \frac{1}{\Gamma(m_1)\Omega_1^{m_1}} y^{m_1-1} \exp\left(-\frac{y}{\Omega_1}\right),$$
$$f_{Z_u}(y|\boldsymbol{b}_L, b_u = 0) = \frac{1}{\Gamma(m_0)\Omega_0^{m_0}} y^{m_0-1} \exp\left(-\frac{y}{\Omega_0}\right) \tag{2.39}$$

where $0 \leq y < \infty$. With the aid of (2.33), the shape and scale parameters in (2.39) are given by

$$m_1 = \frac{\mu_{Z_1}^2}{\sigma_{Z_1}^2}, \ \Omega_1 = \frac{\sigma_{Z_1}^2}{\mu_{Z_1}}$$
$$m_0 = \frac{\mu_{Z_0}^2}{\sigma_{Z_0}^2}, \ \Omega_0 = \frac{\sigma_{Z_0}^2}{\mu_{Z_0}} \tag{2.40}$$

Then, by following (2.34), the miss-probability can be derived as

$$P_M = \frac{1}{2^L} \sum_{\boldsymbol{b}_L \in \mathcal{B}^L} P(Z_u \leq C_T | \boldsymbol{b}_L, b_u = 1)$$
$$= \frac{1}{2^L} \sum_{\boldsymbol{b}_L \in \mathcal{B}^L} \frac{1}{\Gamma(m_1)\Omega_1^{m_1}} \int_0^{C_T} y^{m_1-1} \exp\left(-\frac{y}{\Omega_1}\right) dy \tag{2.41}$$

Using the result of (3.381.1) in [87], we can simplify the above expression to

$$P_M = \frac{1}{2^L} \sum_{\boldsymbol{b}_L \in \mathcal{B}^L} \frac{\gamma(m_1, C_T/\Omega_1)}{\Gamma(m_1)} \tag{2.42}$$

where $\gamma(\alpha, x)$ is the lower incomplete gamma function [87](8.350.1). Furthermore, when m_1 is an integer, or when it is approximated by an integer[1], then, with the aid of [87](8.352.6), (2.42) can be expressed as

$$P_M = \frac{1}{2^L} \sum_{\boldsymbol{b}_L \in \mathcal{B}^L} \left[1 - \exp\left(-\frac{C_T}{\Omega_1}\right) \sum_{n=0}^{m_1-1} \frac{1}{n!} \left(\frac{C_T}{m_1}\right)^n\right] \tag{2.43}$$

Similarly, corresponding to (2.42) and (2.43), the false-alarm probability can be expressed as

$$P_{FA} = 1 - \frac{1}{2^L} \sum_{\boldsymbol{b}_L \in \mathcal{B}^L} \frac{\gamma(m_0, C_T/\Omega_0)}{\Gamma(m_0)} \tag{2.44}$$
$$= 1 - \frac{1}{2^L} \sum_{\boldsymbol{b}_L \in \mathcal{B}^L} \left[1 - \exp\left(-\frac{C_T}{\Omega_0}\right) \sum_{n=0}^{m_0-1} \frac{1}{n!} \left(\frac{C_T}{m_0}\right)^n\right] \tag{2.45}$$

respectively.

Finally, in the general cases, when substituting (2.42) and (2.44) into (2.25), we can obtain the BER expression for the OOK-modulated DMC systems under the Gamma-approximation. By contrast, for the special cases of m_1 and m_0 being integers, corresponding BER expression can be obtained by substituting (2.43) and (2.45) into (2.25).

[1]When m_1 is large, it usually can be approximated by an integer, as the Gamma-distribution in this case is not very sensitive to value of m_1.

2.3.4 Monte-Carlo Approach

So far, we have considered some alternative approaches to deal with the second sum in (2.31). In some cases, such as when communicating at relatively high data rate, the ISI can be very long, which makes exact evaluation of (2.31) impossible, due to the involvement of the first sum of 2^L items, as seen in (2.31). In fact, provided that $L \geq 20$, exact evaluating (2.31) is highly involved, even without considering the second sum in (2.31). In practice, however, the ISI length of L may be significantly larger than 20. Therefore, in this and the next subsections, we provide some approaches for reducing the terms to be considered in the context of the first sum in (2.31), as well as in the BER expressions obtained from the Gaussian- and Gamma-approximation.

Specifically, in this subsection, we consider the Monte-Carlo approach [88] to simplify the computation of the BER expressions obtained under the Poisson, Gaussian-approximation and Gamma-approximation approaches, when L is large. As seen in (2.31), since $\boldsymbol{b}_L$ is a L-length binary random vector distributed in $\mathcal{B}^L$, we can randomly generate W number of binary sequences for $\boldsymbol{b}_L$, which are expressed as $\{\boldsymbol{b}_L^{(1)}, \ldots, \boldsymbol{b}_L^{(W)}\}$. Then, corresponding to (2.31), the BER of the DMC systems employing OOK modulation can be approximately evaluated from the formula

$$P_b \approx \frac{1}{2} + \frac{1}{2W} \sum_{\{\boldsymbol{b}_L^{(1)}, \ldots, \boldsymbol{b}_L^{(W)}\}} \sum_{n=0}^{\lceil V_R C_T \rceil} \left(\frac{\mu_{Y_1}^n e^{-\mu_{Y_1}} - \mu_{Y_0}^n e^{-\mu_{Y_0}}}{n!} \right) \tag{2.46}$$

Provided that W is sufficiently large, the BER estimated by (2.46) should be close to that by (2.31).

Similarly, we can have the approximated BER expressions, when the Gaussian- and Gamma-approximation are respectively employed. As our results in Section 2.5 show, the Monte-Carlo approach is capable of providing close approximation, provided that $W \geq 10^5$.

2.3.5 Simplified Poisson, Gaussian-Approximation and Gamma-Approximation Approaches

From Fig. 2.1 we can see that the concentration becomes flatter and lower, as the propagation time or/and propagation distance increase. This implies that the ISI imposing on a specific data bit is dominated by the several bits sent in the front of the bit. Therefore, when L is large, and assuming that $u >> 1$ and $u > L$, we may re-write the decision variable Z_u of (2.5) as

$$Z_u = \sum_{i=0}^{I} b_{u-i} \left[c_i + n_{(u-i)u} \right] + X_u, \;\; u = 0, 1, \ldots \tag{2.47}$$

where $X_u = \sum_{i=I+1}^{L} b_{u-i} \left[c_i + n_{(u-i)u} \right]$. Since all c_i in X_u have small values and $n_{(u-i)u}$ in X_u are independent random variables, when $(L-I)$ is sufficiently large, we may approximate $Y_u = V_R X_u$ as a Poisson distributed random variable, with the mean and variance given by

$$\mu_y = E\left[V_R X_u\right] = V_R E_{\{b_{u-i}\}} \left[\sum_{i=I+1}^{L} b_{u-i} c_i \right] = \frac{V_R}{2} \sum_{i=I+1}^{L} c_i \tag{2.48}$$

Therefore, X_u has the mean and variance given by

$$\mu_x = \frac{1}{2}\sum_{i=I+1}^{L} c_i,\ \ \sigma_x^2 = \frac{1}{2V_R}\sum_{i=I+1}^{L} c_i \tag{2.49}$$

Consequently, when the Poisson approach is employed, the PDFs of Y_u conditioned on $b_u = 1$ and $b_u = 0$ are given by (2.23) and (2.24), respectively, associated with

$$\begin{aligned}\mu_{Y_1} &= V_R\left(c_0 + \sum_{i=1}^{I} b_{u-i}c_i\right) + \mu_y,\\ \mu_{Y_0} &= V_R\sum_{i=1}^{I} b_{u-i}c_i + \mu_y\end{aligned} \tag{2.50}$$

Finally, following the derivation of (2.31), the BER of the OOK-modulated DMC systems derived from the simplified Poisson approach can be expressed as (2.31) with the parameter L replaced by the parameter I, and $\boldsymbol{b}_L \in \mathcal{B}^L$ replaced by $\boldsymbol{b}_I \in \mathcal{B}^I$ where, by definition, $\boldsymbol{b}_I = [b_{u-I}, \ldots, b_{u-1}]$.

When the simplified Gaussian-approximation is employed, the conditional PDFs of Z_u are respectively given in (2.32) for $b_u = 1$ and $b_u = 0$, associated with

$$\begin{aligned}\mu_{Z_1} &= c_0 + \sum_{i=1}^{I} b_{u-i}c_i + \mu_x;\ \ \sigma_{Z_1}^2 = \frac{c_0}{V_R} + \frac{1}{V_R}\sum_{i=1}^{I} b_{u-i}c_i + \sigma_x^2\\ \mu_{Z_0} &= \sum_{i=1}^{I} b_{u-i}c_i + \mu_x;\ \ \sigma_{Z_0}^2 = \frac{1}{V_R}\sum_{i=1}^{I} b_{u-i}c_i + \sigma_x^2\end{aligned} \tag{2.51}$$

Correspondingly, the BER of the OOK-modulated DMC systems can be derived by following that in Section 2.3.2, which can be expressed as

$$P_b = \frac{1}{2} + \frac{1}{2^{I+1}}\sum_{\boldsymbol{b}_I \in \mathcal{B}^I}\left[Q\left(\frac{C_T - \mu_{Z_0}}{\sigma_{Z_0}}\right) - Q\left(\frac{C_T - \mu_{Z_1}}{\sigma_{Z_1}}\right)\right] \tag{2.52}$$

Finally, when the simplified Gamma-approximation is employed, following the analysis in Section 2.3.2, we can show that the BER of the OOK-modulated DMC systems can be formulated as

$$P_b = \frac{1}{2} + \frac{1}{2^{I+1}}\sum_{\boldsymbol{b}_I \in \mathcal{B}^I}\left[\frac{\gamma\left(m_1, C_T/\Omega_1\right)}{\Gamma(m_1)} - \frac{\gamma\left(m_0, C_T/\Omega_0\right)}{\Gamma(m_0)}\right] \tag{2.53}$$

where $m_1,\ m_0$ and $\Omega_1,\ \Omega_0$ are given in (2.40) with μ_{Z_1}, μ_{Z_0} and $\sigma_{Z_1}^2, \sigma_{Z_0}^2$ given in (2.51).

In comparison to the BER formulas in Sections 2.3.1, 2.3.2 and 2.3.3, which need to consider 2^L terms for the first sum at the RHS of the BER formulas, as seen, e.g., in (2.31), we now only need to compute 2^I terms. In Section 2.5, we will demonstrate the effect of the value of I on the accuracy of evaluated BER, showing that we can choose $I << L$, when L is large. Typically, $I \approx 10$ is sufficient for obtaining near-accurate BER evaluation, provided that the data rate is not too high and, hence, the ISI imposed by any of the other $(L - I)$ data bits is insignificant. Hence, significantly reduced computation is possible, while still achieving sufficiently accurate evaluation.

2.4 BER Analysis of DMC Systems with OOK Modulation and ISI Cancellation

In this section, we analyze the BER of the OOK-modulated DMC systems with the ISIC. Our analysis starts with the decision variable Z_u given by (2.12), and assumes that $\lambda_u = \bar{\lambda}$ is a constant. Furthermore, as in Section 2.3, we assume that the maximum ISI length is L bits, and that $u > L$ is considered. Then, Z_u can be written as

$$\begin{aligned} Z_u = & \underbrace{\sum_{i=0}^{L} b_{u-i} \left[c(iT + \hat{t}_d) + n_{u-i}(uT + \hat{t}_d) \right]}_{Z_{ud}} \\ & \underbrace{- \bar{\lambda} \times \sum_{i=1}^{L} b_{u-i} \left[c(iT) + n_{u-i}(uT) \right]}_{Z_{u0}} \end{aligned} \tag{2.54}$$

Let $c_i = c(iT + \hat{t}_d)$, $n_{(u-i)u} = n_{u-i}(uT + \hat{t}_d)$ and $c'_i = c(iT)$, $n'_{(u-i)u} = n_{u-i}(uT)$. Then, the above equation can be re-written as

$$\begin{aligned} Z_u = & \underbrace{\sum_{i=0}^{L} b_{u-i} c_i + \sum_{i=0}^{L} b_{u-i} n_{(u-i)u}}_{Z_{ud}} \\ & \underbrace{- \bar{\lambda} \times \left[\sum_{i=1}^{L} b_{u-i} c'_i + \sum_{i=1}^{L} b_{u-i} n'_{(u-i)u} \right]}_{Z_{u0}} \end{aligned} \tag{2.55}$$

In order for the analysis to be manageable, we assume that $t_d > \rho^2/D$, so that the two noise samples obtained at $t = uT + \hat{t}_d$ and $t = uT$ are independent [16].

In this section, we derive the BER formulas, when the Poisson approach, simplified Poisson approach, Gaussian-approximation, and simplified Gaussian-approximation are considered. Unfortunately, the PDF for the difference of two Gamma variates distributed with different shaping parameters is unknown in public references, as claimed in [89], the Gamma-approximation approaches will hence not be considered in this section.

2.4.1 Poisson and Simplified Poisson Approaches

Following our analysis in Section 2.3.1, it can be shown that, conditioned on $\boldsymbol{b}_L$ and $b_u = 1$, $Y_{ud} = V_R Z_{ud}$ obeys the Poisson PMF of

$$f_{Y_{ud}}(n|\boldsymbol{b}_L, b_u = 1) = \frac{\mu_{Y_1}^n e^{-\mu_{Y_1}}}{n!}, n = 0, 1, 2, \ldots \tag{2.56}$$

where $\mu_{Y_1} = V_R \left(c_0 + \sum_{i=1}^{L} b_{u-i} c_i \right)$. By contrast, conditioned on $\boldsymbol{b}_L$ and $b_u = 0$, Y_{ud} obeys the Poisson PMF of

$$f_{Y_{ud}}(n|\boldsymbol{b}_L, b_u = 0) = \frac{\mu_{Y_0}^n e^{-\mu_{Y_0}}}{n!}, n = 0, 1, 2, \ldots \tag{2.57}$$

where $\mu_{Y_0} = V_R \sum_{i=1}^{L} b_{u-i} c_i$. As seen in (2.55), Z_{u0} is only dependent on $\boldsymbol{b}_L$ but not on b_u. Hence, the conditional PMF of $Y_{u0} = V_R Z_{u0}$ can be expressed as

$$f_{Y_{u0}}(n|\boldsymbol{b}_L) = \frac{\mu_Y^n e^{-\mu_Y}}{n!}, n = 0, 1, 2, \ldots \tag{2.58}$$

where $\mu_Y = V_R \bar{\lambda} \sum_{i=1}^{L} b_{u-i} c'_i$.

Since the noise samples in Z_{ud} and Z_{u0} are independent, the conditional PMFs of $f_{Y_{ud}}(n|\boldsymbol{b}_L, b_u = 1)$ (or $f_{Y_{ud}}(n|\boldsymbol{b}_L, b_u = 0)$) and $f_{Y_{u0}}(n|\boldsymbol{b}_L)$ are independent. According to the properties of the Poisson distribution, the difference of two independent Poisson distributions obeys the Skellam distribution [90]. Hence, the PMF of $Y_u = V_R Z_u$ conditioned on $(\boldsymbol{b}_L,\ b_u = 1)$ and $(\boldsymbol{b}_L,\ b_u = 0)$ can be expressed as

$$\begin{aligned} f_{Y_u}(k|\boldsymbol{b}_L,\ b_u = 1) &= \exp\left(-[\mu_{Y_1} + \mu_Y]\right) \left(\frac{\mu_{Y_1}}{\mu_Y}\right)^{k/2} \\ &\times I_k\left(2\sqrt{\mu_{Y_1}\mu_Y}\right),\ -\infty < k < \infty \\ f_{Y_u}(k|\boldsymbol{b}_L,\ b_u = 0) &= \exp\left(-[\mu_{Y_0} + \mu_Y]\right) \left(\frac{\mu_{Y_0}}{\mu_Y}\right)^{k/2} \\ &\times I_k\left(2\sqrt{\mu_{Y_0}\mu_Y}\right),\ -\infty < k < \infty \end{aligned} \tag{2.59}$$

respectively. In the above equations, $I_k(z)$ is the modified Bessel function [90].

Having obtained the PMFs of Y_u, as shown in (2.59), then, given a decision threshold C_T in the sense of concentration, the miss-probability can be derived as

$$\begin{aligned} P_M =& \frac{1}{2^L} \sum_{\boldsymbol{b}_L \in \mathcal{B}^L} P(Y_u \le V_R C_T | \boldsymbol{b}_L,\ b_u = 1) \\ =& \frac{1}{2^L} \sum_{\boldsymbol{b}_L \in \mathcal{B}^L} \exp\left(-[\mu_{Y_1} + \mu_Y]\right) \\ & \times \sum_{k=-\infty}^{\lceil V_R C_T \rceil} \left(\frac{\mu_{Y_1}}{\mu_Y}\right)^{k/2} I_k\left(2\sqrt{\mu_{Y_1}\mu_Y}\right) \end{aligned} \tag{2.60}$$

Similarly, for a given decision threshold C_T, the false-alarm probability can be derived as

$$\begin{aligned} P_{FA} =& 1 - \frac{1}{2^L} \sum_{\boldsymbol{b}_L \in \mathcal{B}^L} P(Y_u \le V_R C_T | \boldsymbol{b}_L,\ b_u = 0) \\ =& 1 - \frac{1}{2^L} \sum_{\boldsymbol{b}_L \in \mathcal{B}^L} \exp\left(-[\mu_{Y_0} + \mu_Y]\right) \sum_{k=-\infty}^{\lceil V_R C_T \rceil} \left(\frac{\mu_{Y_0}}{\mu_Y}\right)^{k/2} \\ & \times I_k\left(2\sqrt{\mu_{Y_0}\mu_Y}\right) \end{aligned} \tag{2.61}$$

Finally, the BER of the OOK-modulated DMC with ISIC can be expressed as

$$\begin{aligned} P_b =& \frac{1}{2}(P_M + P_{FA}) \\ =& \frac{1}{2} + \frac{1}{2^{L+1}} \sum_{\boldsymbol{b}_L \in \mathcal{B}^L} \exp(-\mu_Y) \left[\exp\left(-\mu_{Y_1}\right)\right. \\ & \times \sum_{k=-\infty}^{\lceil V_R C_T \rceil} \left(\frac{\mu_{Y_1}}{\mu_Y}\right)^{k/2} I_k\left(2\sqrt{\mu_{Y_1}\mu_Y}\right) \\ & \left. - \exp\left(-\mu_{Y_0}\right) \sum_{k=-\infty}^{\lceil V_R C_T \rceil} \left(\frac{\mu_{Y_0}}{\mu_Y}\right)^{k/2} I_k\left(2\sqrt{\mu_{Y_0}\mu_Y}\right)\right] \end{aligned} \tag{2.62}$$

In the cases that L is large, the BER P_b can be evaluated by the Monte-Carlo approach addressed in Section 2.3.4 or the simplified Poisson approach analyzed in Section 2.3.5. Specifically, when the simplified Poisson approach is desired, the BER has the expression of (2.62) with the following modifications. First, $\boldsymbol{b}_L \in \mathcal{B}^L$ is replaced by $\boldsymbol{b}_I \in \mathcal{B}^I$, where $\boldsymbol{b}_I = [b_{u-I}, \ldots, b_{u-1}]$, when assuming that there are I bits dominating the ISI on the uth bit. Second, μ_{Y_1}, μ_{Y_0} and μ_Y are respectively replaced by the quantities of

$$\begin{aligned} \mu_{Y_1} =& V_R \left(c_0 + \sum_{i=1}^{I} b_{u-i} c_i + \frac{1}{2} \sum_{i=I+1}^{L} c_i\right), \\ \mu_{Y_0} =& V_R \left(\sum_{i=1}^{I} b_{u-i} c_i + \frac{1}{2} \sum_{i=I+1}^{L} c_i\right), \\ \mu_Y =& V_R \bar{\lambda} \left(\sum_{i=1}^{I} b_{u-i} c'_i + \frac{1}{2} \sum_{i=I+1}^{L} c'_i\right) \end{aligned} \tag{2.63}$$

2.4.2 Gaussian-Approximation and Simplified Gaussian-Approximation

According to [91], when both $(\mu_{Y_1} + \mu_Y)$ and $(\mu_{Y_0} + \mu_Y)$ are relatively large, the Skellam PMFs in (2.59) can be approximated by the corresponding Gaussian PDFs. When we directly deal with concentration and have the decision variable given by (2.55), the conditional Gaussian PDFs can be respectively expressed as

$$\begin{aligned} f_{Z_u}(y|\boldsymbol{b}_L, b_u = 1) =& \frac{1}{\sqrt{2\pi}\sigma_{Z_1}} \exp\left(-\frac{[y - \mu_{Z_1}]^2}{2\sigma_{Z_1}^2}\right) \\ f_{Z_u}(y|\boldsymbol{b}_L, b_u = 0) =& \frac{1}{\sqrt{2\pi}\sigma_{Z_0}} \exp\left(-\frac{[y - \mu_{Z_0}]^2}{2\sigma_{Z_0}^2}\right) \end{aligned} \tag{2.64}$$

where $-\infty < y < \infty$, by definition,

$$\begin{aligned}
\mu_{Z_1} =& \frac{1}{V_R}\left(\mu_{Y_1} - \mu_Y\right) = c_0 + \sum_{i=1}^{L} b_{u-i}(c_i - \bar{\lambda}c_i'), \\
\sigma_{Z_1}^2 =& \frac{1}{V_R^2}\left(\mu_{Y_1} + \mu_Y\right) = \frac{1}{V_R}\left[c_0 + \sum_{i=1}^{L} b_{u-i}(c_i + \bar{\lambda}c_i')\right], \\
\mu_{Z_0} =& \frac{1}{V_R}\left(\mu_{Y_0} - \mu_Y\right) = \sum_{i=1}^{L} b_{u-i}(c_i - \bar{\lambda}c_i'), \\
\sigma_{Z_0}^2 =& \frac{1}{V_R^2}\left(\mu_{Y_0} + \mu_Y\right) = \frac{1}{V_R}\left[\sum_{i=1}^{L} b_{u-i}(c_i + \bar{\lambda}c_i')\right]
\end{aligned} \tag{2.65}$$

As seen from the above equations, when the ISI is ideally cancelled, we have $V_R\mu_{Z_1} = V_R c_0$, which represents the average number of molecules in the detection space, and $V_R\mu_{Z_0} = 0$. Hence, for the Skellam distribution to be approximated by the Gaussian distribution, it requires that $V_R\mu_{Z_1}$ is sufficiently large.

Explicitly, the PDFs in (2.64) have the same forms as those in (2.32) in Section 2.3.2. Hence, when given the decision threshold of C_T, the BER of the OOK-modulated DMC systems with ISIC has the same expression as that in Section 2.3.2, with μ_{Z_0}, σ_{Z_0} and μ_{Z_1}, σ_{Z_1} replaced by the corresponding terms given in (2.65).

Furthermore, when the simplified Gaussian-approximation is employed, the BER of the OOK-modulated DMC systems with ISIC can be expressed as (2.52), with μ_{Z_0}, σ_{Z_0} and μ_{Z_1}, σ_{Z_1} provided by the formulas of

$$\begin{aligned}
\mu_{Z_1} =& c_0 + \sum_{i=1}^{I} b_{u-i}(c_i - \bar{\lambda}c_i') + \frac{1}{2}\sum_{i=I+1}^{L}(c_i - \bar{\lambda}c_i'), \\
\sigma_{Z_1}^2 =& \frac{1}{V_R}\left[c_0 + \sum_{i=1}^{I} b_{u-i}(c_i + \bar{\lambda}c_i') + \frac{1}{2}\sum_{i=I+1}^{L}(c_i + \bar{\lambda}c_i')\right], \\
\mu_{Z_0} =& \sum_{i=1}^{I} b_{u-i}(c_i - \bar{\lambda}c_i') + \frac{1}{2}\sum_{i=I+1}^{L}(c_i - \bar{\lambda}c_i'), \\
\sigma_{Z_0}^2 =& \frac{1}{V_R}\left[\sum_{i=1}^{I} b_{u-i}(c_i + \bar{\lambda}c_i') + \frac{1}{2}\sum_{i=I+1}^{L}(c_i + \bar{\lambda}c_i')\right]
\end{aligned} \tag{2.66}$$

As seen at the RHS of the above equations, these quantities are dependent on $\boldsymbol{b}_I$ containing only I data bits.

2.5 Performance Results

In this section, we demonstrate the BER performance of the OOK-modulated DMC systems with or without ISIC, and compare the results obtained by the various analytical approaches considered in Sections 2.3 and 2.4. Furthermore, some results obtained from both the particle-based simulations and the Monte-Carlo simulations [92–94] are provided to validate the analytical results.

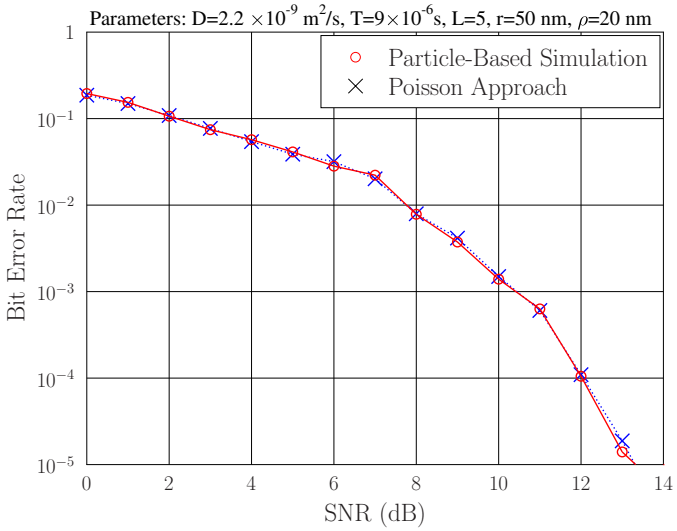

Figure 2.3: Comparison of the BER versus SNR performance of the OOK-modulated DMC systems obtained by the particle-based simulations and Poisson approach.

In order to demonstrate the results, we define the SNR by following the convention in the traditional wireless communications [80] as the ratio between the power received from a single impulse of molecules and the noise power, which is expressed as

$$\gamma_b = \frac{c_0^2}{E[\sigma_0^2]} = \frac{c_0^2}{c_0/V_R} = V_R c_0 \tag{2.67}$$

From this definition and the analysis in Section 2.2, we can know that, given the diffusion coefficient D and the transmission distance r, the SNR is only dependent on the number of molecules Q emitted by one pulse and the volume V_R of the detection space. In our studies, we set $D = 2.2 \times 10^{-9}\ m^2/s$ (squared meter/seconds). For Fig. 2.3 considering the particle-based simulations, we assume relatively short communications distance and set the radius of the spherical detection space to $\rho = 20\ nm$ (nano meter), as the result that particle-based simulation is difficult to cope with a big number of molecules. By contrast, for all the other figures, we consider relatively long communications distance, and set the radius of the spherical detection space to $\rho = 1\ nm$. Furthermore, in our studies, the ISI length L is estimated as

$$L \triangleq \arg_l \{c_l/c_0 \leq 0.1\%\} \tag{2.68}$$

meaning that the ISI from the received pulses having their peak concentration at least 1000 times lower than that of the current pulse is ignored.

Additionally, we note that, for convenience, the parameters used for generating the results are specified with the figures. Furthermore, unless notified, such as in Figs. 2.9 and 2.10, the results are obtained, when the optimum detection thresholds are applied.

First, in Figs. 2.3 and 2.4, we compare the BER versus SNR performance obtained from the analytical and simulation approaches. Specifically, in Fig.2.3, the analytical results were obtained

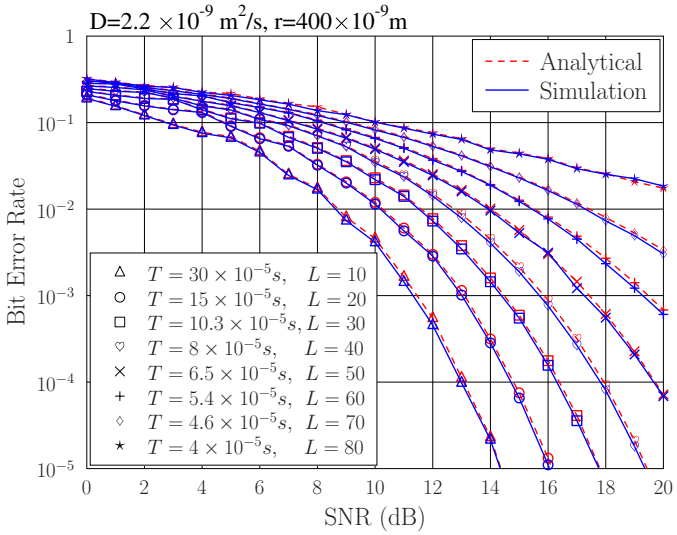

Figure 2.4: Comparison of the BER versus SNR performance of the OOK-modulated DMC systems obtained by the Monte-Carlo simulations and the Poisson or Poisson (Monte-Carlo) approach.

from the Poisson approach of Section 2.3.1, which are compared with the corresponding results obtained from the particle-based simulations. By contrast, in Fig. 2.4, we demonstrate the BER versus SNR performance of the OOK-modulated DMC systems, when the systems are operated with different data rates reflected by the different bit-durations of T. Correspondingly, the length of ISI in different cases is different, as shown in the figure. In the figure, the analytical results were obtained from the Poisson approach of Section 2.3.1 for the cases of $L = 10$ and $L = 20$, while obtained from the Poisson Monte-Carlo approach of Section 2.3.4 for the other cases of $L = 30 - 80$. Note that here the Poisson Monte-Carlo approach was used because, when $L \geq 30$, it is very time-consuming to compute the results by the Poisson approach of Section 2.3.1. The simulation results shown in Fig. 2.4 were obtained from the Monte-Carlo simulations. From the results of Figs. 2.3 and 2.4 we may have the following observations. First, the analytical results agree closely with the simulation results obtained from either the particle-based or the Monte-Carlo simulations. Therefore, the Poisson modelling considered in this chapter is accurate and that the Poisson and Poisson Monte-Carlo approaches are valid. Second, as shown in Fig. 2.4, when the symbol duration decreases, i.e., the data rate increases, the BER performance of the DMC systems degrades due to the increased ISI.

In Fig. 2.5, we show the impact of the parameter I used in the simplified Poisson (Gaussian, and Gamma) approach on the accuracy of the estimated BER performance of the DMC systems, when the OOK modulation without ISIC (Fig. 2.5(a)) and that with ISIC (Fig. 2.5(b)) are employed. Note that, here we consider only the simplified Poisson approach, as our results showed that the simplified Gaussian and Gamma approaches appear the same behavior as the simplified Poisson approach. From the results of Fig. 2.5, we observe that, for both the cases of without/with ISIC, the

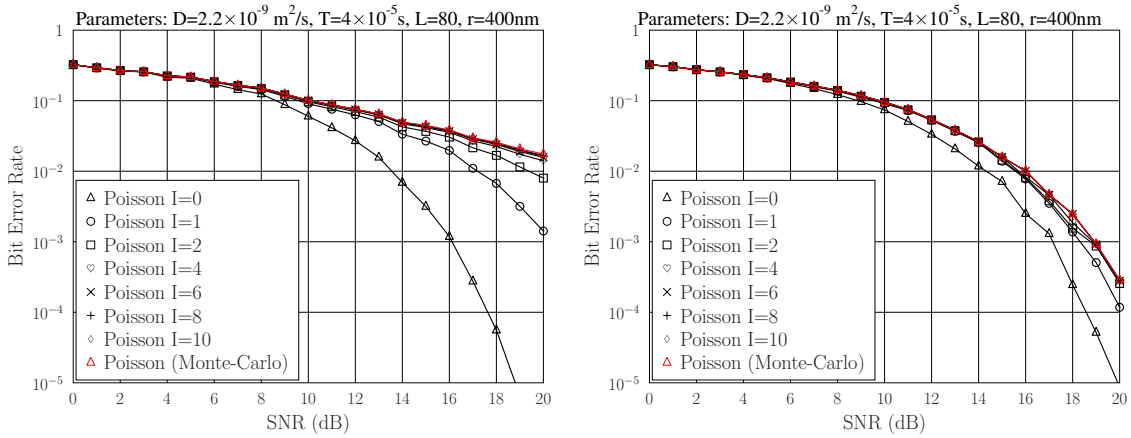

(a) OOK Modulation

(b) OOK modulation with ISIC

Figure 2.5: Impact of parameter I on the accuracy of the BER versus SNR performance of the DMC systems estimated by the simplified Poisson approach.

BER performance evaluated by the simplified approach converges to that obtained by the Monte-Carlo approach, provided that $I \geq 6$ in Fig. 2.5(a) and $I \geq 2$ in Fig. 2.5(b). This observation implies that, when L is relatively large, e.g., $L > 20$, those less dominate ISI can be effectively approximated by a random variable without depending on the specific bit sequence. Hence, the simplified approaches can be efficiently employed for evaluating the error performance of the DMC systems. We should note that in Figs. 2.5(a) and 2.5(b), the Monte-Carlo Poisson approach was used instead of the exact Poisson approach, because it is impossible to evaluate the BER by the exact Poisson approach in the case of $L = 80$, which corresponds to 2^{80} combinations of bit sequences.

When comparing the results (red-colored lines) in Figs. 2.5(a) and 2.5(b), we can observe that the ISIC is capable of providing some performance gain, as shown also by the forthcoming results.

Fig. 2.6 shows the BER performance of the DMC systems without ISIC (top three curves) and that with ISIC (bottom two curves) against the transmission distance, where the results were evaluated by the different approaches as specified in the figure. Explicitly, both the Gaussian- and Gamma-approximation are accurate, which give nearly the same performance results as the exact Poisson approach. As shown in Fig. 2.6, the performance gain provided by the ISIC becomes higher, as the transmission distance increases. The reason behind is that, given the symbol duration T, the ISI increases as the result that the increase of transmission distance results in the expansion of the received pulse, as seen in Fig. 2.1. There is no performance gain available by applying the ISIC, when the transmission distance is below 300nm. In fact, when the transmission distance is short, e.g., 200nm, the ISIC generates negative performance gain. This is because ISIC amplifies noise, as seen in (2.9), due to the randomness of the noise samples.

In Fig. 2.7, we demonstrate the BER versus SNR performance of the DMC systems without/with ISIC, estimated by the different approaches. Notice in the figures that the sets of curves

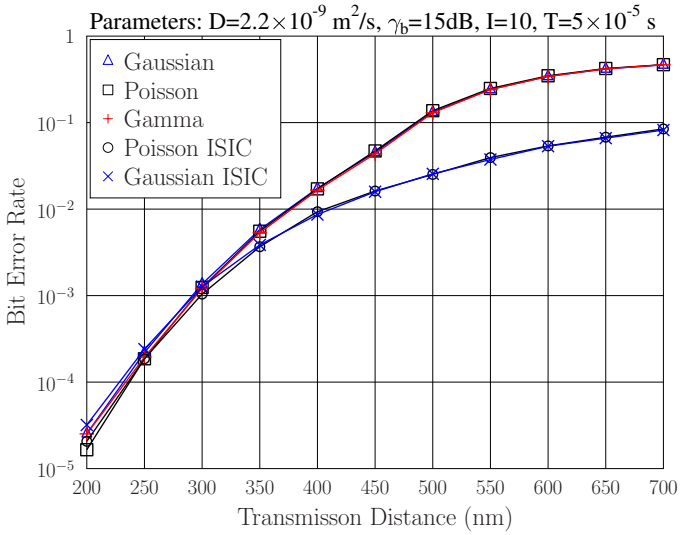

Figure 2.6: Comparison of different approaches for the BER versus transmission distance of the DMC systems with OOK modulation and without/with ISIC.

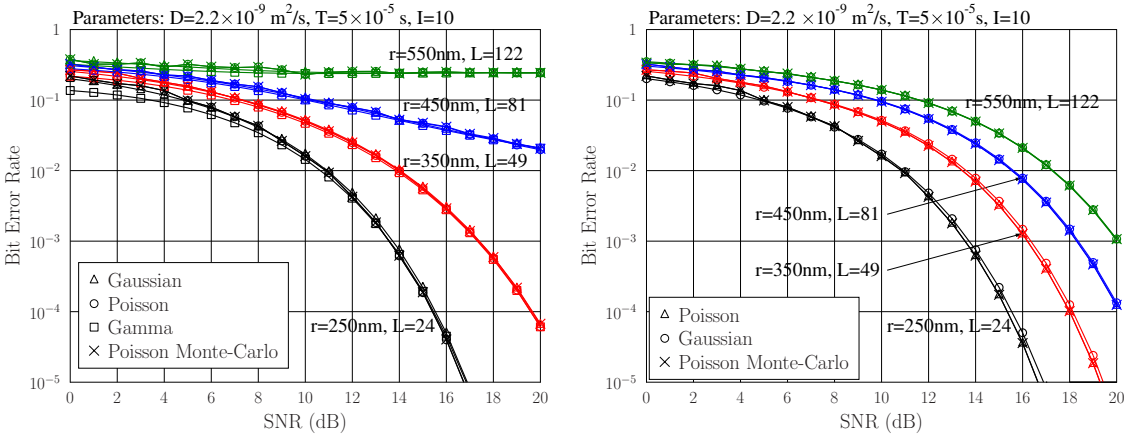

(a) OOK Modulation

(b) OOK modulation with ISIC

Figure 2.7: Comparison of different approaches for the BER versus SNR performance of the DMC systems without/with ISIC.

are distinguished by the transmission distances r and their corresponding ISI length. When comparing the two figures, we can see that the employment of ISIC results in more reliable detection. More performance gain is available, as the transmission distance increases, which follows the observation in Fig. 2.6. In both figures, the BER performance degrades with the increase of transmission distance. Furthermore, all the optional approaches provide near-exact results. However, in the case of without ISIC, when the transmission distance is short, e.g., 250 nm, the BER evaluated by the Gamma-approximation yields marginal difference from the exact one. This is more declared, when the SNR becomes lower. In the case of Fig. 2.7(b) with ISIC, when the transmission distance is relatively short, e.g., 250 nm, the result evaluated by the Gaussian-approximation has a slight

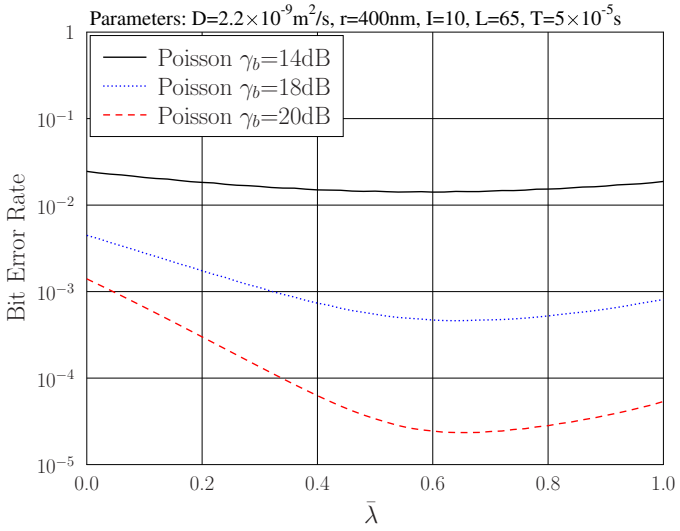

Figure 2.8: BER versus ISIC scaling factor $\bar{\lambda}$ of the OOK-modulated DMC systems with ISIC.

difference from the exact one.

In Fig. 2.8, we show the effect of the ISIC scaling factor $\bar{\lambda}$ on the BER performance of the DMC systems with ISIC. Explicitly, given the other system parameters, there is an optimum value for $\bar{\lambda}$, which results in the lowest BER. As seen in Fig. 2.8, the optimum $\bar{\lambda}$ value is depended on the SNR and is around 0.6 for the cases considered. From these results we are inferred that a good $\bar{\lambda}$ value is around 0.6 for the SNR practically interest, which results in the BER between 10^{-5} and 10^{-2}. Furthermore, the achievable BER performance is not very sensitive to the value of $\bar{\lambda}$, and nearly the same BER performance can be attained, provided that $\bar{\lambda}$ changes within a limited range around the optimum value.

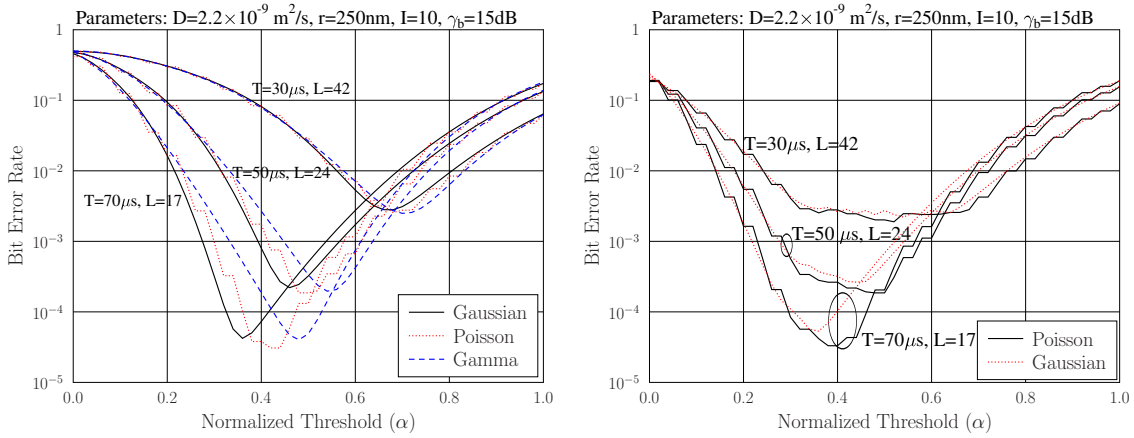

(a) OOK Modulation

(b) OOK modulation with ISIC

Figure 2.9: Comparison of different approaches for the BER versus detection threshold performance of the DMC systems without/with ISIC.

Fig. 2.9 depicts the BER of the DMC systems versus the detection threshold, when ISIC is not employed (Fig. 2.9(a)) or employed (Fig. 2.9(b)). As shown in the figures, three symbol durations are considered, which are $T = 30\mu$s, 50μs and 70μs, which for a given transmission distance of 250nm yields ISI length of $L = 42$, 24 and 17, respectively. Furthermore, in the two figures, we compare the BER evaluated by the different approaches, as marked in the figures. From the results, we may have the following observations. First, for given system parameters, there is an optimum threshold, which yields the lowest BER. Second, for the OOK-modulated DMC systems without ISIC, the BER performance is highly sensitive to the threshold. A threshold slightly different from the optimum one might result in a significant increase of BER. Third, when the OOK-modulated DMC systems employ the proposed ISIC, the BER performance becomes less sensitive to the detection threshold. Forth, for the DMC systems without ISIC (Fig. 2.9(a)), when the optimum thresholds are invoked, both the Gaussian- and Gamma-approximation provide near-accurate approximation to the Poisson approach. By contrast, for the DMC systems with ISIC (Fig. 2.9(b)), even when operated at the optimum thresholds, the Gaussian-approximation yields a BER higher than that given by the Poisson approach, which is clearly seen in the cases of $T = 50\mu$s and 70μs. The reason is that, in this case, the ISI is relatively short, resulting in that the condition for applying the Gaussian approximation is not well satisfied. Additionally, as seen in both the figures, the 'optimum threshold' given by the Gaussian or Gamma approach is actually optimum. There is an explicit difference from the optimum threshold given by the Poisson approach.

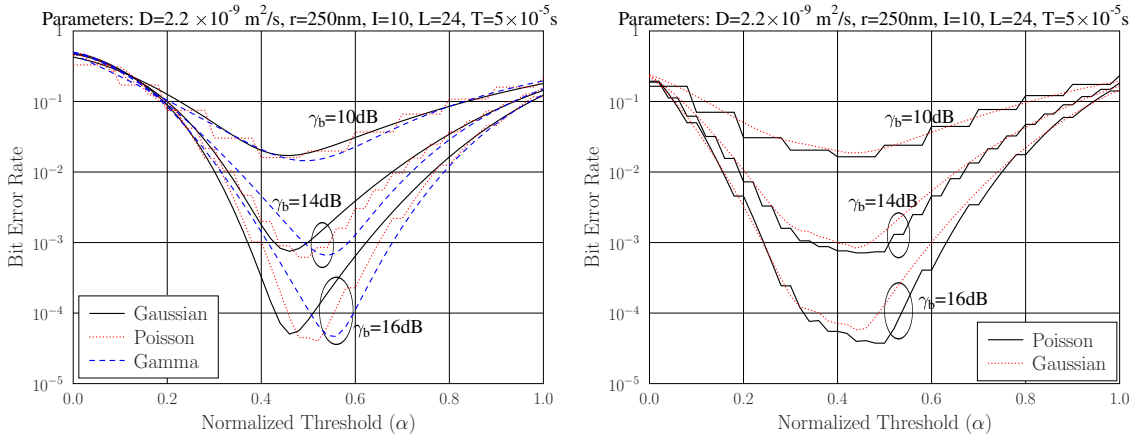

(a) OOK Modulation

(b) OOK modulation with ISIC

Figure 2.10: Comparison of different approaches for the BER versus detection threshold performance of the DMC systems without/with ISIC.

Finally, in Fig. 2.10, we depict the BER versus detection threshold performance of the DMC systems with respect to $\gamma_b = 10$dB, 14dB and 16dB, when without ISIC (Fig. 2.10(a)) or with ISIC (Fig. 2.10(b)). Explicitly, we have similar observations as those from Fig. 2.9(a) and Fig. 2.9(b). It is worthy of noting again that the BER performance of the OOK-modulated DMC systems without ISIC is very sensitive to the detection threshold applied, and employing ISIC mitigates this

sensitivity.

2.6 Conclusions

We have proposed a range of approaches for analyzing and computing the BER of the DMC systems without or with ISIC, based on which exact and approximate BER expressions have respectively been derived. Our studies and comparison show that both the Gaussian- and Gamma-approximation are capable of providing near-accurate BER estimation, provided that the respective optimum thresholds are applied in detection. However, the optimum detection threshold estimated by the Gaussian- or Gamma-approximation is explicitly different from that given by the Poisson modeling, and hence it is practically not optimum. The BER performance of the OOK-modulated DMC systems without ISIC is very sensitive to the change of detection threshold, whereas, the ISIC is able to mitigate the sensitivity to the variation of detection threshold. Furthermore, the employment of ISIC is able to improve the BER performance of the OOK-modulated DMC systems, especially in the scenarios where transmission distance is relatively long or/and transmission rate is high, both resulting in long ISI. However, ISIC amplifies the counting noise, which may result in performance degradation in the case of short ISI. We have shown that, when ISI is long, the Monte-Carlo approach or the different types of simplified approaches may be employed for evaluating the BER of the DMC systems without or with ISIC. The studies and performance results show that all these approaches are effective approaches, and are capable of providing near-accurate BER estimation.

Chapter 3

Performance of Binary Molecular Shift Keying Modulated Diffusive Molecular Communication Systems without/with Inter-Symbol Interference Compression

In this chapter, we analyze and investigate the bit error rate (BER) performance of the diffusive molecular communication (DMC) systems employing binary molecular shift keying (BMoSK) modulation. The DMC systems both without and with inter-symbol interference compression (ISIC) are considered. Specifically, by modelling the number of molecules of one type presenting in a 3-dimensional (3D) detection space as a Poisson, or Gaussian distributed random variable, we derive the BER expressions of the BMoSK-modulated DMC systems without/with ISIC. However, the strong inter-symbol interference (ISI) presenting in DMC systems makes the computation of the above-mentioned BER formulas highly involved or even impossible. Therefore, we introduce some simplified approaches, namely the Monte-Carlo and the simplified Poisson (or simplified Gaussian) approaches, to reduce the computation complexity in the cases of long ISI. Furthermore, based on the statistics of decision variables, we analyze the effect of decision threshold on the BER performance. Finally, the BER performance of the BMoSK-modulated DMC systems without/with ISIC is investigated with considering the impact from different aspects, while the different analytical approaches are compared in terms of the accuracy of the BER evaluated based on these approaches.

3.1 Introduction

Molecular communication (MC) has become one of the most promising approaches for communication between nano-machines, which conveys information between nano-machines via molecules [6, 68]. Among the different MC techniques, diffusive molecular communications (DMC) is one of the most promising approaches for implementation in practice, owing to its merit that no external energy is required for information propagation [7, 66]. Built on non-toxic materials, DMC has been recognized to be the naturally fitting methods for supporting communication inside living bodies and other biological environments, including the applications in biomedical engineering, industrial and consumer goods, military, environmental control, etc. [5, 68, 95–106].

In literature, a lot of research has been carried out in the context of DMC. As some examples, when assuming that transmitter, receiver or both employ channel knowledge, the capacity of different DMC channels has been investigated [51, 70, 107–109]. In terms of signalling, DMC may make use of molecular concentration to form concentration shift keying (CSK) [21, 36, 38, 40, 70, 110], of molecular pulse positions to yield pulse position modulation (PPM) [42], and of molecular types to allow molecular shift keying (MoSK) [39, 40, 72], which constitute the three basic modulation schemes for information transmission in DMC. In addition, these basic modulation schemes may be combined to design hybrid modulation schemes. Specifically, based on CSK and MoSK, molecular concentration shift keying (MCSK) modulation [46] can use both molecular types and their concentration levels to encode information. In the depleted MoSK (D-MoSK) [47], different information bits of a symbol are mapped to different types of molecules, which are then encoded to different concentration levels. By contrast, in [73], the authors have proposed a hybrid molecular modulation scheme by combining MoSK with PPM. Concerning the signal detection in DMC, in addition to the fundamental detectors, which usually make no effort to mitigate ISI, for the above-mentioned basic modulation schemes, some more advanced detection schemes have also been proposed and investigated. These include the sequence detectors in the principles of maximum *a-posteriori* (MAP) and maximum likelihood (ML) [20, 22, 30, 74, 75], linear minimum mean-square error (MMSE) detector [22], decision-feedback detectors [22, 76], etc. The main motivation of these advanced detectors is to mitigate the effect of severe inter-symbol interference (ISI) existing in DMC systems. Moreover, some advanced issues have recently been investigated in the context of DMC and the networking based on DMC. These include error-control coding [111, 112], multiple-input multiple-output (MIMO), relay and multi-hop communications [51, 78], adaptive rate transmission [113], multiple access [56, 61], and even security and privacy [114], Internet of molecular things [115], neuroscience application [98–102], etc.

This chapter focuses on analyzing the bit error rate (BER) of the DMC systems with binary MoSK (BMoSK) modulation. In literature, the error rate of DMC systems with different signalling and detection schemes has been analyzed in a range of references. Specifically, considering binary CSK, MoSK or MCSK modulation, the error performance of DMC systems with Poisson modeling

has been addressed in [46], when assuming that a bit being detected is affected only by one bit previously transmitted. Assuming that both ISI and counting noise can be approximated as Gaussian noise, the false-alarm probability, detection probability, as well as error probabilities of the DMC systems with binary and M-ary CSK modulations have been analyzed in [21, 62]. Again, with the Gaussian modelling of counting noise and ISI, some closed-form expressions have been derived in [63] for the error rate of the DMC systems with pulse-based modulation, and supported by energy or amplitude detection. In [64], the authors have derive the error probability and capacity of the DMC systems relying on M-ary amplitude modulation. By contrast, with the aid of the binomial modelling of the molecules hitting receiver, [65, 116] have analyzed the capacity and error rate of the DMC systems with CSK and MoSK modulations. Very recently, the error rate of the DMC systems with binary CSK (or on-off keying (OOK)) modulation has been addressed in [110], where different approaches are introduced for deriving the BER expressions of the DMC systems with/without ISI compression (ISIC).

Following [110], in this chapter, we provide some approaches for analysing and evaluating the BER performance of the BMoSK-modulated DMC systems with or without ISIC. In comparison with the OOK modulation considered in [110], where only one type of molecules is used, there are two types of molecules when BMoSK is employed. Correspondingly, the detection of BMoSK-modulated information has to handle the difference between two types of molecules, which demands new tools for BER analysis. For this purpose, we model the number of molecules of one type presenting in a detection space as a Poisson (or Gaussian) distributed random variable. Then, the distribution of the difference between two Poisson (or Gaussian) distributed random variables is derived, and based on which we derive the BER expressions. Moreover, due to the fact that DMC usually experiences strong ISI, which makes the formulas derived as above-mention very hard, and sometimes even impossible, to evaluate. Therefore, we introduce some approximation approaches to reduce the computation. Specifically, as done in [110], we introduce the Monte-Carlo and simplified Poisson (or Gaussian) approaches for BER evaluation. Our studies show that, when appropriately set, these approaches are usually efficient to obtain accurate BER estimation.

The other parts of the chapter is structured as follows. Section 3.2 considers the modelling of DMC systems, and the principles of BMoSK-modulated DMC. In Section 3.3, we analyze the BER of the BMoSK-modulated DMC without ISIC, while in Section 3.4 we analyze the BER of the BMoSK-modulated DMC with ISIC. Section 3.5 demonstrates performance results associated with discussion. Finally, in 3.6, we summaries the main observations from research.

3.2 System Model and Assumptions

We consider a DMC system consisting of a transmitter, a molecular propagation channel and a receiver. At the transmitter side, information is released via molecular pulses. After propagated over a molecular diffusion channel, information is recovered at receiver according to the molec-

ular concentration that varies following the molecular pulses released by transmitter. Following references, such as [38, 110], in this chapter, we assume a point transmitter, a 3-dimensional (3D) spherical receiver having a radius of ρ, and that the transmission and receiving processes are independent. Then, when an impulse of Q molecules is released at $t = 0$, according to Fick's law of diffusion [38], the molecular concentration observed by receiver can be expressed as

$$c(t) = \frac{Q}{(4\pi Dt)^{\frac{3}{2}}} \exp\left(-\frac{r^2}{4Dt}\right), t > 0, \tag{3.1}$$

where r is the distance between transmitter and receiver, t is the observation time, while D is the diffusion coefficient of molecular medium.

As demonstrated in [38, 110], $c(t)$ is a time-domain pulse function, whose shape is dependent on the distance r between transmitter and receiver. The concentration expected at receiver is time-variant, which reaches maximum at the time of $t_d = r^2/(6D)$ [38, 110]. Substituting this value into (3.1), the maximum value of $c(t)$ for a given r is

$$c_{\max} = \left(\frac{3}{2\pi e}\right)^{\frac{3}{2}} \frac{Q}{r^3}, \; r \geq 0, \tag{3.2}$$

which reduces with r^3. Hence, DMC is usually only suitable for communication over very short distance.

3.2.1 DMCs Employing BMoSK Modulation

Let $\{b_j\} = \{b_0, b_1, \ldots, b_j, \ldots\}$ be a binary data sequence, where $b_j \in \{0, 1\}$. Then, with BMoSK, the transmitter sends an impulse of Type-A molecules for sending $b_j = 1$, while sends an impulse of Type-B molecules for sending $b_j = 0$. At the receiver, at time t, $uT \leq t < (u+1)T$, the difference between the concentrations of Type-A and Type-B molecules is

$$\begin{aligned} z(t) =& z_A(t) - z_B(t) \\ =& \sum_{j=0}^{u} b_j [c_A(t - jT) + n_{A,j}(t)] \\ & - \sum_{j=0}^{u} (1 - b_j)[c_B(t - jT) + n_{B,j}(t)], \end{aligned} \tag{3.3}$$

where $z_A(t)$ and $z_B(t)$ represent the concentation of Type-A and Type-B molecules, respectively, observed by the receiver at time t, T is the bit duration, and $u = [t/T]$ is an integer, and $(u+1)$ is the number of bits transmitted during $[0, t)$. Note that, bit duration T and information rate R is related by the relationship of $R = 1/T$, where R has the unit of bits per second (bps). In (3.3), $c_A(t)$ and $c_B(t)$ are respectively the concentration of Type-A and Type-B molecules, taking the form of (3.1), $n_{A,j}(t)$ and $n_{B,j}(t)$ are the noise, referred to as particle counting noise, generated, respectively, by the Type-A and Type-B molecules diffused in the channel.

By inspecting the shape of $c(t)$, we can know that, given an impulse of molecules transmitted at $t = 0$, the receiver is desired to sample at $t = t_d$ to obtain the maximum molecular concentration. Hence, for detecting the u-th bit, we assume that an observation for the molecule concentration is obtained via sampling at $t = uT + \hat{t}_d$, where $\hat{t}_d$ represents the estimate to t_d, yielding the decision variable

$$\begin{aligned} Z_u =& z_A(t = uT + \hat{t}_d) - z_B(t = uT + \hat{t}_d) \\ =& \sum_{j=0}^{u} b_j \left[c_A([u-j]T + \hat{t}_d) + n_{A,j}(uT + \hat{t}_d)\right] \\ &- \sum_{j=0}^{u} (1 - b_j) \left[c_B([u-j]T + \hat{t}_d) + n_{B,j}(uT + \hat{t}_d)\right], \\ & u = 0, 1, \ldots \end{aligned} \tag{3.4}$$

To simplify the above representation, let us define $c_{x,u-j} = c_x([u-j]T + \hat{t}_d)$ and $n_{x,ju} = n_{x,j}(uT + \hat{t}_d)$. Then, we have

$$\begin{aligned} Z_u =& \sum_{j=0}^{u} b_j \left[c_{A,u-j} + n_{A,ju}\right] \\ &- \sum_{j=0}^{u} (1 - b_j) \left[c_{B,u-j} + n_{B,ju}\right], \quad u = 0, 1, \ldots, \end{aligned} \tag{3.5}$$

which explicitly shows that the u-th bit experiences ISI. Assume that LT is the length of ISI, which in our experiments is determined by a value relative to the peak of $c(t)$, as seen in Section 3.5. Then, using the transform of $i = u - j$, we can express Z_u as

$$\begin{aligned} Z_u =& \sum_{j=\max\{0,u-L\}}^{u} b_j \left[c_{A,u-j} + n_{A,ju}\right] \\ &- \sum_{j=\max\{0,u-L\}}^{u} (1 - b_j) \left[c_{B,u-j} + n_{B,ju}\right] \\ =& \sum_{i=0}^{\min\{L,u\}} b_{u-i} \left[c_{A,i} + n_{A,(u-i)u}\right] \\ &- \sum_{i=0}^{\min\{L,u\}} (1 - b_{u-i}) \left[c_{B,i} + n_{B,(u-i)u}\right], \\ & u = 0, 1, \ldots. \end{aligned} \tag{3.6}$$

Moreover, for clarity of forthcoming description, we write (3.6) as

$$\begin{aligned} Z_u =& \underbrace{\sum_{i=0}^{\min\{L,u\}} b_{u-i} c_{A,i} + n_{A,u}}_{Z_{uA}} \\ &- \underbrace{\sum_{i=0}^{\min\{L,u\}} (1 - b_{u-i})\, c_{B,i} + n_{B,u}}_{Z_{uB}}, \quad u = 0, 1, \ldots, \end{aligned} \tag{3.7}$$

where $n_{A,u} = \sum_{i=0}^{\min\{L,u\}} b_{u-i} n_{A,(u-i)u}$ and $n_{B,u} = \sum_{i=0}^{\min\{L,u\}} (1-b_{u-i})\, n_{B,(u-i)u}$.

Let $V_R = \frac{4}{3}\pi\rho^3$ be the volume of the 3D spherical detection space. According to [16], $Y_{uA} = V_R Z_{uA}$ and $Y_{uB} = V_R Z_{uB}$, which are the numbers of Type-A and Type-B molecules presenting in the detection space, can be closely modelled as the Poisson distributed random variables, with the mean and variance for Type-A given by $\mu_A = V_R \sum_{i=0}^{\min\{L,u\}} b_{u-i} c_{A,i}$, and for Type-B given as $\mu_B = V_R \sum_{i=0}^{\min\{L,u\}} (1-b_{u-i}) c_{B,i}$ [110]. The difference between two independent Poisson distributions Y_{uA} and Y_{uB} obeys the Skellam distribution [90]. Let $Y_u = V_R Z_u$. Then, the PMF of Y_u can be expressed as

$$f_{Y_u}(k|\boldsymbol{b}_L) = \exp\left(-[\mu_{Y_A} + \mu_{Y_B}]\right) \left(\frac{\mu_{Y_A}}{\mu_{Y_B}}\right)^{k/2} I_k\left(2\sqrt{\mu_{Y_A}\mu_{Y_B}}\right), \quad -\infty < k < \infty, \tag{3.8}$$

where $I_k(z)$ is the modified Bessel function [90].

Moreover, when μ_{Y_A} and μ_{Y_B} are sufficiently large, making the Gaussian approximation applicable, Z_u in (3.7) can be approximated to obey the Gaussian distribution with the probability density function (PDF) [74]

$$Z_u \sim \mathcal{N}(\mu_Z, \sigma_Z^2), \tag{3.9}$$

where

$$\begin{aligned} \mu_Z &= \sum_{i=0}^{\min\{L,u\}} \left[b_{u-i} c_{A,i} - (1-b_{u-i})\, c_{B,i}\right], \\ \sigma_Z^2 &= \frac{1}{V_R} \sum_{i=0}^{\min\{L,u\}} \left[b_{u-i} c_{A,i} + (1-b_{u-i})\, c_{B,i}\right], \end{aligned} \tag{3.10}$$

Finally, the decision for the u-th bit is made according to the rule of

$$\hat{b}_u = \begin{cases} 1, & \text{if } Y_u > 0, \text{ or } Z_u > 0 \\ 0, & \text{if } Y_u \leq 0, \text{ or } Z_u \leq 0 \end{cases} \tag{3.11}$$

Note that, in the conventionally BMoSK type of communication schemes such as the binary orthogonal modulation, the decision rule is given by [80]

$$\hat{b}_u = \begin{cases} 1, & \text{if } Z_{uA} > Z_{uB} \\ 0, & \text{if } Z_{uB} \geq Z_{uA} \end{cases} \tag{3.12}$$

where Z_{uA} and Z_{uB} are given in (3.6). It is noteworthy that the decision rule of (3.11) is equivalent to that of (3.12). This is because $Z_{uA} \geq 0$ and $Z_{uB} \geq 0$. Hence, whenever $Z_{uA} > Z_{uB}$ is satisfied in (3.12), we have $Z_u = Z_{uA} - Z_{uB} > 0$ in (3.11). Otherwise, if $Z_{uA} \leq Z_{uB}$ in (3.12), we certainly have $Z_u = Z_{uA} - Z_{uB} \leq 0$ in (3.11). Therefore, there is no difference between the decision rule of (3.11) and that of (3.12).

As seen, e.g., in (3.6), the BMoSK-modulated DMC experiences ISI, which can be very strong, if data rate is high. In the next subsection, we introduce an approach for the ISI mitigation.

3.2.2 Mitigation of Inter-Symbol Interference

In [77], we have introduced an ISIC scheme, whose performance is further studied in [110] in the context of a DMC system with OOK modulation. Below we extend this ISIC scheme to the BMoSK-modulated DMC systems. Following [77, 110] with ISIC being considered, we form the decision variable for the u-th bit as

$$\begin{aligned} Z_u =& \underbrace{\left[z_A(t = uT + \hat{t}_d) - z_A(t = uT)\right]}_{Z'_{u,A}} \\ & - \underbrace{\left[z_B(t = uT + \hat{t}_d) - z_B(t = uT)\right]}_{Z'_{u,B}} \\ =& \Bigg\{ \sum_{j=0}^{u} b_j \left[c_A([u-j]T + \hat{t}_d) + n_{A,j}(uT + \hat{t}_d)\right] \\ & - \sum_{j=0}^{u} b_j \left[c_A([u-j]T) + n_{A,j}(uT)\right] \Bigg\} \\ & - \Bigg\{ \sum_{j=0}^{u} (1-b_j) \left[c_B([u-j]T + \hat{t}_d) + n_{B,j}(uT + \hat{t}_d)\right] \\ & - \sum_{j=0}^{u} (1-b_j) \left[c_B([u-j]T) + n_{B,j}(uT)\right] \Bigg\}, \\ & u = 0, 1, \ldots. \end{aligned} \tag{3.13}$$

From the above equations we can know that $z_X(t = uT)$ consists of only the remaining molecules of type-A or type-B from previous bits. Hence, this observation can be used as the estimate to the ISI imposing on the u-th bit having the observation obtained at time $uT + \hat{t}_d$. Therefore, by subtracting $z_X(t = uT)$ from $z_X(t = uT + \hat{t}_d)$, some ISI can be cancelled.

From the function of $c(t)$ we can be inferred that, when the transmission rate $1/T$ is relatively low, the ISI at $t = uT$ may be very similar to that at $t = uT + \hat{t}_d$. In this case, most of the ISI can be eliminated by the ISIC of (3.13). However, in the case of high transmission rate, the ISI estimated at $t = uT$ may be very different from that at $t = uT + \hat{t}_d$. This may result in over cancelling and noise amplification. In order to mitigate these problems, we modify the ISIC of (3.13) to the form of [110]

$$\begin{aligned} Z_u =& \Big\{ z_A(t = uT + \hat{t}_d) - \lambda_u z_A(t = uT) \Big\} \\ & - \Big\{ z_B(t = uT + \hat{t}_d) - \lambda_u z_B(t = uT) \Big\}, \end{aligned} \tag{3.14}$$

where a scaling parameter λ_u, $0 \leq \lambda_u \leq 1$, is introduced. Then, following (3.13), (3.14) can be

expressed as

$$\begin{aligned} Z_u =& \Big\{ b_u c_A(\hat{t}_d) - (1-b_u) c_B(\hat{t}_d) \Big\} \\ &+ \sum_{j=0}^{u-1} \Big\{ b_j \left[c_A([u-j]T + \hat{t}_d) - \lambda_u c_A([u-j]T) \right] \\ &- (1-b_j) \left[c_B([u-j]T + \hat{t}_d) - \lambda_u c_B([u-j]T) \right] \Big\} \\ &+ \sum_{j=0}^{u} \Big\{ b_j \left[n_{A,j}(uT + \hat{t}_d) - \lambda_u n_{A,j}(uT) \right] \\ &- (1-b_j) \left[n_{B,j}(uT + \hat{t}_d) - \lambda_u n_{B,j}(uT) \right] \Big\}, \\ & u = 0, 1, \ldots. \end{aligned} \tag{3.15}$$

It can be seen that, in (3.15), the desired term is not affected by the ISIC. However, the problem of noise amplification may be reduced due to $\lambda_u < 1$. Moreover, in (3.14), the scaling factor λ_u may be estimated in different ways, as shown in [110].

Below we analyze the BER of the BMoSK-modulated DMC systems without/with ISIC.

3.3 BER Analysis of DMC Systems Employing BMoSK Modulation

As in [110], we consider a range of approaches to analyze the BER of the BMoSK-modulated DMC systems. Throughout the analysis, we assume that $u >> L$, meaning that the DMC process is in static state. In this case, the decision variable of (3.6) can be written as

$$\begin{aligned} Z_u =& \underbrace{\sum_{i=0}^{L} b_{u-i} \left[c_{A,i} + n_{A,(u-i)u} \right]}_{Z_{uA}} \\ &- \underbrace{\sum_{i=0}^{L} (1-b_{u-i}) \left[c_{B,i} + n_{B,(u-i)u} \right]}_{Z_{uB}}. \end{aligned} \tag{3.16}$$

In our analysis, we also assume that the bit duration T satisfies $T > \rho^2/D$ [16], so that adjacent noise samples are independent. Moreover, we assume that the binary data transmitted obeys the uniform distribution with the probabilities of $P(1) = P(0) = 0.5$.

3.3.1 Poisson Approximation

According to [110], the observations of Type-A and Type-B molecules, given by $Y_{uA} = V_R Z_{uA}$ and $Y_{uB} = V_R Z_{uB}$, can be closely approximated as the Poisson distributed random variables with the PMF expressed as $\mathcal{P}(\mu_{Y_A})$ and $\mathcal{P}(\mu_{Y_B})$. Let $\boldsymbol{b}_L = [b_{u-L}, ..., b_{u-1}]^T$ be a vector containing the

L bits imposing ISI on b_u. Then, by considering $b_u = 1$ or 0, μ_{Y_A} and μ_{Y_B} can be expressed as

$$\begin{aligned}
\mu_{Y_{A1}} =& V_R \left[c_{A,0} + \sum_{i=1}^{L} b_{u-i} c_{A,i} \right], \\
\mu_{Y_{A0}} =& V_R \sum_{i=1}^{L} b_{u-i} c_{A,i}, \\
\mu_{Y_{B1}} =& V_R \sum_{i=1}^{L} (1 - b_{u-i})\, c_{B,i}, \\
\mu_{Y_{B0}} =& V_R \left[c_{B,0} + \sum_{i=1}^{L} (1 - b_{u-i})\, c_{B,i} \right],
\end{aligned} \tag{3.17}$$

where $\mu_{Y_{A1}}$ and $\mu_{Y_{B1}}$ are the mean values corresponding to $b_u = 1$, while $\mu_{Y_{A0}}$ and $\mu_{Y_{B0}}$ are the mean values corresponding to $b_u = 0$. Therefore, the Poisson PMFs of Y_{uA} and Y_{uB} for given $b_u = 1$ and $b_u = 0$ can be expressed as

$$\begin{aligned}
f_{Y_{uA}}(n|\boldsymbol{b}_L, b_u = 1) =& \frac{\mu_{Y_{A1}}^n e^{-\mu_{Y_{A1}}}}{n!},\ n = 0, 1, 2, \ldots, \\
f_{Y_{uA}}(n|\boldsymbol{b}_L, b_u = 0) =& \frac{\mu_{Y_{A0}}^n e^{-\mu_{Y_{A0}}}}{n!},\ n = 0, 1, 2, \ldots, \\
f_{Y_{uB}}(n|\boldsymbol{b}_L, b_u = 1) =& \frac{\mu_{Y_{B1}}^n e^{-\mu_{Y_{B1}}}}{n!},\ n = 0, 1, 2, \ldots, \\
f_{Y_{uB}}(n|\boldsymbol{b}_L, b_u = 0) =& \frac{\mu_{Y_{B0}}^n e^{-\mu_{Y_{B0}}}}{n!},\ n = 0, 1, 2, \ldots.
\end{aligned} \tag{3.18}$$

Considering that the observations of Type-A and Type-B molecules are independent, we can deduce that the PMFs of Y_{uA} and Y_{uB} are independent. Hence, the difference between Y_{uA} and Y_{uB} obeys the Skellam distribution [90]. Let $Y_u = V_R Z_u$, where Z_u is given by (3.16). Then, the PMF of Y_u for $b_u = 1$ and $b_u = 0$ can be expressed as

$$\begin{aligned}
f_{Y_u}(k|\boldsymbol{b}_L,\ b_u = 1) =& \exp\left(-[\mu_{Y_{A1}} + \mu_{Y_{B1}}]\right) \left(\frac{\mu_{Y_{A1}}}{\mu_{Y_{B1}}} \right)^{k/2} \\
& \times I_k \left(2\sqrt{\mu_{Y_{A1}} \mu_{Y_{B1}}} \right),\ -\infty < k < \infty, \\
f_{Y_u}(k|\boldsymbol{b}_L,\ b_u = 0) =& \exp\left(-[\mu_{Y_{A0}} + \mu_{Y_{B0}}]\right) \left(\frac{\mu_{Y_{A0}}}{\mu_{Y_{B0}}} \right)^{k/2} \\
& \times I_k \left(2\sqrt{\mu_{Y_{A0}} \mu_{Y_{B0}}} \right),\ -\infty < k < \infty,
\end{aligned} \tag{3.19}$$

respectively.

Therefore, given the decision threshold $C_T = 0$, the miss probability can be derived as

$$\begin{aligned} P_M =& P(\hat{b}_u = 0|b_u = 1) = P(Y_u < 0|b_u = 1) \\ =& 1 - P(Y_u \geq 0|b_u = 1) \\ =& 1 - \sum_{\boldsymbol{b}_L \in \mathcal{B}^L} P(\boldsymbol{b}_L) P(Y_u \geq 0|\boldsymbol{b}_L, b_u = 1) \\ =& 1 - \frac{1}{2^L} \sum_{\boldsymbol{b}_L \in \mathcal{B}^L} \exp\left(-[\mu_{Y_{A1}} + \mu_{Y_{B1}}]\right) \\ & \times \sum_{k=0}^{\infty} \left(\frac{\mu_{Y_{A1}}}{\mu_{Y_{B1}}}\right)^{k/2} I_k\left(2\sqrt{\mu_{Y_{A1}}\mu_{Y_{B1}}}\right), \end{aligned} \tag{3.20}$$

where $\mathcal{B} = \{1, 0\}$, $P(\boldsymbol{b}_L)$ is the probability of the occurrence of a specific sequence of $\boldsymbol{b}_L$. When assuming that $P(1) = P(0) = 0.5$, we have $P(\boldsymbol{b}_L) = 1/2^L$.

Similarly, the false alarm probability can be derived, given as

$$\begin{aligned} P_{FA} =& \sum_{\boldsymbol{b}_L \in \mathcal{B}^L} P(\boldsymbol{b}_L) P(Y_u \geq 0|\boldsymbol{b}_L, b_u = 0) \\ =& \frac{1}{2^L} \sum_{\boldsymbol{b}_L \in \mathcal{B}^L} \exp\left(-[\mu_{Y_{A0}} + \mu_{Y_{B0}}]\right) \\ & \times \sum_{k=0}^{\infty} \left(\frac{\mu_{Y_{A0}}}{\mu_{Y_{B0}}}\right)^{k/2} I_k\left(2\sqrt{\mu_{Y_{A0}}\mu_{Y_{B0}}}\right). \end{aligned} \tag{3.21}$$

After combining (3.20) and (3.21), the BER of the BMoSK-modulated DMC systems can be expressed as

$$\begin{aligned} P_b =& \frac{1}{2}(P_M + P_{FA}) \\ =& \frac{1}{2} + \frac{1}{2^{L+1}} \sum_{\boldsymbol{b}_L \in \mathcal{B}^L} \Bigg[\exp\left(-[\mu_{Y_{A0}} + \mu_{Y_{B0}}]\right) \\ & \times \sum_{k=0}^{\infty} \left(\frac{\mu_{Y_{A0}}}{\mu_{Y_{B0}}}\right)^{k/2} I_k\left(2\sqrt{\mu_{Y_{A0}}\mu_{Y_{B0}}}\right) \\ & - \exp\left(-[\mu_{Y_{A1}} + \mu_{Y_{B1}}]\right) \\ & \times \sum_{k=0}^{\infty} \left(\frac{\mu_{Y_{A1}}}{\mu_{Y_{B1}}}\right)^{k/2} I_k\left(2\sqrt{\mu_{Y_{A1}}\mu_{Y_{B1}}}\right) \Bigg]. \end{aligned} \tag{3.22}$$

3.3.2 Gaussian-Approximation

When both $(\mu_{Y_{A1}} + \mu_{Y_{B1}})$ and $(\mu_{Y_{A0}} + \mu_{Y_{B0}})$ are relatively large, the Skellam PMFs in (3.19) can be approximated as the Gaussian PDFs [91]. Then, the conditional Gaussian PDFs for given $b_u = 1$

and $b_u = 0$ can be expressed as

$$\begin{aligned} f_{Z_u}(y|\boldsymbol{b}_L, b_u = 1) =& \frac{1}{\sqrt{2\pi}\sigma_{Z_1}} \exp\left(-\frac{[y-\mu_{Z_1}]^2}{2\sigma_{Z_1}^2}\right), \\ & -\infty < y < \infty, \\ f_{Z_u}(y|\boldsymbol{b}_L, b_u = 0) =& \frac{1}{\sqrt{2\pi}\sigma_{Z_0}} \exp\left(-\frac{[y-\mu_{Z_0}]^2}{2\sigma_{Z_0}^2}\right), \\ & -\infty < y < \infty, \end{aligned} \tag{3.23}$$

respectively, associated with defining

$$\begin{aligned} \mu_{Z_1} =& c_{A,0} + \sum_{i=1}^{L} b_{u-i}\left(c_{A,i} + c_{B,i}\right) - \sum_{i=1}^{L} c_{B,i}, \\ \sigma_{Z_1}^2 =& \frac{c_{A,0}}{V_R} + \frac{1}{V_R}\left[\sum_{i=1}^{L} b_{u-i}\left(c_{A,i} - c_{B,i}\right) + \sum_{i=1}^{L} c_{B,i}\right]; \\ \mu_{Z_0} =& \sum_{i=1}^{L} b_{u-i}\left(c_{A,i} + c_{B,i}\right) - \sum_{i=1}^{L} c_{B,i} - c_{B,0}, \\ \sigma_{Z_0}^2 =& \frac{1}{V_R}\left[\sum_{i=1}^{L} b_{u-i}\left(c_{A,i} - c_{B,i}\right) + \sum_{i=1}^{L} c_{B,i}\right] + \frac{c_{B,0}}{V_R}, \end{aligned} \tag{3.24}$$

which are all functions of $\boldsymbol{b}_L$. Based on (3.23), the miss-probability P_M can be derived as

$$\begin{aligned} P_M =& \frac{1}{2^L} \sum_{\boldsymbol{b}_L \in \mathcal{B}^L} P(Z_u \le 0|\boldsymbol{b}_L, b_u = 1) \\ =& 1 - \frac{1}{2^L} \sum_{\boldsymbol{b}_L \in \mathcal{B}^L} P(Z_u > 0|\boldsymbol{b}_L, b_u = 1) \\ =& 1 - \frac{1}{2^L} \sum_{\boldsymbol{b}_L \in \mathcal{B}^L} \frac{1}{\sqrt{2\pi}\sigma_{Z_1}} \int_0^{\infty} \exp\left(-\frac{[y-\mu_{Z_1}]^2}{2\sigma_{Z_1}^2}\right) dy \\ =& \frac{1}{2^L} \sum_{\boldsymbol{b}_L \in \mathcal{B}^L} Q\left(\frac{\mu_{Z_1}}{\sigma_{Z_1}}\right), \end{aligned} \tag{3.25}$$

where $Q(x)$ is the Gaussian Q-function [80] defined as $Q(x) = (2\pi)^{-1/2} \int_x^{\infty} e^{-t^2/2} dt$. Similarly, the false-alarm probability P_{FA} can be derived as

$$\begin{aligned} P_{FA} =& \frac{1}{2^L} \sum_{\boldsymbol{b}_L \in \mathcal{B}^L} P(Z_u > 0|\boldsymbol{b}_L, b_u = 0) \\ =& \frac{1}{2^L} \sum_{\boldsymbol{b}_L \in \mathcal{B}^L} \frac{1}{\sqrt{2\pi}\sigma_{Z_0}} \int_0^{\infty} \exp\left(-\frac{[y-\mu_{Z_0}]^2}{2\sigma_{Z_0}^2}\right) dy \\ =& 1 - \frac{1}{2^L} \sum_{\boldsymbol{b}_L \in \mathcal{B}^L} Q\left(\frac{\mu_{Z_0}}{\sigma_{Z_0}}\right). \end{aligned} \tag{3.26}$$

Consequently, the BER of the BMoSK-modulated DMC systems obtained from the Gaussian-approximation can be expressed as

$$P_b = \frac{1}{2} + \frac{1}{2^{L+1}} \sum_{\boldsymbol{b}_L \in \mathcal{B}^L} \left[Q\left(\frac{\mu_{Z_1}}{\sigma_{Z_1}}\right) - Q\left(\frac{\mu_{Z_0}}{\sigma_{Z_0}}\right)\right]. \tag{3.27}$$

3.3.3 Improved Threshold

Above $C_T = 0$ is assumed in our analysis, which is simple but does not reflect the distributions of Z_u conditioned on $b_u = 1$ and 0, due to its dependence on ISI. According to the detection theory, an improved threshold C_{IT} can be given by

$$\begin{aligned} C_{IT} =& \frac{\mu_{Z_0} + \mu_{Z_1}}{2} \\ =& \frac{(\mu_{A_0} - \mu_{B_0}) + (\mu_{A_1} - \mu_{B_1})}{2}, \end{aligned} \tag{3.28}$$

which is obtained by assuming that the distributions of $Z_u(b_u = 1)$ and $Z_u(b_u = 0)$ are similar, except their different means of μ_{Z_1} and μ_{Z_0}.

However, the means shown in the above equation are depended on the bit sequence of $\{b_j\}$ transmitted before the u-th bit, as shown, for example, in (3.24). In practice, these bits can only be replaced by the detected bits $\{\hat{b}_j\}$ for estimating the improved threshold C_{IT} for detection of the u-th bit. Therefore, with the aid of (3.17), the improved threshold C_{IT} can be evaluated as

$$C_{IT} = \frac{c_{A,0} - c_{B,0}}{2} + \left[\sum_{i=1}^{L} \hat{b}_{u-i} \left(c_{A,i} + c_{B,i} \right) - c_{B,i} \right]. \tag{3.29}$$

Correspondingly, under the Poisson approximation, the BER of the BMoSK-modulated DMC systems with the optimal threshold assisted detection can be modified from (3.22), which is

$$\begin{aligned} P_b =& \frac{1}{2} + \frac{1}{2^{L+1}} \sum_{\boldsymbol{b}_L \in \mathcal{B}^L} \Bigg[\exp\left(-[\mu_{Y_{A0}} + \mu_{Y_{B0}}] \right) \\ & \times \sum_{k=V_R C_{IT}}^{\infty} \left(\frac{\mu_{Y_{A0}}}{\mu_{Y_{B0}}} \right)^{k/2} I_k \left(2\sqrt{\mu_{Y_{A0}} \mu_{Y_{B0}}} \right) \\ & - \exp\left(-[\mu_{Y_{A1}} + \mu_{Y_{B1}}] \right) \\ & \times \sum_{k=V_R C_{IT}}^{\infty} \left(\frac{\mu_{Y_{A1}}}{\mu_{Y_{B1}}} \right)^{k/2} I_k \left(2\sqrt{\mu_{Y_{A1}} \mu_{Y_{B1}}} \right) \Bigg]. \end{aligned} \tag{3.30}$$

Similarly, when the Gaussian approximation is employed, according to (3.27), the BER of the BMoSK-modulated DMC systems with the optimal threshold assisted detection can be expressed as

$$P_b = \frac{1}{2} + \frac{1}{2^{L+1}} \sum_{\boldsymbol{b}_L \in \mathcal{B}^L} \left[Q\left(\frac{C_{IT} - \mu_{Z_0}}{\sigma_{Z_0}} \right) - Q\left(\frac{C_{IT} - \mu_{Z_1}}{\sigma_{Z_1}} \right) \right]. \tag{3.31}$$

3.3.4 Monte-Carlo Approach

As shown in (3.22) and (3.30) for the Poisson approximation, and in (3.27) and (3.31) for the Gaussian approximation, the complexity of BER evaluation is mainly determined by the length of ISI. When data rate is relatively high or transmission distance is relatively long, the ISI can be very long. Since the number of combinations of a L-length binary sequence is 2^L, it will become impossible

to evaluate the BER based on the above mentioned formulas, if the ISI length L is large. In fact, provided that $L \geq 20$, exact evaluating the above-mentioned formulas is highly involved. Whereas, in practice, the ISI length L may be significantly larger than 20. Therefore, in order to circumvent this problem, in this and the next subsections, we introduce some approximation approaches to reduce the computation, while without trading much off the accuracy of BER estimation.

First, we consider the Monte-Carlo approach [89] to simplify the computation of (3.22) or (3.27), when L is large. Let us assume that $\boldsymbol{b}_L$ is a L-length random binary vector distributed in $\mathcal{B}^L$. Then, Q number of binary sequences for $\boldsymbol{b}_L$ can be randomly generated, which are expressed as $\{\boldsymbol{b}_L^{(1)}, \ldots, \boldsymbol{b}_L^{(Q)}\}$. According to Monte-Carlo theory, the statistical properties of $\boldsymbol{b}_L$ can be guaranteed, provided that Q is sufficiently large. Therefore, when Q is sufficiently large, corresponding to (3.22), the BER of the BMoSK-modulated DMC systems can be approximately evaluated as

$$\begin{aligned} P_b \approx \frac{1}{2} + \frac{1}{2Q} \sum_{\{\boldsymbol{b}_L^{(1)}, \ldots, \boldsymbol{b}_L^{(Q)}\}} \Bigg[& \exp\left(-[\mu_{Y_{A0}} + \mu_{Y_{B0}}]\right) \\ & \times \sum_{k=0}^{\infty} \left(\frac{\mu_{Y_{A0}}}{\mu_{Y_{B0}}}\right)^{k/2} I_k\left(2\sqrt{\mu_{Y_{A0}}\mu_{Y_{B0}}}\right) \\ & - \exp\left(-[\mu_{Y_{A1}} + \mu_{Y_{B1}}]\right) \\ & \times \sum_{k=0}^{\infty} \left(\frac{\mu_{Y_{A1}}}{\mu_{Y_{B1}}}\right)^{k/2} I_k\left(2\sqrt{\mu_{Y_{A1}}\mu_{Y_{B1}}}\right) \Bigg]. \end{aligned} \tag{3.32}$$

Similarly, (3.27) can be evaluated using the Monte-Carlo approach, when the Gaussian-approximation is employed.

3.3.5 Simplified Poisson and Gaussian-Approximation Approaches

When L is large, we can deduce that most ISI terms on a bit are nearly flat and small. This implies that the ISI imposed on a data bit is only dominated by some bits sent in the front of it. Therefore, when L is large and $u > L$, the decision variable Z_u of (3.6) can be expressed as

$$\begin{aligned} Z_u = & \underbrace{\left\{\sum_{i=0}^{I} b_{u-i}\left[c_{A,i} + n_{A,(u-i)u}\right] + X_{uA}\right\}}_{Z_{uA}} \\ & - \underbrace{\left\{\sum_{i=0}^{I} (1-b_{u-i})\left[c_{B,i} + n_{B,(u-i)u}\right] + X_{uB}\right\}}_{Z_{uB}}, \\ & u = 0, 1, \ldots, \end{aligned} \tag{3.33}$$

where $X_{uA} = \sum_{i=I+1}^{L} b_{u-i}\left[c_{A,i} + n_{A,(u-i)u}\right]$ and $X_{uB} = \sum_{i=I+1}^{L} (1-b_{u-i})\left[c_{B,i} + n_{B,(u-i)u}\right]$, contain the counting noise as well as the less-dominant ISI. Hence, we may approximate $Y_{uA} = V_R X_{uA}$ and $Y_{uB} = V_R X_{uB}$ as the Poisson distributed random variables, with the mean (also vari-

ance) of Type-A and Type-B molecules given by

$$\begin{aligned}\mu_{A,Y} =& E\left[V_R X_{uA}\right] = V_R E_{b_{u-i}}\left[\sum_{i=I+1}^{L} b_{u-i}c_{A,i}\right]\\ =& \frac{V_R}{2}\sum_{i=I+1}^{L} c_{A,i}, \end{aligned} \tag{3.34}$$

$$\begin{aligned}\mu_{B,Y} =& E\left[V_R X_{uB}\right] = V_R E_{b_{u-i}}\left[\sum_{i=I+1}^{L} \left(1-b_{u-i}\right)c_{B,i}\right]\\ =& \frac{V_R}{2}\sum_{i=I+1}^{L} c_{B,i}, \end{aligned} \tag{3.35}$$

respectively. Correspondingly, X_{uA} and X_{uB} have the mean and variance given, respectively, by

$$\mu_{A,X} = \frac{1}{2}\sum_{i=I+1}^{L} c_{A,i},\ \ \sigma_{A,X}^2 = \frac{1}{2V_R}\sum_{i=I+1}^{L} c_{A,i}; \tag{3.36}$$

$$\mu_{B,X} = \frac{1}{2}\sum_{i=I+1}^{L} c_{B,i},\ \ \sigma_{B,X}^2 = \frac{1}{2V_R}\sum_{i=I+1}^{L} c_{B,i}. \tag{3.37}$$

Consequently, when the Poisson approach is employed, the PMF of Y_u conditioned on $b_u = 1$ and $b_u = 0$ are given in (3.19), associated with

$$\begin{aligned}\mu_{Y_{A1}} =& V_R\left[c_{A,0} + \sum_{i=1}^{I} b_{u-i}c_{A,i}\right] + \mu_{A,Y},\\ \mu_{Y_{A0}} =& V_R\left(\sum_{i=1}^{I} b_{u-i}c_{A,i}\right) + \mu_{A,Y},\\ \mu_{Y_{B1}} =& V_R\left[\sum_{i=1}^{I}\left(1-b_{u-i}\right)c_{B,i}\right] + \mu_{B,Y},\\ \mu_{Y_{B0}} =& V_R\left[c_{B,0} + \sum_{i=1}^{I}\left(1-b_{u-i}\right)c_{B,i}\right] + \mu_{B,Y}. \end{aligned} \tag{3.38}$$

Finally, according to (3.22), the BER of the BMoSK-modulated DMC systems can be expressed as

$$\begin{aligned}P_b =& \frac{1}{2} + \frac{1}{2^{I+1}}\sum_{\boldsymbol{b}_I\in\mathcal{B}^I}\Bigg[\exp\left(-\left[\mu_{Y_{A0}} + \mu_{Y_{B0}}\right]\right)\\ &\times\sum_{k=0}^{\infty}\left(\frac{\mu_{Y_{A0}}}{\mu_{Y_{B0}}}\right)^{k/2} I_k\left(2\sqrt{\mu_{Y_{A0}}\mu_{Y_{B0}}}\right)\\ &-\exp\left(-\left[\mu_{Y_{A1}} + \mu_{Y_{B1}}\right]\right)\\ &\times\sum_{k=0}^{\infty}\left(\frac{\mu_{Y_{A1}}}{\mu_{Y_{B1}}}\right)^{k/2} I_k\left(2\sqrt{\mu_{Y_{A1}}\mu_{Y_{B1}}}\right)\Bigg], \end{aligned} \tag{3.39}$$

where, by definition, $\boldsymbol{b}_I = \left[b_{u-I},\ldots,b_{u-1}\right]^T$.

Similarly, when the simplified Gaussian-approximation is employed, the conditional PDFs of

Z_u are respectively given in (3.23) for $b_u = 1$ and $b_u = 0$, associated with

$$\begin{aligned}
\mu_{Z_1} =& \mu_{A,X} + c_{A,0} + \sum_{i=1}^{I} b_{u-i}\left(c_{A,i} + c_{B,i}\right) \\
& - \sum_{i=1}^{I} c_{B,i} - \mu_{B,X}, \\
\sigma^2_{Z_1} =& \frac{c_{A,0}}{V_R} + \frac{1}{V_R}\left[\sum_{i=1}^{I} b_{u-i}\left(c_{A,i} - c_{B,i}\right) + \sum_{i=1}^{I} c_{B,i}\right] \\
& + \sigma^2_{A,X} + \sigma^2_{B,X}; \\
\mu_{Z_0} =& \sum_{i=1}^{I} b_{u-i}\left(c_{A,i} + c_{B,i}\right) - \sum_{i=1}^{I} c_{B,i} - c_{B,0} + \mu_{A,X} \\
& - \mu_{B,X}, \\
\sigma^2_{Z_0} =& \frac{1}{V_R}\left[\sum_{i=1}^{I} b_{u-i}\left(c_{A,i} - c_{B,i}\right) + \sum_{i=1}^{I} c_{B,i}\right] + \frac{c_{B,0}}{V_R} \\
& + \sigma^2_{A,X} + \sigma^2_{B,X}.
\end{aligned} \tag{3.40}$$

Correspondingly, the BER of the BMoSK-modulated DMC systems can be expressed as

$$P_b = \frac{1}{2} + \frac{1}{2^{I+1}} \sum_{\boldsymbol{b}_I \in \mathcal{B}^I} \left[Q\left(\frac{\mu_{Z_1}}{\sigma_{Z_1}}\right) - Q\left(\frac{\mu_{Z_0}}{\sigma_{Z_0}}\right)\right]. \tag{3.41}$$

As seen in the formulas in Sections 3.3.1 and 3.3.2, 2^L terms are required to be considered for the first sum at the righthand side of (3.22) and (3.27). By contrast, as seen in (3.39) and (3.41), there are only 2^I terms need to be computed. Hence, with the simplified Poisson- or Gaussian-approach, the computation can be significantly reduced, if choosing $I << L$ is allowed, as shown in Section 3.5.

3.4 BER Analysis of BMoSK-Modulated DMC Systems with ISI Mitigation

Having analyzed the BER of the BMoSK-modulated DMC systems, let us now consider the BER of the BMoSK-modulated DMC systems employing ISIC. Our analysis is based on the decision variable Z_u of (3.14). For simplicity, we assume that $\lambda_u = \bar{\lambda}$ is a constant. Then, we can write Z_u

as

$$
\begin{aligned}
Z_u = \Bigg\{ & \underbrace{\sum_{i=0}^{L} b_{u-i} \left[c_A(iT + \hat{t}_d) + n_{A,u-i}(uT + \hat{t}_d) \right]}_{Z_{u,A1}} \\
& \underbrace{- \bar{\lambda} \times \sum_{i=1}^{L} b_{u-i} \left[c_A(iT) + n_{A,u-i}(uT) \right]}_{Z_{u,A0}} \Bigg\} \\
& - \Bigg\{ \underbrace{\sum_{i=0}^{L} (1 - b_{u-i}) \left[c_B(iT + \hat{t}_d) + n_{B,u-i}(uT + \hat{t}_d) \right]}_{Z_{u,B1}} \\
& \underbrace{- \bar{\lambda} \times \sum_{i=1}^{L} (1 - b_{u-i}) \left[c_B(iT) + n_{B,u-i}(uT) \right]}_{Z_{u,B0}} \Bigg\}. \qquad (3.42)
\end{aligned}
$$

Let $c_{x,i} = c_x(iT + \hat{t}_d)$, $n_{x,(u-i)u} = n_{x,u-i}(uT + \hat{t}_d)$ and $c'_{x,i} = c_x(iT)$, $n'_{x,(u-i)u} = n_{x,u-i}(uT)$. Then, the above equation can be re-written as

$$
\begin{aligned}
Z_u = \Bigg\{ & \underbrace{\sum_{i=0}^{L} b_{u-i} \left[c_{A,i} + n_{A,(u-i)u} \right]}_{Z_{u,A1}} \\
& \underbrace{- \bar{\lambda} \times \sum_{i=1}^{L} b_{u-i} \left[c'_{A,i} + n'_{A,(u-i)u} \right]}_{Z_{u,A0}} \Bigg\} \\
& - \Bigg\{ \underbrace{\sum_{i=0}^{L} (1 - b_{u-i}) \left[c_{B,i} + n_{B,(u-i)u} \right]}_{Z_{u,B1}} \\
& \underbrace{- \bar{\lambda} \times \sum_{i=1}^{L} (1 - b_{u-i}) \left[c'_{B,i} + n'_{B,(u-i)u} \right]}_{Z_{u,B0}} \Bigg\} \\
= & Z_{uC} - Z_{uD}, \qquad (3.43)
\end{aligned}
$$

where, by definition,

$$Z_{uC} = \left\{ \underbrace{\sum_{i=0}^{L} b_{u-i} \left[c_{A,i} + n_{A,(u-i)u} \right]}_{Z_{u,A1}} + \underbrace{\bar{\lambda} \times \sum_{i=1}^{L} (1 - b_{u-i}) \left[c'_{B,i} + n'_{B,(u-i)u} \right]}_{Z_{u,B0}} \right\},$$

$$Z_{uD} = \left\{ \underbrace{\sum_{i=0}^{L} (1 - b_{u-i}) \left[c_{B,i} + n_{B,(u-i)u} \right]}_{Z_{u,B1}} + \underbrace{\bar{\lambda} \times \sum_{i=1}^{L} b_{u-i} \left[c'_{A,i} + n'_{A,(u-i)u} \right]}_{Z_{u,A0}} \right\}.$$

3.4.1 Poisson and Simplified Poisson Approaches

Following the analysis in 3.3.1, it can be shown that, $Y_{u,A1} = V_R Z_{u,A1}$, $Y_{u,A0} = V_R Z_{u,A0}$, $Y_{u,B1} = V_R Z_{u,B1}$ and $Y_{u,B0} = V_R Z_{u,B0}$, all obey the Poisson distributions. According to the properties of Poisson distribution [79], we can deduce that both $Y_{uC} = V_R Z_{uC}$ and $Y_{uD} = V_R Z_{uD}$ also follow the Poisson distributions, with the parameters $\mu_{Y_{uC}} = \mu_{Y_{u,A1}} + \mu_{Y_{u,B0}}$ and $\mu_{Y_{uD}} = \mu_{Y_{u,B1}} + \mu_{Y_{u,A0}}$, respectively. When considering the condition of $b_u = 1$ or 0, we have

$$\begin{aligned}
\mu_{Y_{uC_1}} =& V_R \left\{ c_{A,0} + \sum_{i=1}^{L} \left[b_{u-i} \left(c_{A,i} - \bar{\lambda} c'_{B,i} \right) + \bar{\lambda} c'_{B,i} \right] \right\}, \\
\mu_{Y_{uC_0}} =& V_R \sum_{i=1}^{L} \left[b_{u-i} \left(c_{A,i} - \bar{\lambda} c'_{B,i} \right) + \bar{\lambda} c'_{B,i} \right], \\
\mu_{Y_{uD_1}} =& V_R \sum_{i=1}^{L} \left[b_{u-i} \left(\bar{\lambda} c'_{A,i} - c_{B,i} \right) + c_{B,i} \right], \\
\mu_{Y_{uD_0}} =& V_R \left\{ c_{B,0} + \sum_{i=1}^{L} \left[b_{u-i} \left(\bar{\lambda} c'_{A,i} - c_{B,i} \right) + c_{B,i} \right] \right\}.
\end{aligned} \tag{3.44}$$

Therefore, when given $b_u = 1$ and $b_u = 0$, the Poisson PMFs of Y_{uC} and Y_{uD} conditioned on $\boldsymbol{b}_L$ can be expressed as

$$\begin{aligned}
f_{Y_{uC}}(n|\boldsymbol{b}_L, b_u = 1) &= \frac{\mu_{Y_{uC_1}}^n e^{-\mu_{Y_{uC_1}}}}{n!},\ n = 0, 1, 2, \ldots, \\
f_{Y_{uC}}(n|\boldsymbol{b}_L, b_u = 0) &= \frac{\mu_{Y_{uC_0}}^n e^{-\mu_{Y_{uC_0}}}}{n!},\ n = 0, 1, 2, \ldots, \\
f_{Y_{uD}}(n|\boldsymbol{b}_L, b_u = 1) &= \frac{\mu_{Y_{uD_1}}^n e^{-\mu_{Y_{uD_1}}}}{n!},\ n = 0, 1, 2, \ldots, \\
f_{Y_{uD}}(n|\boldsymbol{b}_L, b_u = 0) &= \frac{\mu_{Y_{uD_0}}^n e^{-\mu_{Y_{uD_0}}}}{n!},\ n = 0, 1, 2, \ldots.
\end{aligned} \tag{3.45}$$

Since the noise samples in Z_{uC} and Z_{uD} are independent, the conditional PMFs of Y_{uC} and Y_{uD} are independent. Therefore, the difference of Y_{uC} and Y_{uD} obeys the Skellam distribution, and the PMF of $Y_u = V_R Z_u$ for given $b_u = 1$ and $b_u = 0$ can be expressed as

$$\begin{aligned}
f_{Y_u}(k|\boldsymbol{b}_L, b_u = 1) &= \exp\left(-[\mu_{Y_{uC_1}} + \mu_{Y_{uD_1}}]\right) \left(\frac{\mu_{Y_{uC_1}}}{\mu_{Y_{uD_1}}}\right)^{k/2} \\
&\quad \times I_k\left(2\sqrt{\mu_{Y_{uC_1}}\mu_{Y_{uD_1}}}\right), \\
f_{Y_u}(k|\boldsymbol{b}_L, b_u = 0) &= \exp\left(-[\mu_{Y_{uC_0}} + \mu_{Y_{uD_0}}]\right) \left(\frac{\mu_{Y_{uC_0}}}{\mu_{Y_{uD_0}}}\right)^{k/2} \\
&\quad \times I_k\left(2\sqrt{\mu_{Y_{uC_0}}\mu_{Y_{uD_0}}}\right),
\end{aligned} \tag{3.46}$$

in the range of $\infty < k < \infty$.

Consequently, given the decision threshold $C_T = 0$, the miss-probability can be derived, which is

$$\begin{aligned}
P_M &= 1 - \frac{1}{2^L} \sum_{\boldsymbol{b}_L \in \mathcal{B}^L} P(Y_u \geq 0|\boldsymbol{b}_L,\ b_u = 1) \\
&= 1 - \frac{1}{2^L} \sum_{\boldsymbol{b}_L \in \mathcal{B}^L} \exp\left(-[\mu_{Y_{uC_1}} + \mu_{Y_{uD_1}}]\right) \\
&\quad \times \sum_{k=0}^{\infty} \left(\frac{\mu_{Y_{uC_1}}}{\mu_{Y_{uD_1}}}\right)^{k/2} I_k\left(2\sqrt{\mu_{Y_{uC_1}}\mu_{Y_{uD_1}}}\right).
\end{aligned} \tag{3.47}$$

Similarly, the false-alarm probability can be expressed as

$$\begin{aligned}
P_{FA} &= \frac{1}{2^L} \sum_{\boldsymbol{b}_L \in \mathcal{B}^L} P(Y_u \geq 0|\boldsymbol{b}_L,\ b_u = 0) \\
&= \frac{1}{2^L} \sum_{\boldsymbol{b}_L \in \mathcal{B}^L} \exp\left(-[\mu_{Y_{uC_0}} + \mu_{Y_{uD_0}}]\right) \\
&\quad \times \sum_{k=0}^{\infty} \left(\frac{\mu_{Y_{uC_0}}}{\mu_{Y_{uD_0}}}\right)^{k/2} I_k\left(2\sqrt{\mu_{Y_{uC_0}}\mu_{Y_{uD_0}}}\right).
\end{aligned} \tag{3.48}$$

Finally, the BER of the BMoSK-modulated DMC with ISIC can be expressed as

$$\begin{aligned}
P_b =& \frac{1}{2}(P_M + P_{FA}) \\
=& \frac{1}{2} + \frac{1}{2^{L+1}} \sum_{\boldsymbol{b}_L \in \mathcal{B}^L} \Bigg[\exp\left(-[\mu_{Y_{uC_0}} + \mu_{Y_{uD_0}}]\right) \\
& \times \sum_{k=0}^{\infty} \left(\frac{\mu_{Y_{uC_0}}}{\mu_{Y_{uD_0}}}\right)^{k/2} I_k\left(2\sqrt{\mu_{Y_{uC_0}}\mu_{Y_{uD_0}}}\right) \\
& - \exp\left(-[\mu_{Y_{uC_1}} + \mu_{Y_{uD_1}}]\right) \\
& \times \sum_{k=0}^{\infty} \left(\frac{\mu_{Y_{uC_1}}}{\mu_{Y_{uD_1}}}\right)^{k/2} I_k\left(2\sqrt{\mu_{Y_{uC_1}}\mu_{Y_{uD_1}}}\right) \Bigg].
\end{aligned} \tag{3.49}$$

Similarly, following the analysis in Section 3.3.4 and Section 3.3.5, when L is sufficiently large, we can evaluate P_b of (3.49) by the Monte-Carlo approach or the simplified Poisson-approach. Specifically, when the simplified Poisson approach is considered, the BER has the expression of (3.49) with the following modifications. First, $\boldsymbol{b}_L \in \mathcal{B}^L$ is replaced by $\boldsymbol{b}_I \in \mathcal{B}^I$, $I << L$. Second, μ_{uC_1}, μ_{uC_0}, μ_{uD_1} and μ_{uD_0} are respectively replaced by

$$\begin{aligned}
\mu_{Y_{uC_1}} =& V_R \left\{ c_{A,0} + \sum_{i=1}^{I} \left[b_{u-i} \left(c_{A,i} - \bar{\lambda} c'_{B,i} \right) + \bar{\lambda} c'_{B,i} \right] \right. \\
& \left. + \frac{1}{2} \sum_{i=I+1}^{L} \left(c_{A,i} + \bar{\lambda} c'_{B,i} \right) \right\}, \\
\mu_{Y_{uC_0}} =& V_R \left\{ \sum_{i=1}^{I} \left[b_{u-i} \left(c_{A,i} - \bar{\lambda} c'_{B,i} \right) + \bar{\lambda} c'_{B,i} \right] \right. \\
& \left. + \frac{1}{2} \sum_{i=I+1}^{L} \left(c_{A,i} + \bar{\lambda} c'_{B,i} \right) \right\}, \\
\mu_{Y_{uD_1}} =& V_R \left\{ \sum_{i=1}^{I} \left[b_{u-i} \left(\bar{\lambda} c'_{A,i} - c_{B,i} \right) + c_{B,i} \right] \right. \\
& \left. + \frac{1}{2} \sum_{i=I+1}^{L} \left(\bar{\lambda} c'_{A,i} + c_{B,i} \right) \right\}, \\
\mu_{Y_{uD_0}} =& V_R \left\{ c_{B,0} + \sum_{i=1}^{I} \left[b_{u-i} \left(\bar{\lambda} c'_{A,i} - c_{B,i} \right) + c_{B,i} \right] \right. \\
& \left. + \frac{1}{2} \sum_{i=I+1}^{L} \left(\bar{\lambda} c'_{A,i} + c_{B,i} \right) \right\}.
\end{aligned} \tag{3.50}$$

3.4.2 Gaussian-Approximation and Simplified Gaussian-Approximation

When the Gaussian-approximation is employed, the decision variable given by (3.43), conditioned on $b_u = 1$ or 0, can be respectively expressed as

$$\begin{aligned} f_{Z_u}(y|\boldsymbol{b}_L, b_u = 1) =& \frac{1}{\sqrt{2\pi}\sigma_{Z_1}} \exp\left(-\frac{[y-\mu_{Z_1}]^2}{2\sigma_{Z_1}^2}\right), \\ & -\infty < y < \infty \\ f_{Z_u}(y|\boldsymbol{b}_L, b_u = 0) =& \frac{1}{\sqrt{2\pi}\sigma_{Z_0}} \exp\left(-\frac{[y-\mu_{Z_0}]^2}{2\sigma_{Z_0}^2}\right), \\ & -\infty < y < \infty \end{aligned} \tag{3.51}$$

where, by definition,

$$\begin{aligned} \mu_{Z_1} =& \frac{1}{V_R}\left(\mu_{Y_{uC_1}} - \mu_{Y_{uD_1}}\right) \\ =& c_{A,0} + \sum_{i=1}^{L}\left[b_{u-i}\left(c_{A,i} + c_{B,i} - \bar{\lambda}c'_{B,i} - \bar{\lambda}c'_{A,i}\right)\right. \\ & \left. + \bar{\lambda}c'_{B,i} - c_{B,i}\right], \\ \sigma_{Z_1}^2 =& \frac{1}{V_R^2}\left(\mu_{Y_{uC_1}} + \mu_{Y_{uD_1}}\right) \\ =& \frac{1}{V_R}\left\{c_{A,0} + \sum_{i=1}^{L}\left[b_{u-i}(c_{A,i} - c_{B,i} - \bar{\lambda}c'_{B,i} + \bar{\lambda}c'_{A,i})\right.\right. \\ & \left.\left. + \bar{\lambda}c'_{B,i} + c_{B,i}\right]\right\}, \end{aligned}$$

$$\begin{aligned} \mu_{Z_0} =& \frac{1}{V_R}\left(\mu_{Y_{uC_0}} - \mu_{Y_{uD_0}}\right) \\ =& \sum_{i=1}^{L}\left[b_{u-i}\left(c_{A,i} + c_{B,i} - \bar{\lambda}c'_{B,i} - \bar{\lambda}c'_{A,i}\right)\right. \\ & \left. + \bar{\lambda}c'_{B,i} - c_{B,i}\right] - c_{B,0}, \\ \sigma_{Z_0}^2 =& \frac{1}{V_R^2}\left(\mu_{Y_{uC_0}} + \mu_{Y_{uD_0}}\right) \\ =& \frac{1}{V_R}\left\{\sum_{i=1}^{L}\left[b_{u-i}\left(c_{A,i} - c_{B,i} - \bar{\lambda}c'_{B,i} + \bar{\lambda}c'_{A,i}\right)\right.\right. \\ & \left.\left. + \bar{\lambda}c'_{B,i} + c_{B,i}\right] + c_{B,0}\right\}. \end{aligned} \tag{3.52}$$

From the above equations, we can see that, when ISI is fully cancelled, we have $V_R\mu_{Z_1} = V_R c_{A,0}$ and $|V_R\mu_{Z_0}| = V_R c_{B,0}$, which represent, respectively, the average number of Type-A and Type-B molecules in the measurement space. Hence, for applying the Gaussian-approximation to the Skellam distribution, both $V_R\mu_{Z_1}$ and $|V_R\mu_{Z_0}|$ are required to be sufficiently large.

Explicitly, the PDFs in (3.51) take the same forms as those in (3.23) in Section 3.3.2. Hence, when given the threshold $C_T = 0$ for decision making, the BER of the BMoSK-modulated DMC

systems with ISIC is given by (3.27) with μ_{Z_0}, σ_{Z_0} and μ_{Z_1}, σ_{Z_1} replaced by the corresponding terms shown in (3.52).

By contrast, when the simplified Gaussian-approximation is employed, the BER of the BMoSK-modulated DMC systems with ISIC can be expressed as (3.41), associated with μ_{Z_0}, σ_{Z_0} and μ_{Z_1}, σ_{Z_1} given by

$$\begin{aligned}
\mu_{Z_1} =& c_{A,0} + \sum_{i=1}^{I} \left[b_{u-i} \left(c_{A,i} + c_{B,i} - \bar{\lambda} c'_{B,i} - \bar{\lambda} c'_{A,i} \right) \right. \\
& \left. + \bar{\lambda} c'_{B,i} - c_{B,i} \right] \\
& + \frac{1}{2} \sum_{i=I+1}^{L} \left(c_{A,i} - \bar{\lambda} c'_{A,i} + \bar{\lambda} c'_{B,i} - c_{B,i} \right), \\
\sigma_{Z_1}^2 =& \frac{1}{V_R} \left\{ c_{A,0} + \sum_{i=1}^{I} \left[b_{u-i} \left(c_{A,i} - c_{B,i} - \bar{\lambda} c'_{B,i} + \bar{\lambda} c'_{A,i} \right) \right. \right. \\
& \left. + \bar{\lambda} c'_{B,i} + c_{B,i} \right] \\
& \left. + \frac{1}{2} \sum_{i=I+1}^{L} \left(c_{A,i} + \bar{\lambda} c'_{A,i} + \bar{\lambda} c'_{B,i} + c_{B,i} \right) \right\}; \\
\mu_{Z_0} =& \sum_{i=1}^{I} \left[b_{u-i} \left(c_{A,i} + c_{B,i} - \bar{\lambda} c'_{B,i} - \bar{\lambda} c'_{A,i} \right) \right. \\
& \left. + \bar{\lambda} c'_{B,i} - c_{B,i} \right] - c_{B,0} \\
& + \frac{1}{2} \sum_{i=I+1}^{L} \left(c_{A,i} - \bar{\lambda} c'_{A,i} + \bar{\lambda} c'_{B,i} - c_{B,i} \right), \\
\sigma_{Z_0}^2 =& \frac{1}{V_R} \left\{ \sum_{i=1}^{I} \left[b_{u-i} \left(c_{A,i} - c_{B,i} - \bar{\lambda} c'_{B,i} + \bar{\lambda} c'_{A,i} \right) \right. \right. \\
& \left. + \bar{\lambda} c'_{B,i} + c_{B,i} \right] + c_{B,0} \\
& \left. + \frac{1}{2} \sum_{i=I+1}^{L} \left(c_{A,i} + \bar{\lambda} c'_{A,i} + \bar{\lambda} c'_{B,i} + c_{B,i} \right) \right\}.
\end{aligned} \tag{3.53}$$

3.4.3 Improved Threshold

In the above description and analysis, we assumed the threshold for decision to be $C_T = 0$. However, due to the dependence of the decision variable Z_u in (3.43) on the transmitted data bits, an improved threshold may be engaged, as done in Section 3.3.3. This improved threshold C_{IT} for the BMoSK-modulated DMC systems with ISIC is given by

$$\begin{aligned}
C_{IT} =& \frac{\left(\mu_{Y_{uC_0}} - \mu_{Y_{uD_0}} \right) + \left(\mu_{Y_{uC_1}} - \mu_{Y_{uD_1}} \right)}{2} \\
=& \frac{c_{A,0} - c_{B,0}}{2} \\
& + \left[\sum_{i=1}^{L} \hat{b}_{u-i} \left(c_{A,i} + c_{B_i} - \bar{\lambda} c'_{B,i} - \bar{\lambda} c'_{A,i} \right) + \bar{\lambda} c'_{B,i} - c_{B,i} \right].
\end{aligned} \tag{3.54}$$

Then, according to (3.49), the BER of the BMoSK-modulated DMC systems with ISIC under the Poisson-approximation can be expressed as

$$P_b = \frac{1}{2} + \frac{1}{2^{L+1}} \sum_{\boldsymbol{b}_L \in \mathcal{B}^L} \Bigg[\exp\left(-[\mu_{Y_{uC_0}} + \mu_{Y_{uD_0}}]\right) \times \sum_{k=C_{IT}}^{\infty} \left(\frac{\mu_{Y_{uC_0}}}{\mu_{Y_{uD_0}}}\right)^{k/2} I_k\left(2\sqrt{\mu_{Y_{uC_0}}\mu_{Y_{uD_0}}}\right) - \exp\left(-[\mu_{Y_{uC_1}} + \mu_{Y_{uD_1}}]\right) \times \sum_{k=C_{IT}}^{\infty} \left(\frac{\mu_{Y_{uC_1}}}{\mu_{Y_{uD_1}}}\right)^{k/2} I_k\left(2\sqrt{\mu_{Y_{uC_1}}\mu_{Y_{uD_1}}}\right) \Bigg]. \tag{3.55}$$

Similarly, when the decision threshold of (3.54) is employed, the BER of the BMoSK-modulated DMC systems with ISIC under the Gaussian-approximation can be expressed as (3.31).

3.5 Performance Results

Below we provide a range of BER results to show the performance of the BMoSK-modulated DMC systems without or with ISIC, when various approaches introduced in Section 3.3 and 3.4 are considered. Moreover, the simulation results in some cases are provided to validate our analysis. In the figures, the BER is depicted versus the SNR, which according to [110], is defined as $\gamma_b = c_0^2/E[\sigma_0^2] = V_R c_0$. Therefore, when given a transmission distance r, and a diffusion coefficient D, the SNR is determined by the number of molecules Q sent in one pulse and the volume V_R. In our studies, we fix the parameters $D = 2.2 \times 10^{-9}\ m^2$ (squared meter/seconds) and $\rho = 1\ nm$ (nano meter), i.e., V_R. Hence, the SNR is changed by changing the number of molecules sent in one pulse. Furthermore, for the length of ISI, the value of L is determined by the constraint of

$$L \triangleq \arg_J \left\{ \frac{c_J}{c_0} \leq 0.1\% \right\}. \tag{3.56}$$

Note that, the parameter values used to generate the results of a figure are given in detail with the figure.

Let us first show the BER performance of the BMoSK-modulated DMC systems without ISIC in Fig. 3.1, to show the effect of bit-durations of T on the BER performance. In the figure, the analytical results for $L = 15$ and $L = 25$ were computed from the Poisson approach, and that for $L = 35 - 85$ were evaluated from the Poisson Monte-Carlo approach, due to the fact that it is hard to directly use the Poisson approach to evaluate the BER, when $L > 30$. Note furthermore that, given a distance as shown in the caption, a smaller bit-duration T (corresponding to higher data rate) results in longer ISI computed based on (3.56), as noted in the figure. From the figure we can observe that the analytical results are close to the corresponding results obtained from simulations, implying that the Poisson modelling is very accurate. The results also show that the Poisson Monte-Carlo approach is also capable of providing near-accurate BER estimation. Additionally, in terms

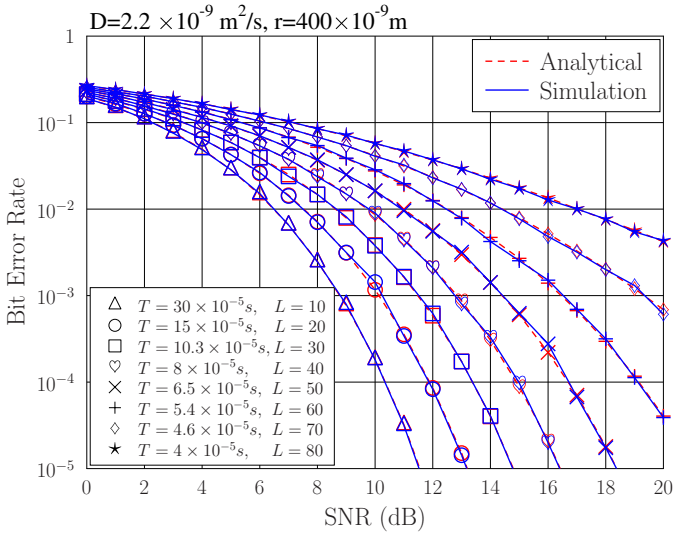

Figure 3.1: BER versus SNR performance of BMoSK-modulated DMC systems, obtained by simulations and the Poisson or Poisson (Monte-Carlo) approach, with the transmission distance of $r = 400$ nm.

of the effect of data rate, the BER increases as the data rate (or bit-duration) increases (decreases), since higher data rate (lower bit-duration) results in severe ISI.

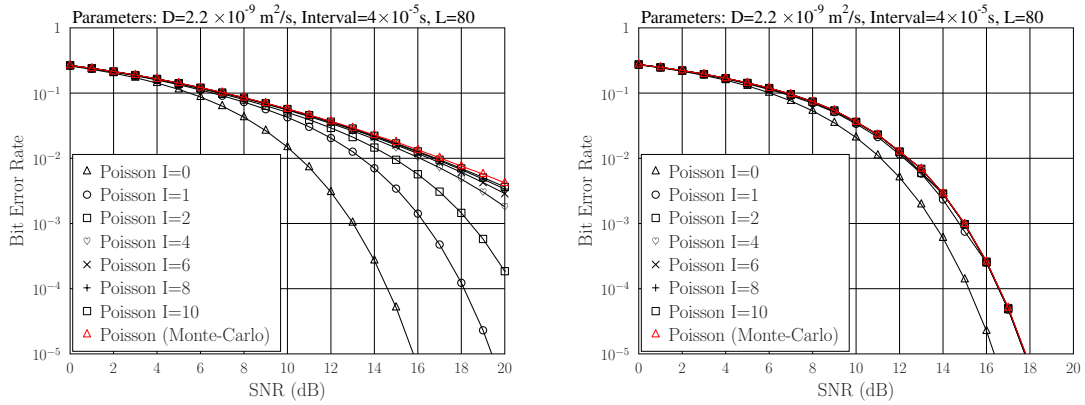

(a) BMSK Modulation

(b) BMSK modulation with ISIC

Figure 3.2: Effect of I on the accuracy of the BER versus SNR performance of the BMoSK-modulated DMC systems estimated by the simplified Poisson approach, with the parameters: $r = 400$ nm, $T = 40$ μs, and $L = 80$.

In Fig.3.2, we show the effect of I, which was introduced with the simplified Poisson approach, on the accuracy of the evaluated BER. The BMoSK-modulated DMC systems both without ISIC (Fig.3.2(a)) and with ISIC (Fig.3.2(b)) are considered. From the results we can see that, in the case of no ISIC, the BER evaluated from the simplified Poisson approach becomes close to that obtained by the Poisson Monte-Carlo approach, provided that $I \geq 6$. By contrast, with ISIC, the

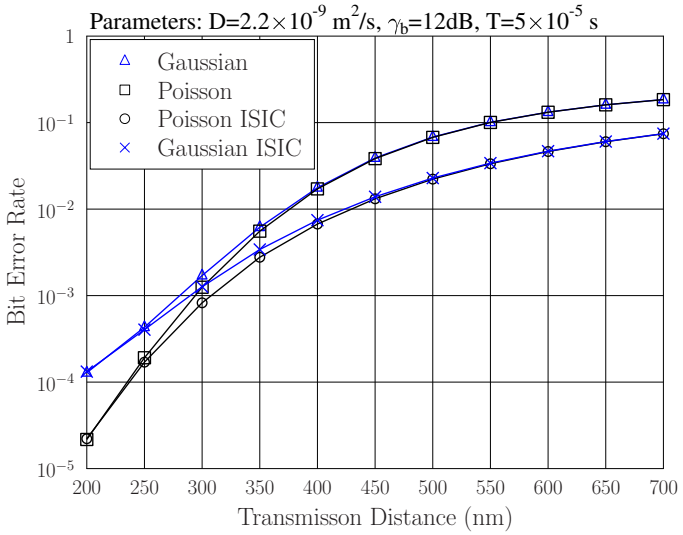

Figure 3.3: Comparison of the Poisson and Gaussian approaches for the BMoSK-modulated DMC systems without or with ISIC, with the parameters: $T = 50$ μs and $\gamma_b = 12$ dB.

BER evaluated from the simplified Poisson approach is very close to that obtained from the Poisson Monte-Carlo approach, provided that $I \geq 2$. These observations imply that, when L is large, such as $L \geq 20$, the effect of ISI is dominated by the several bits sent in the front of a reference bit considered, and the remaining ISI can be well approximated by a Poisson (or Gaussian) random variable having fixed statistics. Correspondingly, when L is large, the simplified Poisson (also Gaussian) approach can be confidently used for evaluating the BER of the BMoSK-modulated DMC systems, while significantly reducing the amount of computation. Additionally, by comparing Fig.3.2(a) with Fig.3.2(b), we can observe that the ISIC scheme is efficient, which can significantly improve the BER performance.

In Fig. 3.3, we compare the Poisson and Gaussian approaches, when the BMoSK-modulated DMC systems with or without ISIC are considered. From the previous results as shown in Fig. 3.1, we can know that the Poisson approach is very accurate. Hence, Fig. 3.3 infers that the Gaussian modelling becomes inaccurate for the scenarios considered, when the transmission distance is shorter than 400 nm. The reason behind is that short transmission distance yields low ISI, making the number of molecules presenting in the detection space insufficient to apply the Gaussian approximation. By contrast, when the transmission is sufficient large, such as $>$ 400 nm, the Gaussian modelling becomes accurate. Additionally, the BER performance in both cases degrades, as the transmission distance increases, due to the increased ISI.

In Fig. 3.4, we depict the BER performance of the BMoSK-modulated DMC systems with/without ISIC, when the detector uses $C_T = 0$ and $C_T = C_{IT}$, respectively. Explicitly, using the improved detection threshold is capable of improving the BER performance, but at the cost

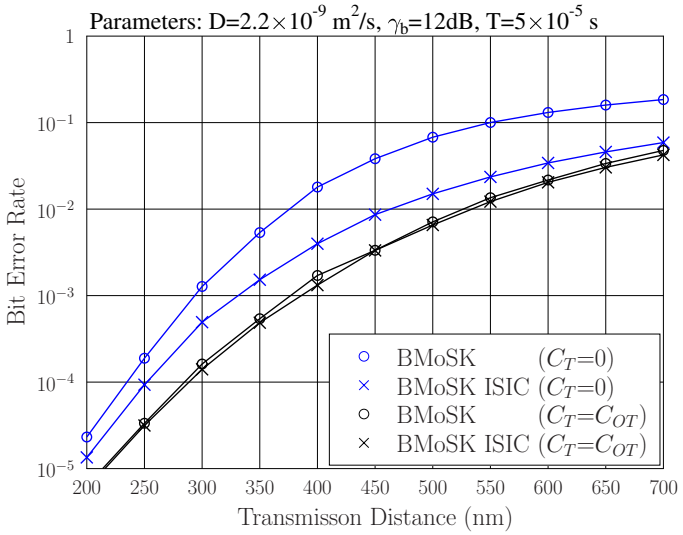

Figure 3.4: Comparison of BER versus transmission distance performance of the BMoSK-modulated DMC systems employing respectively the threshold of $C_T = 0$ and the improved threshold C_{IT} for detection, with the parameters: $T = 50$ μs, and $\gamma_b = 12$ dB.

of increased computation as well as the increased space for storing the detected data bits. As shown in Fig. 3.4, when there is no ISIC, assisted by the improved threshold, significant performance improvement can be obtained, when comparing with the case with $C_T = 0$. By contrast, when ISIC is employed, the performance improvement provided by the improved threshold becomes smaller, in particular, when the transmission distance becomes larger. This is because, when ISIC is used to mitigate the effect of strong ISI, the distributions of $Z_u(b_u = 1)$ and $Z_u(b_u = 0)$ become more similar and symmetric, making $C_T = 0$ closer to optimal. Note that, as discussed in 3.3.1, in practice, it is usually hard to operate the BMoSK-modulated DMC systems with the improved threshold, due to its dependence on the transmitted data. Therefore, low-complexity high-efficiency ISIC, such as that considered in this chapter, is highly important.

In Fig. 3.5, we compare the Gaussian and Poisson approaches, when both of them are used to evaluate the BER performance of the BMoSK-modulated DMC systems with/without ISIC. The curves in the figure are distinguished by the length of ISI, which is determined by the transmission distance r. First, the same as shown in some previous figures, such as in Figs. 3.3 and 3.4, the BER performance degrades, as the transmission distance increases. Second, by comparing the two figures, we can realize that the introduced ISIC scheme is very effective, especially, in the case of severe ISI. Moreover, as shown in both figures, the BER evaluated from the Gaussian approach is different from the BER evaluated from the Poisson Monte-Colo approach, which is accurate as shown in Fig. 3.1, when transmission distance is shorter than 350nm in the case of without ISIC, and shorter than 450nm in the case of with ISIC. Otherwise, the Gaussian approach also provides very accurate BER evaluation.

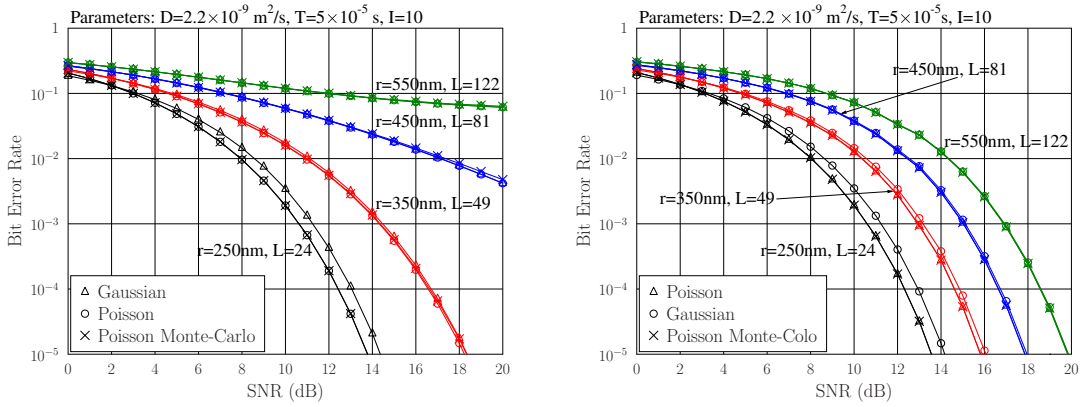

(a) BMSK Modulation

(b) BMSK modulation with ISIC

Figure 3.5: BER versus SNR performance of the BMoSK-modulated DMC systems without/with ISIC, evaluated by the Gaussian or Poisson approaches, with the parameters: $T = 50$ μs, and $I = 10$.

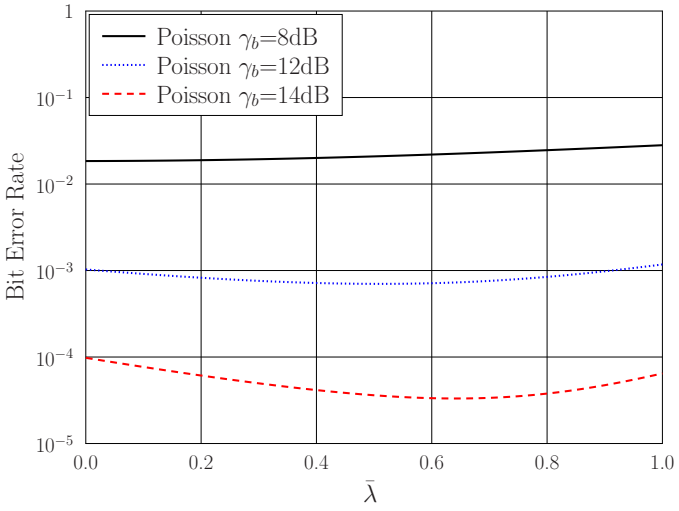

Figure 3.6: Impact of ISIC scaling factor $\bar{\lambda}$ on the BER performance of the BMoSK-modulated DMC systems with ISIC, with the parameters: $r = 250$ nm, $T = 50$ μs, and $L = 35$.

Finally, in Fig. 3.6, the effect of the ISIC scaling factor $\bar{\lambda}$ on the BER performance of the BMoSK-modulated DMC systems with ISIC is investigated. When the SNR is small, such as, 8 dB, the BER performance always degrades, as $\bar{\lambda}$ increases. This is the result of the extra noise introduced by the ISIC operation. By contrast, when the SNR is relatively high, such as 12 dB or 14 dB, we can observe that there is an optimal ISIC scaling factor to achieve the lowest BER. From this we can see that ISIC makes a trade-off between ISI mitigation and noise enhancement. However, as seen in Fig. 3.6, the achievable BER is in general robust to the value of $\bar{\lambda}$, yielding a similar BER performance over a relatively big range of $\bar{\lambda}$.

Below we compare the performance between the OOK and BMoSK modulation schemes based on simulation results.

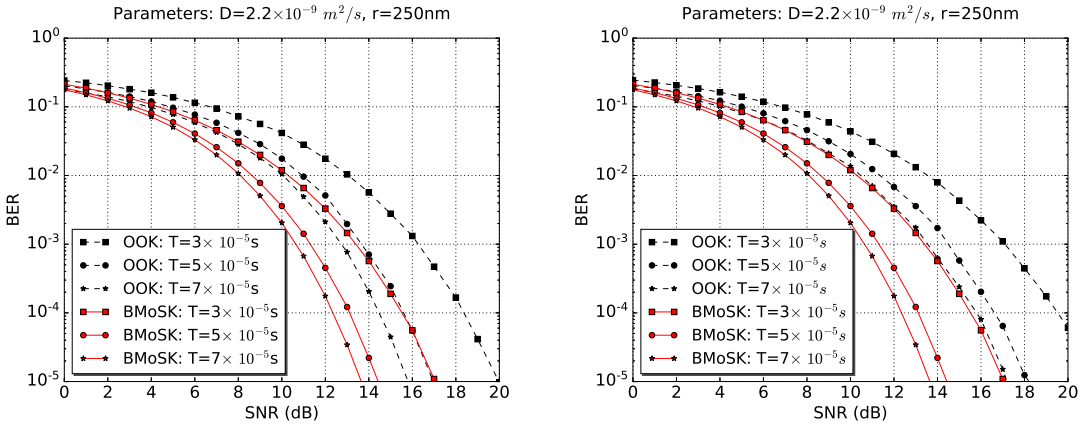

(a) OOK with optimal threshold

(b) OOK with non-optimal threshold

Figure 3.7: Comparison of BER versus SNR performance of the OOK with optimal/non-optimal threshold and the BMoSK, in terms of different symbol intervals of T.

In Figs. 3.7, we compare the BER versus SNR performance of the OOK with that of the BMoSK, when different symbol intervals are assumed. In (Fig.3.7(a)), the optimal threshold is employed by the OOK, while in (Fig.3.7(b)), we assume the non-ideal threshold applied. In the case that the threshold is non-ideal, we assume that it obeys the Gaussian distribution with its mean given by the optimum threshold, and a variance of 0.01, i.e.,

$$\alpha \sim \mathcal{N}(\alpha_{optimal}, 0.01) \tag{3.57}$$

From Figs. 3.7, we observe that the BER performance of the BMoSK is always better than that of the OOK. Typically, even when the optimum threshold is employed by the OOK, as seen in (Fig.3.7(a)), the BMoSK is at least 2 dB better than the OOK, provided that the BER is lower than 10^{-2}. By contrast, when non-ideal threshold is employed by the OOK, as shown in (Fig.3.7(b)), the BMoSK outperforms the OOK by about 3 dB, when the BER is in the range below 10^{-3}. Additionally, from these figures, we are implied that the performance loss of the OOK is about 1 dB, even when the threshold has only very small random changes (reflected by the variance of 0.01) around the optimum threshold.

Finally, in Fig. 3.8, we compare the BER versus transmission distance r performance of the OOK with optimum threshold, the BMoSK, and the BMoSK with ISIC. In our simulations, SNR is retained to 15 dB, by correspondingly increasing the number of emitted molecules, when the communication distance increases. From our analysis in the previous sections, we know that, as the transmission distance increases, the width of received pulses expands, which results in higher ISI for a given transmission rate R or symbol interval T. Therefore, as seen in Fig. 3.8, for all the schemes considered, the BER performance becomes worse, as the transmission distance increases,

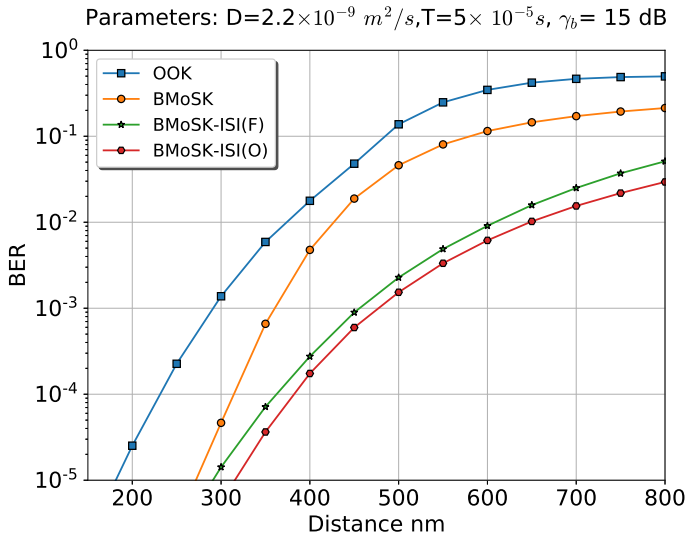

Figure 3.8: Comparison of BER performance of the OOK with optimum threshold, BMoSK and the BMoSK with ISIC.

as the result of increased ISI at given T. Over all the transmission ranges considered, the BMoSK significantly outperforms the OOK, while the ISIC brings a big gain to the BMoSK. Again, the performance achieved by applying the ISIC scaling factors obtained from formulas is near-optimum.

3.6 Conclusions

In this chapter, different approaches have been introduced for analyzing and evaluating the BER performance of the BMoSK-modulated DMC systems without or with ISIC. Correspondingly, a range of BER expressions have been obtained, which have also been validated using simulations and analysis. Based on our studies and performance results, we can conclude that the Poisson modelling is in general near-accurate. By contrast, the Gaussian-approximation is not very accurate, if the average number of molecules presenting within the detection space is insufficient to apply the Gaussian approximation, which may be due to the insufficient number of molecules transmitted and/or insufficient residue molecules resulted from ISI. Our studies also show that, when ISI is very long, the Monte-Carlo approach or the simplified Poisson approach allows to attain near-accurate BER with relatively low computation complexity. With respect to detection, the studies show that, if an increased computation complexity and extra storage of detected information are available, an improved detection threshold may be employed by DMC systems to achieve significantly improved BER performance, especially, when the DMC systems without ISIC is considered. By contrast, when the DMC systems use ISIC, the BER performance improvement resulted from applying the improved threshold becomes moderate. This implies that the ISIC operation makes the distributions of the decision variables conditioned on $b_u = 1$ and 0 more symmetric with re-

spect to zero, making the decision threshold $C_T = 0$ closer to optimum. Furthermore, our studies demonstrate that the threshold relied by the OOK scheme is highly sensitive to the environment changes, and hence difficult to manage in practice, while the threshold in the BMoSK is always near zero, which is feasible for practical implementation.

Chapter 4

Equalization and Performance of Diffusive Molecular Communication Systems with Binary Molecular-Shift Keying Modulation

This chapter investigates the equalization techniques for the diffusive molecular communication (DMC) systems with binary molecular-shift keying (BMoSK) modulation, referred to as the BMoSK-DMC systems, in order to mitigate the effect of inter-symbol interference (ISI). We first show that in terms of receiving equalization, a BMoSK-DMC system is in fact equivalent to a conventional binary phase-shift keying (BPSK) modulated radio communication system encountering ISI. Hence, a wealth of equalization techniques developed with the conventional radio communication systems may be introduced for equalization of BMoSK-DMC signals. However, considering the limited capability of molecular transceivers on computation and storage, in this chapter, we investigate only the linear equalizers (LEQ) in the principles of matched-filtering (MF), zero-forcing (ZF) and minimum mean-square error (MMSE). We characterize the effects of the different aspects related to DMC signaling and propagation on the achievable performance of the BMoSK-DMC systems with these linear equalizers. Our studies and performance results demonstrate that both the ZF- and MMSE-LEQ are capable of efficiently suppressing the ISI and attaining promising performance, while still have low-complexity to facilitate implementation.

4.1 Introduction

Design of the communication schemes operable at nano-scale has been motivated by researchers in order to implement, such as, intelligent drug delivery, network of nano-robots, etc. Inspired by

nature, diffusive molecular communications (DMC) has become an emerging nano-scale communication paradigm, where information may be conveyed by encoding it into the value of molecular concentration, molecular type and release time at the transmitter [68]. During signal transmission, molecules can be driven by the Brownian motion with or without drift from the communication medium. Hence, DMC can be a highly energy efficient communication scheme operable at nano-scale.

DMC has been investigated from different perspectives, as shown, for example, by the survey and tutorial paper [68] and the references therein. Specifically in the context of the DMC channel modeling, various channel and noise models have been proposed [16, 51, 117]. It is shown that due to the random diffusive movements of molecules, DMC usually experiences strong inter-symbol interference (ISI), in addition to the noise generated from the random movements of information molecules as well as from the other possible noisy sources in the environment [16]. In literature, various ISI mitigation techniques have been proposed and investigated. These techniques can in general be classified into the transmitter signaling design and the receiver signal processing. In a little more detail, in the class of the transmitter signaling design, the molecular shift keying (MoSK) modulation scheme [40, 72] has the embedded capability of ISI mitigation, as multiple types of molecules are used for information encoding, resulting in that the same type of molecules has a relatively small probability to become active. Relying on two types of molecules, the molecular transition shift keying (MTSK) modulation [118] has been proposed specifically for ISI mitigation. With the MTSK, no molecules are emitted for transmitting bit 0, while a type of molecules is released for transmitting a bit 1 followed by a bit 1, and the second type of molecules is emitted for transmitting a bit 1 followed by a bit 0. Furthermore, a modulation scheme based on multiple types of molecules has been proposed in [119]. With this transmission scheme, the same type of molecules is only allowed to be activated after a pre-defined time period.

In the context of the receiver signal processing techniques for ISI mitigation/suppression. One way is to use the interference suppression/cancellation [74, 77, 110, 120–123], which first generates an estimate to the ISI and then subtracts the estimated ISI from the observation for information detection. Another approach is to use the equalization techniques. In literature, various equalization methods have been proposed, as shown, e.g., in [20, 22, 30, 74]. In more detail, these equalization techniques include the sequence detectors in the principles of maximum a-posteriori (MAP) or maximum likelihood (ML) [20, 22, 30, 74, 75], linear equalizer in minimum mean-square error (MMSE) principle [22] or in zero-forcing (ZF) principle [124, 125], the decision-feedback based equalization [22, 76], etc. In all these references considering the equalization techniques, concentration-shift keying (CSK) modulation has been considered.

Following the research in literature, in this chapter, we consider the equalization in the binary molecular shift keying DMC (BMoSK-DMC) systems. We assume that in the BMoSK-DMC system, two types of molecules having the same propagation property are used for binary data modulation, where one type is activated to transmit bit 1, while the other type is activated to transmit bit 0.

At the receiver, the differences between the sampled concentrations of the two types of molecules are used as the observations for information detection. We demonstrate that the differences between the sampled concentrations of the two types of molecules have an equivalent structure as the observations in the conventional radio-based communication systems with binary phase-shift keying (BPSK) modulation and experiencing ISI [80]. Therefore in theory, various equalization techniques introduced to the conventional radio-based communications can be employed to equalize the DMC channel and improve the detection reliability of the BMoSK-DMC system. However, we should be aware of that at nano-scale, the transceivers deployed with DMC usually have limited signal processing capability, and hence the non-linear high-complexity equalization techniques based on, e.g., MAP or ML, may be impractical. Therefore, in this chapter, we investigate and compare the performance of the BMoSK-DMC systems with only the linear equalization (LEQ) based on the matched-filtering (MF), zero-forcing (ZF) and minimum mean-square error (MMSE) principles, referred to as the MF-LEQ, ZF-LEQ and MMSE-LEQ, respectively.

In summary, the main contributions and novelties of the chapter are as follows.

- Signal detection and equalization are investigated in the context of the BMoSK-DMC system, in contrast to the references where equalization has been mainly investigated with the CSK modulation.
- An expression is derived for representing the received signals in the BMoSK-DMC system, which has the same form as the received signals in the conventional radio-based BPSK-modulated communication systems experiencing ISI. Hence, it enables the feasibility to be empowered by the equalization techniques developed with the conventional radio-based communications.
- Hence, the MF-LEQ, ZF-LEQ and MMSE-LEQ are introduced to the BMoSK-DMC system.
- Furthermore, the performance of the BMoSK-DMC system with MF-LEQ, ZF-LEQ and MMSE-LEQ is investigated and compared based on numerical simulations.

In the rest of chapter, the system model is first introduced in Section 4.2. Section 4.3 provides the expressions for the received signals, which are beneficial to the derivation of equalizers. In Section 4.4, we detail the equalization schemes. Performance results are demonstrated in Section 4.5. Finally in Section 4.6, we conclude the chapter with a summary of the research.

4.2 System Model

The BMoSK-DMC system to be considered consists of a point-source transmitter and a point-like receiver. The locations of transmitter and receiver are separated by a distance r, as shown in Fig. 4.1. Information is transmitted by releasing a pulse of Q number of molecules at the beginning

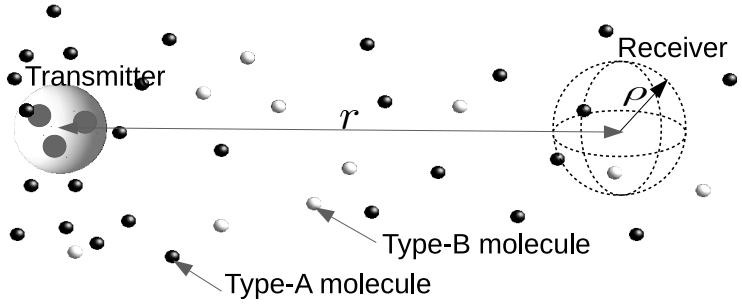

Figure 4.1: System model for DMC systems with BMoSK modulation, where the dark and light colored small spheres represent the Type-A and Type-B molecules.

of each fixed bit duration T_b. We assume that the receiver is capable of counting the number of information molecules inside a spherical detection space with a radius of ρ, and hence a volume of $V = 4\pi\rho^3/3$. The transmitter uses BMoSK modulation to send binary information data $\{b_j\} = \{b_0, b_1, \ldots, b_j, \ldots\}$, where $b_j \in \{0, 1\}$, with the aid of two types of molecules, recorded as Type-A and Type-B. Type-A is assigned for signaling $b_j = 1$ and Type-B is for signaling $b_j = 0$. We assume that the number Q of molecules emitted per pulse obeys the Poisson distribution with a rate λ within a sufficiently short time. Furthermore, we assume that the fluid medium is stable with a constant diffusion coefficient D. Additionally, we assume that synchronization is achieved between transmitter and receiver.

Based on the above assumptions and assuming that a pulse of Q molecules is emitted by the transmitter at $t = 0$, the concentration measured by the receiver at time $t > 0$ follows the Fick's Law, and is expressed as

$$c(t) = \frac{Q}{(4\pi Dt)^{\frac{3}{2}}} \exp\left(-\frac{r^2}{4Dt}\right), t > 0 \tag{4.1}$$

which is a time-domain pulse function when observed at the receiver, and reaches its maximum at the time $t_d = r^2/6D$. By substituting this value into Eq. (4.1), its peak concentration value is given by $c_{\max} = \left(\frac{3}{2\pi e}\right)^{\frac{3}{2}} \frac{Q}{r^3}$, which decreases shapely with the increase of transmission distance. For this sake and when there is no drift, DMC is usually only suitable for the communications over short distance.

When assuming that the receiver is capable of identifying the two types of molecules, the concentration difference between Type-A and Type-B molecules sensed by the receiver for the uth

bit can be expressed as

$$\begin{aligned} z(t) =& z_A(t) - z_B(t) \\ =& \sum_{j=0}^{u} b_j[c_A(t - jT_b) + n_{A,j}(t)] \\ & - \sum_{j=0}^{u}(1 - b_j)[c_B(t - jT_b) + n_{B,j}(t)], \\ & uT_b \leq t < (u+1)T_b \end{aligned} \tag{4.2}$$

where $c_X(t - jT_b)$, $X \in \{A, B\}$, is the concentration sensed at time t, $uT_b \leq t < (u+1)T_b$, generated by the molecular pulse for sending the jth bit b_j sent during $jT_b \leq t < (j+1)T_b$. This is the interference of the jth transmitted bit on the receiving of the uth bit. Hence, BMoSK-DMC experiences inter-symbol interference (ISI), which can be very severe, and significantly degrades the communication reliability, especially, when the transmission rate is relatively high, or when the transmission distance is relatively long. In Eq. (4.2), $n_{A,j}(t)$ and $n_{B,i}(t)$ are the particle counting noise caused by the corresponding types of molecules emitted by the jth pulse of molecules [16]. Considering one particular type of molecules, since the number of emitted molecules per pulse is assumed to obey the Poisson distribution with a rate λ, we can readily know that $V[c_A(t - jT_b) + n_{A,j}(t)]$ (or $V[c_B(t - jT_b) + n_{B,j}(t)]$) obeys the Poisson distribution with the rate $\lambda V c_A(t - jT_b)$ (or $V c_B(t - jT_b)$). Hence, according to [16, 74], when Q in Eq. (4.1) is sufficiently large, $n_{A,j}(t)$ (or $n_{B,j}(t)$) can be approximated as the Gaussian noise with zero mean and a variance of $\sigma^2_{A,j}(t) = V^{-1} b_j c_A(t - jT_b)$ (or $\sigma^2_{B,j}(t) = V^{-1}(1 - b_j)c_B(t - jT_b)$), when $b_j = 1$ (or $b_j = 0$) is transmitted. For convenience, these normal distributions can be expressed as $n_{A,j}(t) \sim \mathcal{N}\left(0, \sigma^2_{A,j}(t)\right)$ or $n_{B,j}(t) \sim \mathcal{N}\left(0, \sigma^2_{B,j}(t)\right)$.

In order to detect the uth bit, the receiver samples for the concentrations at $t = uT_b + \hat{t}_d$, where $\hat{t}_d$ is the estimated t_d. Then, the concentration difference between Type-A and Type-B molecules at the sampling time $t = uT_b + \hat{t}_d$ can be expressed as

$$\begin{aligned} z_u =& z_A(t = uT_b + \hat{t}_d) - z_B(t = uT_b + \hat{t}_d) \\ =& \sum_{j=0}^{u} b_j[c_A((u-j)T_b + \hat{t}_d) + n_{A,j,u}] \\ & - \sum_{j=0}^{u}(1 - b_j)[c_B((u-j)T_b + \hat{t}_d) + n_{B,j,u}], \\ & u = 0, 1, \ldots \end{aligned} \tag{4.3}$$

where $n_{A,j,u} = n_{A,j}(uT_b + \hat{t}_d)$ and $n_{B,j,u} = n_{B,j}(uT_b + \hat{t}_d)$, which are the noise added on the uth bit but due to the transmission of the jth bit. Explicitly, the detection of bit u experiences the ISI imposed from the bits sent in the front of bit u, i.e., via the indices of $j = 0, 1, \ldots, u-1$, as seen in Eq. (4.3). Let us assume that the maximum length of ISI is L bits. The value of L can be derived by letting the ISI to be ignorable in relative to the desired signal, as done, for example, in [110].

Then, z_u in Eq. (4.3) can be expressed in the form of

$$\begin{aligned} z_u = & \sum_{j=\max\{0,u-L\}}^{u} b_j[c_A((u-j)T_b + \hat{t}_d) + n_{A,j,u}] \\ & - \sum_{j=\max\{0,u-L\}}^{u} (1-b_j)[c_B((u-j)T_b + \hat{t}_d) + n_{B,j,u}], \\ & u = 0, 1, \ldots \end{aligned} \tag{4.4}$$

Let $i = u - j$, $c_{A,i} = c_A(iT_b + \hat{t}_d)$ and $c_{B,i} = c_B(iT_b + \hat{t}_d)$, we can re-represent Eq.Eq. (4.4) as

$$\begin{aligned} z_u = & \sum_{i=0}^{\min\{u,L\}} [b_{u-i}c_{A,i} - (1-b_{u-i})c_{B,i}] \\ & + \sum_{i=0}^{\min\{u,L\}} [b_{u-i}n_{A,u-i,u} - (1-b_{u-i})n_{B,u-i,u}], \\ & u = 0, 1, \ldots \end{aligned} \tag{4.5}$$

where, again, $n_{A,u-i,u}$ and $n_{B,u-i,u}$ are the Type-A and Type-B noise imposing on the uth bit, but generated by the transmission of the $(u-i)$th bit. It can be shown that $n_{A,u-i,u}$ and $n_{B,u-i,u}$ obey the distributions of $n_{A,u-i,u} \sim \mathcal{N}\left(0, \sigma^2_{A,u-i,u}\right)$ and $n_{B,u-i,u} \sim \mathcal{N}\left(0, \sigma^2_{B,u-i,u}\right)$, where $\sigma^2_{A,u-i,u} = V^{-1}c_{A,i}$ and $\sigma^2_{B,u-i,u} = V^{-1}c_{B,i}$.

4.3 Representation of Received Molecular Signals

Despite that the types of molecules for Type-A and Type-B are different, as implied from Eq. (4.1), we have $c_{A,i} = c_{B,i} = c_i$, when the number Q of molecules per transmission pulse, and the medium diffusion coefficient D are the same. Furthermore, let $n_{u-i} = b_{u-i}n_{A,u-i,u} - (1-b_{u-i})n_{B,u-i,u}$. Then, we can readily show that n_{u-i} has the distribution of $n_{u-i} \sim \mathcal{N}\left(0, \sigma^2_{u-i}\right)$ with $\sigma^2_{u-i} = V^{-1}c_i$, when the Gaussian approximation is applied. When applying these results into Eq. (4.5), we can obtain z_u as

$$\begin{aligned} z_u = & \sum_{i=0}^{\min\{u,L\}} \left(2b_{u-i} - 1\right)c_i \\ & + \sum_{i=0}^{\min\{u,L\}} n_{u-i},\ u = 0, 1, \ldots \end{aligned} \tag{4.6}$$

Here we should note that, although the Gaussian approximation of n_{u-i} may not be accurate, the Gaussian approximation of $\sum_{i=0}^{\min\{u,L\}} n_{u-i}$ can usually be sufficiently accurate for studying the performance of DMC systems, as demonstrated in [110]. In order to facilitate the mathematical derivation, let in Eq. (4.6) $\tilde{b}_{u-i} = 2b_{u-i} - 1$, where we now have $\tilde{b}_{u-i} \in \{-1, 1\}$, and $n_u = \sum_{i=0}^{\min\{u,L\}} n_{u-i}$, which follows the distribution of $n_u \sim \mathcal{N}\left(0, \sigma^2_n = V^{-1}\sum_{i=0}^{\min\{u,L\}} c_i\right)$. Then, we can modify Eq. (4.6) to

$$z_u = \sum_{i=0}^{\min\{u,L\}} \tilde{b}_{u-i}c_i + n_u,\ u = 0, 1, \ldots \tag{4.7}$$

Let us assume that the system is operated in its static state, meaning that $u >> L$. Also, let us assume that there is a $(N+L)$-length bit sequence expressed as $\boldsymbol{b} = [b_{-L}, \ldots, b_{-1}, b_0, b_1, \ldots, b_{N-1}]^T$, where $b_{-L}, \ldots, b_{-1}$ are the L bits sent in the front of b_0. Corresponding to $\boldsymbol{b}$, we have $\tilde{\boldsymbol{b}}$, whose elements have values in $\{+1, -1\}$. Let the signals received in correspondence to $[b_0, b_1, \ldots, b_{N-1}]^T$ be expressed as $\boldsymbol{y} = [z_0, z_1, \ldots, z_{N-1}]^T$, the corresponding noise samples be expressed as $\boldsymbol{n} = [n_0, n_1, \ldots, n_{N-1}]^T$. Then, the received signals $\boldsymbol{y}$ can be expressed in matrix form as

$$\boldsymbol{y} = \boldsymbol{H}\tilde{\boldsymbol{b}} + \boldsymbol{n} \tag{4.8}$$

where $\boldsymbol{H}$ is the $N \times (N+L)$ dimensional matrix due to channel impulse responses. The (i,j)th element of $\boldsymbol{H}$ is given by

$$h_{i,j} = \begin{cases} c_{i-j+L}, & \text{when } -L \leq i-j \leq 0 \\ 0, & \text{otherwise} \end{cases}, \tag{4.9}$$
$$i = 0, 1, \ldots, N-1; j = 0, 1, \ldots, N+L-1$$

In more detail, $\boldsymbol{H}$ is in the form of

$$\boldsymbol{H} = \begin{pmatrix} c_L & \cdots & c_1 & c_0 & 0 & \cdots & \cdots & \cdots & \cdots & 0 \\ 0 & c_L & \cdots & c1 & c_0 & 0 & \cdots & \cdots & \cdots & 0 \\ \vdots & \ddots & \ddots & \ddots & \ddots & \ddots & \ddots & \ddots & \ddots & \vdots \\ 0 & \cdots & \cdots & \cdots & \cdots & \cdots & c_L & \cdots & c_1 & c_0 \end{pmatrix} \tag{4.10}$$

In Eq. (4.8), $\boldsymbol{n}$ is a Gaussian noise vector, which has zero mean and a covariance matrix of $\sigma_n^2 \boldsymbol{I}_N$, with $\sigma_n^2 = V^{-1} \sum_{i=0}^{L} c_i$ and $\boldsymbol{I}_N$ being the identity matrix of size $(N \times N)$.

Furthermore, if we express $\tilde{\boldsymbol{b}} = [\tilde{\boldsymbol{b}}_I^T, \tilde{\boldsymbol{b}}_d^T]^T$, where $\tilde{\boldsymbol{b}}_I = [\tilde{b}_{-L}, \tilde{b}_{-L+1}, \ldots, \tilde{b}_{-1}]^T$, and $\tilde{\boldsymbol{b}}_d = [\tilde{b}_0, \tilde{b}_1, \ldots, \tilde{b}_{N-1}]^T$. Again, corresponding to $\tilde{\boldsymbol{b}}_I$ and $\tilde{\boldsymbol{b}}_d$, we have their one-to-one mappings to $\boldsymbol{b}_I$ and $\boldsymbol{b}_d$. Corresponding to $\tilde{\boldsymbol{b}}_I$ and $\tilde{\boldsymbol{b}}_d$, let us divide $\boldsymbol{H}$ into $\boldsymbol{H}_I$ and $\boldsymbol{H}_d$, which consist of the first L columns and the other N columns of $\boldsymbol{H}$, respectively. Then, we can rewrite Eq. (4.8) as

$$\boldsymbol{y} = \boldsymbol{H}_d \tilde{\boldsymbol{b}}_d + \boldsymbol{H}_I \tilde{\boldsymbol{b}}_I + \boldsymbol{n} \tag{4.11}$$

From this representation, explicitly, $\boldsymbol{H}_I \tilde{\boldsymbol{b}}_I$ is the interference imposed by the last data block on the current data block $\tilde{\boldsymbol{b}}_d$.

4.4 Equalization Algorithms

In this section, we consider some equalization schemes for detecting the received information in the BMoSK-DMC system. Since nano-machines are usually tiny size with very limited power for computation, we consider only low-complexity linear equalization schemes. Specifically, we consider the equalization schemes in the principles of matched-filtering (MF), zero-forcing (ZF)

and minimum mean-square error (MMSE). For all these three equalization schemes, the decision variables for detecting $\tilde{\boldsymbol{b}}_d$, and hence $\boldsymbol{b}_d$, can be obtained from the linear processing

$$\tilde{\boldsymbol{z}} = \boldsymbol{G}\boldsymbol{y} \tag{4.12}$$

where $\boldsymbol{G}$ is a $(N \times N)$ linear processing matrix for generating N decision variables, which are determined in the principles of MF, ZF and MMSE, as detailed below.

4.4.1 Matched-Filtering Linear Equalization

When substituting $\boldsymbol{y}$ from Eq. (4.11) into Eq. (4.12), we obtain

$$\tilde{\boldsymbol{z}} = \boldsymbol{G}\boldsymbol{H}_d\tilde{\boldsymbol{b}}_d + \boldsymbol{G}\boldsymbol{H}_I\tilde{\boldsymbol{b}}_I + \boldsymbol{G}\boldsymbol{n} \tag{4.13}$$

which gives N decision variables for the N bits in $\tilde{\boldsymbol{b}}_d$.

In the context of the MF-assisted linear equalization (MF-LEQ), we choose $\boldsymbol{G}$ as [80]

$$\boldsymbol{G}_{MF} = \boldsymbol{H}_d^T \tag{4.14}$$

Assume that $n > 2L$. In this case, the interference term $\boldsymbol{G}\boldsymbol{H}_I\tilde{\boldsymbol{b}}_I$ in Eq. (4.13) will not show in the decision variable for $\tilde{b}_n$. It can be shown that the last a few of decision variables for $\tilde{b}_n$ can be expressed as

$$\begin{aligned}
\tilde{z}_{N-1} =& c_0^2\tilde{b}_{N-1} + \sum_{i=1}^{L} c_0 c_i \tilde{b}_{N-i-1} + n'_N \\
\tilde{z}_{N-2} =& (c_0^2 + c_1^2)\tilde{b}_{N-2} + \sum_{i=1}^{L} c_0 c_i \tilde{b}_{N-2-i} \\
&+ \sum_{i=0, i\neq 1}^{L} c_1 c_i \tilde{b}_{N-1-i} + n'_{N-1} \\
\tilde{z}_{N-3} =& (c_0^2 + c_1^2 + c_2^2)\tilde{b}_{N-3} + \sum_{i=1}^{L} c_0 c_i \tilde{b}_{N-3-i} \\
&+ \sum_{i=0, i\neq 1}^{L} c_1 c_i \tilde{b}_{N-2-i} + \sum_{i=0, i\neq 2}^{L} c_2 c_i \tilde{b}_{N-1-i} + n'_{N-1} \\
\tilde{z}_{N-4} =& \left(\sum_{i=0}^{3} c_i^2\right)\tilde{b}_{N-4} + \sum_{i=1}^{L} c_0 c_i \tilde{b}_{N-4-i} \\
&+ \sum_{i=0, i\neq 1}^{L} c_1 c_i \tilde{b}_{N-3-i} + \sum_{i=0, i\neq 2}^{L} c_2 c_i \tilde{b}_{N-2-i} \\
&+ \sum_{i=0, i\neq 3}^{L} c_2 c_i \tilde{b}_{N-1-i} + n'_{N-1}
\end{aligned} \tag{4.15}$$

Similarly, we can write out the other decision variables. From the above equations we can know that, when the value of n decreases from $N-1$ to $N-L-1$, the decision variable $\tilde{z}_n$ is capable of collecting more power from the diffusive channels. However, the number of interference terms also

increases. In Section 4.5, we will investigate this issue to illustrate which of them is more dominant to the achievable performance.

The MF-LEQ has a low complexity for implementation. From Eq. (4.15) we can readily know that the complexity for detecting a bit is mainly contributed by the multiplication operations. Since the maximum number of non-zero elements in a column of $\boldsymbol{H}_d$ is $(L+1)$, the number of operations, including both multiplications and additions, is about $2L$. Hence, the complexity of the MF-LEQ is $\mathcal{O}(L)$ per bit. Furthermore, as above-mentioned, the best error performance should not be attained with $N-L-1$, but with a value close to $N-1$, as the result that the molecular density of Eq. (4.1) decreases sharply with the increase of time. As shown by our performance results in Section 4.5, the best performance can usually be achieved for $N-1$ or $N-2$. In these cases, the number of operations required for detecting a bit is only about 2 or 4, which can be significantly lower than $\mathcal{O}(L)$.

4.4.2 Zero-Forcing Linear Equalization

Upon treating the inter-block interference $\boldsymbol{G}\boldsymbol{H}_I\tilde{\boldsymbol{b}}_I$ as Gaussian noise, the ZF linear equalizer (ZF-LEQ) can be directly obtained from Eq. (4.13) by the implementation of $\boldsymbol{G}\boldsymbol{H}_d = \boldsymbol{I}_N$. From Eq. (4.10) we can deduce that $\boldsymbol{H}_d$ is invertible, and its inverse is also a lower triangular matrix. Hence, we can readily obtain that

$$\boldsymbol{G}_{ZF} = \boldsymbol{H}_d^{-1} \tag{4.16}$$

Upon substituting this result into Eq. (4.13), the decision variable vector $\tilde{\boldsymbol{z}}$ can be expressed as

$$\tilde{\boldsymbol{z}} = \tilde{\boldsymbol{b}}_d + \boldsymbol{H}_d^{-1}\boldsymbol{H}_I\tilde{\boldsymbol{b}}_I + \boldsymbol{H}_d^{-1}\boldsymbol{n} \tag{4.17}$$

The ZF-LEQ has the following characteristics. First, it is capable of fully suppressing the ISI within $\tilde{\boldsymbol{b}}_d$. However, there is still some ISI from the bits sent in the front of $\tilde{b}_0$. Second, when given the transmission distance and sampling interval, $\boldsymbol{H}_d$ is a fixed matrix, and hence its inverse is also fixed and only required to be computed once. Therefore, the complexity of the ZF-LEQ is the same as that of the MF-LEQ. Finally, it is well known that ZF-LEQ has the problem of noise amplification [126]. However, from Eq. (4.13) we can know that $\boldsymbol{H}_d$ is a square matrix of diagonal elements significantly dominant, if the transmission distance is relatively short. Hence, we can expect that the N eigenvalues of $\boldsymbol{H}_d$ are all smaller but very close to one. Therefore, the noise amplification problem in the ZF-LEQ for DMC systems is usually not severe, as demonstrated in Section4.5.

4.4.3 Minimum Mean-Square Error Linear Equalization

For the MMSE-LEQ, the optimum linear processing matrix $\boldsymbol{G}$ seen in Eq. (4.12) can be derived from the optimization problem expressed as

$$\boldsymbol{G}_{MMSE} = \arg\min_{\boldsymbol{G}} \mathbb{E}\left\{\|\tilde{\boldsymbol{b}}_d - \boldsymbol{G}\boldsymbol{y}\|^2\right\} \tag{4.18}$$

Solving this optimization problem gives the MMSE-LEQ solution of [126]

$$\boldsymbol{G}_{MMSE} = \boldsymbol{R}_{\boldsymbol{y}\tilde{\boldsymbol{b}}_d}^T \boldsymbol{R}_{\boldsymbol{y}}^{-1} \tag{4.19}$$

where $\boldsymbol{R}_{\boldsymbol{y}}$ is the autocorrelation matrix of $\boldsymbol{y}$, given by

$$\begin{aligned}\boldsymbol{R}_{\boldsymbol{y}} = \mathbb{E}\left\{\boldsymbol{y}\boldsymbol{y}^T\right\} =& \boldsymbol{H}\boldsymbol{H}^T + \sigma_n^2 \boldsymbol{I}_N \\ =& \boldsymbol{H}_d\boldsymbol{H}_d^T + \boldsymbol{H}_I\boldsymbol{H}_I^T + \sigma_n^2\boldsymbol{I}_N\end{aligned} \tag{4.20}$$

and $\boldsymbol{R}_{\boldsymbol{y}\tilde{\boldsymbol{b}}_d}$ is the cross-correlation matrix between $\boldsymbol{y}$ and $\tilde{\boldsymbol{b}}_d$, given by

$$\boldsymbol{R}_{\boldsymbol{y}\tilde{\boldsymbol{b}}_d} = \mathbb{E}\left\{\boldsymbol{y}\tilde{\boldsymbol{b}}_d^T\right\} = \boldsymbol{H}_d \tag{4.21}$$

Substituting Eq. (4.20) and Eq. (4.21) into Eq. (4.19), we obtain $\boldsymbol{G}_{MMSE}$ as

$$\boldsymbol{G}_{MMSE} = \boldsymbol{H}^T\left(\boldsymbol{H}\boldsymbol{H}^T + \sigma_n^2\boldsymbol{I}\right)^{-1} \tag{4.22}$$

The MMSE-LEQ employs the similar properties as the ZF-LEQ. It is also a low-complexity LEQ, although the number of operations is more than that of the MF-LEQ and that of the ZF-LEQ. This can be seen from Eq. (4.22), where the $(N+L)\times(N+L)$ inverse matrix is a fixed matrix, only required to be computed once. Therefore, $\boldsymbol{G}_{MMSE}$ is also fixed, with the dimensions of $N\times(N+L)$. In $\boldsymbol{G}_{MMSE}$ there will be more non-zero elements than in $\boldsymbol{G}_{MF}$ as well as in $\boldsymbol{G}_{ZF}$, and each column of $\boldsymbol{G}_{MMSE}$ has about $2L$ non-zero elements, if $N \geq 2L$. Hence, the number of operations required to compute $\tilde{\boldsymbol{z}} = \boldsymbol{G}\boldsymbol{y}$ is about $4L$. However, the benefit to employ the MMSE-LEQ is that it also has the capability to mitigate counting noise, which is useful in the case of high counting noise.

4.4.4 Decision Making

Having obtained the decision variable $\tilde{z}_u$, the uth bit can be detected relying on a threshold expressed as C_T. However, as the result of the ISI imposing on the current detection, we have to consider all the previously transmitted bits to compute the optimal threshold. For this objective, the receiver has to store all the estimated bits for current detection, and the estimation error would further decrease the error performance of the DMC system. In order to reduce the complexity of receiver and avoid the effect of error propagation from the previous detections, we consider the

sub-optimal threshold based decision making. Specifically, when assuming that the binary information bits are uniformly distributed, we can approximately set $C_T = 0$ in decision making. In this case, the uth bit can be detected as

$$b_u = \begin{cases} 1, & \text{when } \tilde{z}_u > 0 \\ 0, & \text{when } \tilde{z}_u \leq 0 \end{cases} \tag{4.23}$$

Let us below provide some numerical results to demonstrate the performance of the equalizers considered in this section.

4.5 Performance Results and Analysis

In this section, we investigate and compare the bit error rate (BER) performance of the BMoSK-DMC systems employing different equalization schemes, as proposed in Sections 4.4. In our simulations, we assume that the coefficient of the two types of molecules diffusing in a liquid is $D = 2.2 \times 10^{-9}\ nm/s$, the radius of receiver is set to $\rho = 15$ nm. As in [110], the SNR is defined as the ratio between the power received from a single pulse of molecules and the corresponding noise power generated by this molecular pulse, which is expressed as

$$\gamma_b = \frac{c_0^2}{E[\sigma_0^2]} = \frac{c_0^2}{\frac{1}{V}c_0} = Vc_0 \tag{4.24}$$

Hence, for a given SNR of γ_b, we can obtain $c_0 = \gamma_b/V = 3\gamma_b/(4\pi\rho^3)$. Applying this value and the associated values for $t = t_d$ and r into Eq. (4.1), we can obtain the number of molecules required to emit per pulse in simulations.

From the previous analysis we can know that the ISI length L is dependent on both the bit duration T_b and the transmission distance r. Correspondingly, in the following studies, L is estimated as

$$L \triangleq \arg_l \{c_l/c_0 \leq 1/1000\} \tag{4.25}$$

In other words, the ISI from the samples having the concentration values at least 1000 times (30 dB) lower than c_0 of the pulse's peak value is ignored.

First, in Fig. 4.2, we compare the BER performance of the BMoSK-DMC systems employ the MF-LEQ, ZF-LEQ and MMSE-LEQ, respectively. In addition to the common parameters mentioned at the start of this section, the other parameters used in our simulation are provided with the figure and in the corresponding caption, the same are in the following figures. From Fig. 4.2, we can observe that for any LEQ scheme, the BER performance degrades as the transmission distance increases, which results in stronger ISI for a given bit rate of $1/T_b$. The results show that after suppressing the ISI, both the ZF-LEQ and MMSE-LEQ are capable of achieving much better performance than the MF-LEQ. Specifically, at the BER of 0.01, using the ZF-LEQ

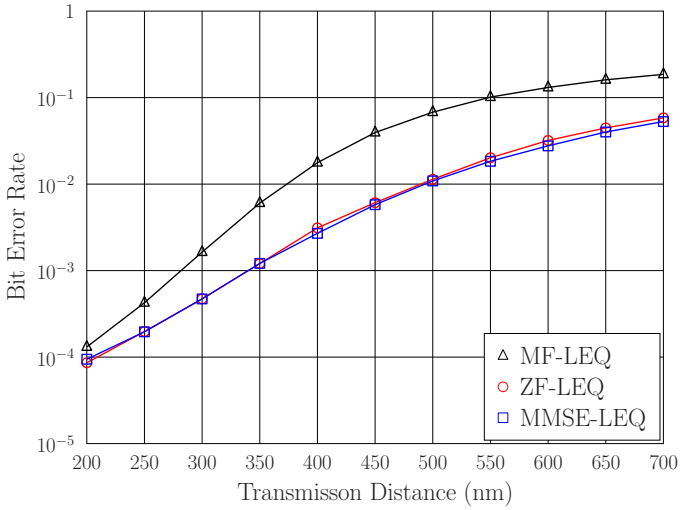

Figure 4.2: Comparison of the BER performance of the BMoSK-DMC systems employing MF-LEQ, ZF-LEQ and MMSE-LEQ, when $N = 2L+1$, $\gamma_b = 12$ dB and $T_b = 5 \times 10^{-5}$ s.

or MMSE-LEQ allows the BMoSK-DMC system to increase a transmission distance by about 125 nm, when compared with the MF-LEQ. Furthermore, Fig. 4.2 shows that both the ZF-LEQ and MMSE-LEQ achieve nearly the same performance, provided that the transmission distance is shorter than 500 nm. Beyond this distance, the MMSE-LEQ slightly outperforms the ZF-LEQ, owing to the MMSE-LEQ's noise suppression capability. Note that, as we mentioned previously in Section 4.4.2, in the BMoSK-DMC systems, the channel matrix $\boldsymbol{H}_d$ is a diagonal dominant matrix. Hence, the noise amplification problem of the ZF-LEQ operated in BMoSK-DMC systems is not severe. This can be explicitly evidenced by the results shown in Fig. 4.2, and also in the following figures.

In Figs. 4.3-4.5, we exam the BER of the bits at different locations of the detected blocks. Following Eq. (4.15), $I = 0$ represents the bit detected from $\tilde{z}_{N-1}$, $I = 1$ represents the bit detected from $\tilde{z}_{N-2}$, and so on. From Fig. 4.3 we can observe that when the value of I increases, the BER performance degrades. As what we analyzed associated with Eq. (4.15), when I increases, the decision variable is able to collect more energy for detection, but also experiences higher interference. The results in Fig. 4.3 confirm that, when the MF-LEQ is employed, the added interference outweighs the extra energy collected from the ISI components, and hence dominates the final achievable performance. Therefore, in order to achieve the best possible performance by the MF-LEQ, we can simply form the decision variable as

$$\tilde{z}_u = c_0 z_u \triangleq z_u \tag{4.26}$$

for detecting the uth bit, where z_u is given by Eq. (4.7). Here we have '$\triangleq$' due to c_0 being a positive constant. Note furthermore that the detector based on Eq. (4.26) is a symbol-based detector and has

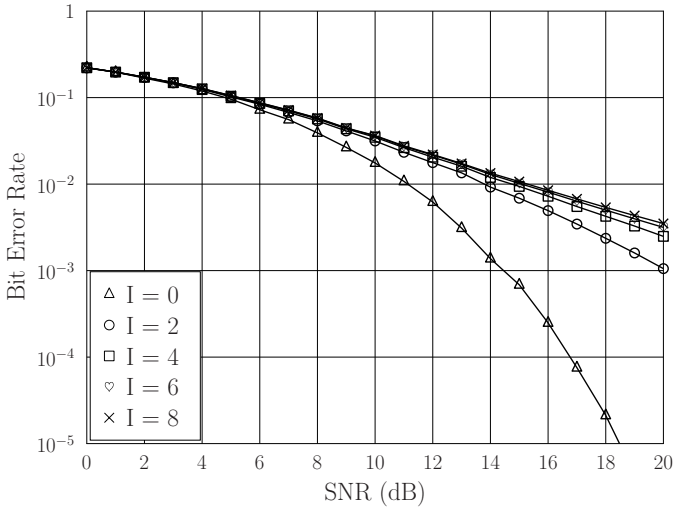

Figure 4.3: BER performance of the different bits in the BMoSK-DMC systems with MF-LEQ, when $N = 2L + 1$, $r = 350nm$ and $T_b = 5 \times 10^{-5}$ s.

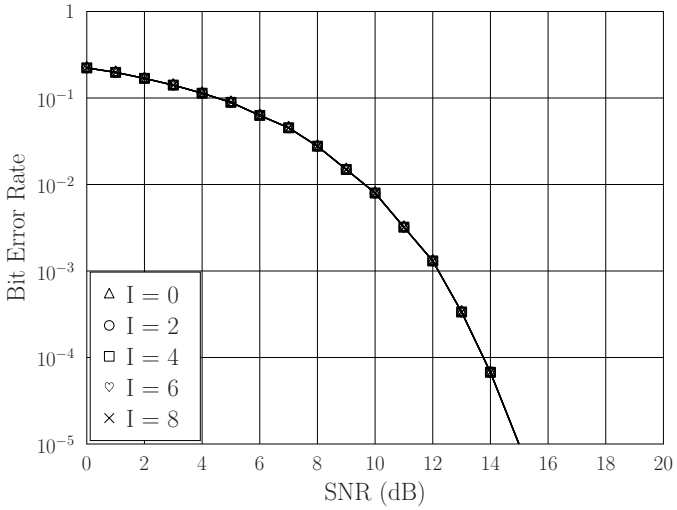

Figure 4.4: BER performance of the different bits in the BMoSK-DMC systems with ZF-LEQ, when $N = 2L + 1$, $r = 650nm$ and $T_b = 8 \times 10^{-5}$ s.

the lowest detection complexity.

By contrast, as shown in Figs. 4.4 and 4.5, after the ISI is suppressed by the ZF-LEQ or MMSE-LEQ, the detections of all the bits in one block achieve a similar BER performance, which is slightly better than that of MF-LEQ with $I = 0$.

In Fig.4.6, we show the effect of bit duration T_b (or bit rate $R_b = 1/T_b$ of the system) on the BER performance of the BMoSK-DMC systems employing the MF-LEQ, ZF-LEQ and MMSE-LEQ, respectively. Explicitly, as the bit rate decrease (or as the bit duration increases), the BER performance in all cases improves. This is because for a fixed transmission distance, the ISI reduces

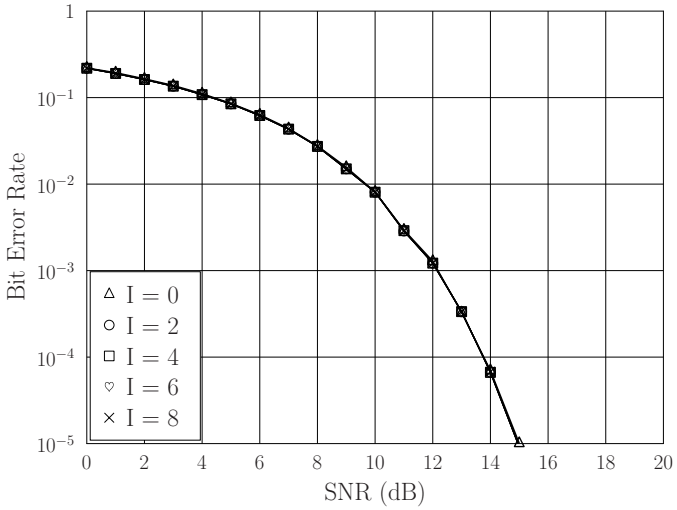

Figure 4.5: BER performance of the different bits in the BMoSK-DMC systems with MMSE-LEQ, when $N = 2L + 1$, $r = 650nm$ and $T_b = 8 \times 10^{-5}$ s.

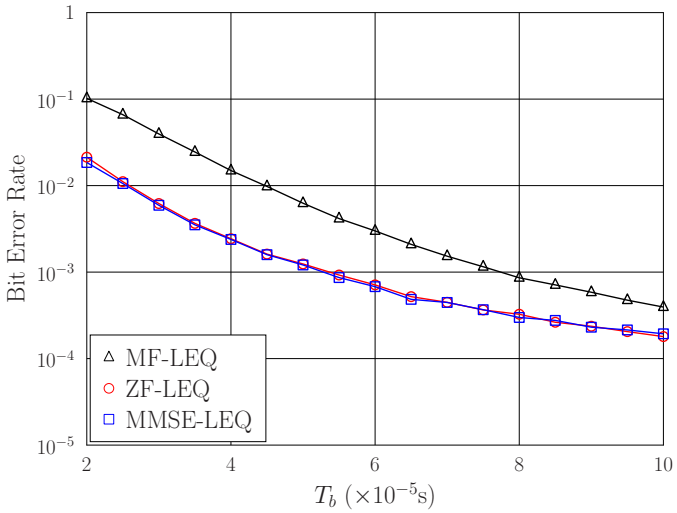

Figure 4.6: Comparison of the BER versus bit duration T_b performance of the BMoSK-DMC systems employing MF-LEQ, ZF-LEQ and MMSE-LEQ, when $N = 2L + 1$, $r =$ 350 nm and $\gamma_b = 12$ dB.

as the bit duration increases. Furthermore, both the ZF-LEQ and MMSE-LEQ achieve a similar BER performance, which outperform the MF-LEQ.

In the context of Fig.4.7, we investigate the impact of transmission distance on the BER performance of the BMoSK-DMC systems employing the MF-LEQ, ZF-LEQ and MMSE-LEQ, when a fixed bit duration is assumed. In this case, when the transmission distance becomes longer, the ISI length also increases, according to the properties of Eq. (4.1). The ISI length corresponding to different transmission distance is explicitly shown with the figure. Explicitly, due to the increase of

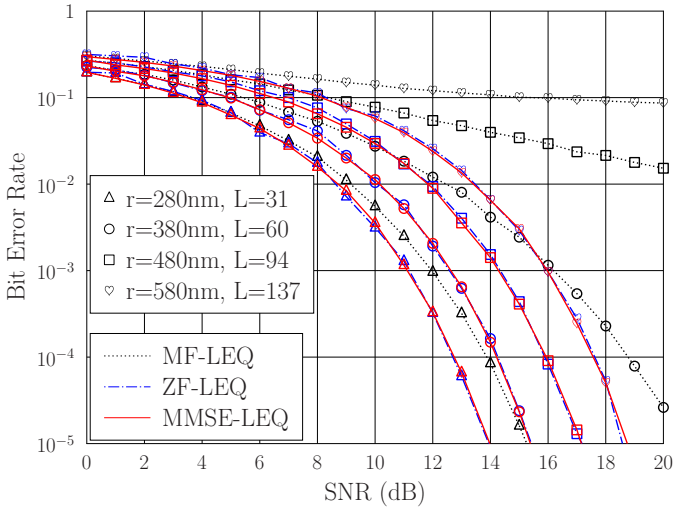

Figure 4.7: Comparison of the BER performance of the BMoSK-DMC systems with MF-LEQ, ZF-LEQ and MMSE-LEQ, when $N = 2L + 1$, $T_b = 5 \times 10^{-5}$ s.

the ISI resulted from the increase of transmission distance, for all the three LEQ schemes, the BER performance degrades as the transmission distance increases. From the results of Fig.4.7 we can be inferred that, provided that the SNR is sufficiently high, both the ZF-LEQ and MMSE-LEQ perform well, even when the transmission distance is as high as $r = 580$ nm. The BER performance achieved by the ZF-LEQ or MMSE-LEQ can significantly outperform that of the MF-LEQ, which becomes more declared, as the transmission distance becomes longer.

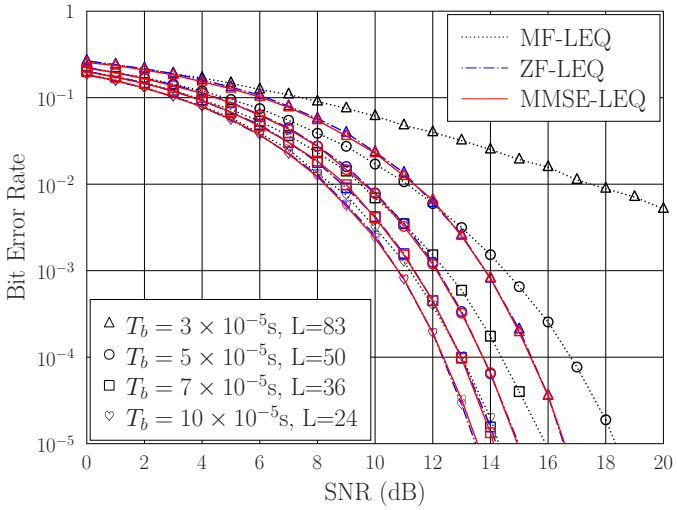

Figure 4.8: Comparison of the BER performance of the BMoSK-DMC systems with MF-LEQ, ZF-LEQ and MMSE-LEQ, when $N = 2L + 1$ and $r = 350$ nm.

Finally in Fig.4.8, we demonstrate the impact of bit duration T_b on the BER performance of

the BMoSK-DMC systems with MF-LEQ, ZF-LEQ and MMSE-LEQ, when a fixed transmission distance of $r = 350$ nm is assumed. In this case, when T_b is smaller, means that the bit rate is higher, the ISI becomes longer. Correspondingly, as seen in Fig.4.8, for all the three LEQ schemes, the BER performance improves, as T_b becomes larger or the bit rate becomes lower. Again, the BER performance attained by the ZF-LEQ or MMSE-LEQ outperforms that of the MF-LEQ, which is more significant, when ISI becomes stronger.

To this point, we would like to note that, regardless of which LEQ is employed, the BER performance of the BMoSK-DMC system at a given SNR degrades, whenever the ISI becomes stronger, no matter what the source is to make the ISI increase. This can be explicitly seen, e.g., in Figs. 4.6-4.8. This result is different from that in the conventional radio-based communication systems [80], where the advanced equalizers, including the ZF- and MMSE-based equalizers, are usually capable of achieving the performance of their corresponding systems without ISI. The reason behind is that in the conventional radio-based communication systems, the additive white Gaussian noise (AWGN) is experienced, whose statistics have nothing to do with the transmitted signals. By contrast, in the DMC communication systems including the BMoSK-DMC system considered in this chapter, as seen in Eq. (4.3)-Eq. (4.6), the noise components are related to the transmitted signals. It can be known that even when uniformly distributed data bits are assumed, the second moment of the noise components, i.e., the noise power, increases with the increase of ISI. Due to this increase of noise power, we can know that for a SNR given by Eq. (4.24), the actual SNR determining the achievable performance in fact decreases with the increase of ISI. Hence, the resultant BER performance always degrades, as the ISI becomes stronger.

4.6 Conclusion

In this chapter, we have investigated the receiving equalization techniques for the ISI mitigation and signal detection in BMoSK-DMC systems. Three types of LEQs have been considered, namely the MF-LEQ, ZF-LEQ and MMSE-LEQ. We have examined the effects of the different parameters defining transmit signals and characterizing DMC channels on the error performance of the BMoSK-DMC systems. Our studies and performance results show that to achieve the best possible performance, the MF-LEQ is reduced to a symbol-based detector, which detects individual bits independently under the ISI. In BMoSK-DMC systems, the channel matrix is diagonal dominant, which makes the ZF-LEQ highly efficient, achieving nearly the same performance as the MMSE-LEQ, although MMSE-LEQ has a slightly higher complexity than the ZF-LEQ. Both the ZF-LEQ and MMSE-LEQ are capable of effectively suppressing the ISI, yielding significantly improved detection reliability beyond the MF-LEQ. Nevertheless, both the ZF-LEQ and MMSE-LEQ are still low-complexity equalizers that are feasible for implementation, although their complexity is slightly higher than that of the MF-LEQ.

Chapter 5

Molecular Code-Division Multiple-Access: Signaling, Signal Detection and Performance

In this chapter, relying on two types of molecules, we design a molecular code-division multiple-access (MoCDMA) scheme to enable multiple nano-users (NUs) to share a common molecular communication media, and to simultaneously communicate with a receiver. We mirror the proposed MoCDMA to the conventional radio-based CDMA (RdCDMA) with binary phase-shift keying (BPSK) modulation, based on which we derive the various expressions for received signals, so that the information conveyed by different NUs can be flexibly detected on either symbol-by-symbol or block-by-block basis. Correspondingly, we introduce a range of relatively low-complexity detectors in the principles of matched-filtering (MF), zero-forcing (ZF) and minimum mean-square error (MMSE), which are operated at either symbol or block level. Furthermore, at block level, we derive the frequency (F)-domain detectors operated also in the principles of MF, ZF or MMSE. We analyze the noise characteristics in MoCDMA systems, and the complexity of the various detection schemes. Moreover, we investigate and compare the error performance of the MoCDMA systems with various detection schemes based on numerical simulations. Our studies and performance results demonstrate that the MoCDMA constitutes a promising scheme for supporting multiple-access in molecular communications, and that the various detection schemes may be implemented to attain a required complexity-reliability trade-off.

5.1 Introduction

Molecular communication (MC) belongs to a bio-inspired communication paradigm, which enables molecules to convey information from one device, such as a nano-machine, to another one

that are separated with a certain distance [7]. In MC, the diffusion-based molecular communication (DMC) has been recognized as one of the most practical transmission methods, owing to the merit that in DMC, the movements of information molecules are solely driven by the diffusion process in liquid or gas medium. In this way, DMC systems can be highly energy-efficient. In DMC systems, information can be conveyed via modifying the concentration levels of molecules at the transmitter, and correspondingly, the receiver decodes the information according to the concentration levels obtained from its detection space [1]. However, due to the random diffusive movements of molecules, DMC usually experiences long transmission delay and strong inter-symbol interference (ISI), in addition to the noise generated from the random movements of information molecules as well as from the other noisy sources in the communications environment [16].

DMC has been investigated from different perspectives, including the fundamental issues, such as, DMC channel modeling, capacity of DMC channels, data modulation and demodulation, signal detection and performance, etc., as shown in some tutorial and survey papers [7, 19, 66, 68]. DMC has also been investigated in the context of the more advanced issues, such as, ISI mitigation and advanced DMC signal detection (equalization) [20, 22, 30, 74–77, 110, 120–123], error-control coding [111, 112, 127–129], multiple-input multiple-output (MIMO) DMC [124, 125, 130–132], relay and multi-hop communications [51, 78], network coding [52–54], adaptive rate transmission [113], security and privacy [114], Internet of molecular things [115], etc. In DMC, one of the important challenges is to enable multiple molecular communication terminals, which we refer to as the nano-users (NUs) in the following description, to share a common DMC medium. For example, in an intra-body DMC-based sensor network, there are possibly a number of molecular sensors distributed at different locations, which may require to share a common DMC media in order to connect with a molecular fusion center that may be further connected with an external network or even Internet. Therefore, multiple-access DMC is one of the important techniques for DMC networking, which has hence attracted some research interest [55–59, 133].

As in the conventional radio-based wireless communications, in principle, multiple-access DMC can be implemented in different domains. The most straightforward one is the molecular-division multiple-access (MDMA) [1], which is in parallel with the frequency-division multiple-access (FDMA) in the conventional wireless communications. With MDMA, different NUs communicating with a common receiver are assigned with different types of molecules. MDMA is simple, however, when there are many NUs communicating at the same time, many types of molecules are required, which is highly challenging in terms of the generation and storage of molecules, and the design of molecular transceivers. Furthermore, separate receiving mechanisms for sensing the different types of molecules have to be implemented, which may demand a high-complexity receiver. Multiple-access DMC can also be achieved in the time (T)-domain using molecular time-division multiple-access (MoTDMA) [57, 60]. To implement MoTDMA, the time axis can be divided into frames, and a frame is further divided into a number of time slots. In this way, messages of different NUs can be delivered to the receiver using only one type of molecules via schedul-

ing different NUs to transmit on different time slots of a frame. It is well-known that a crucial requirement for implementing TDMA is that all the transmitted signals should be precisely synchronized. However, this is hardly achieved in DMC, unless all the transmit NUs have the same distance from their common receiver. This is because in DMC, the channel impulse response is non-linear, which is highly sensitive to the transmission distance, making both the amplitude and width of the received pulses from different NUs very different, if they have different distances from the receiver [38]. Furthermore, in principle, multiple-access DMC may also be achieved via space-division multiple-access, forming the MoSDMA, which distinguishes different transmit NUs based on their locations (channels) relative to the receiver. However, MoSDMA relies very much on the instantaneous channels from different NUs, which are hard to estimate due to the multiple-access interference (MAI) between different NUs.

Furthermore, multiple-access DMC can be achieved in the principles of code-division multiple-access (CDMA), forming the molecular CDMA (MoCDMA) [56, 61], via assigning different NUs the different signature codes (sequences), which can then be exploited by the receiver to detect the information conveyed by the NUs. Explicitly, MoCDMA has the advantage that it only requires a small number (typically 1 or 2) of the types of molecules. Furthermore, depending on the DMC scenarios, MoCDMA may be operated in synchronous mode or asynchronous mode, and even in the scenarios where different NUs have different distances from their common receiver or/and transmit at different data rate. In detail, in [56], a MoCDMA scheme has been proposed on the basis of a single type of molecules with the aid of the on-off keying (OOK) modulation. Correspondingly, in this type of MoCDMA, the optical spreading sequences having their elemental values in the additive group of $\{0, 1\}$ are used. Due to the on-off nature of the signature sequences, the performance results in [56] show that the achievable error performance of this MoCDMA system is in general poor, even when the number of NUs supported is as low as 2 or 4 for a spreading factor of 10. By contrast, the authors in [61] have proposed a MoCDMA scheme based on two types of molecules and the binary molecule-shift keying (BMoSK) modulation. The comparison between this MoSK-based MoCDMA with the OOK-based MoCDMA shows that the former one has the potential to significantly outperform the latter one. However, the studies in [61] are very specific, which assumes only the Walsh codes for spreading and the adaptive threshold detection. Furthermore, the system model is not sufficiently generalized for use and the performance results are only limited to the cases of 4 NUs.

Based on the above observations, in this chapter, we propose a MoCDMA scheme, which uses the spreading sequences having their chip-elements take values in the multiplicative group of $\{+1, -1\}$. This is because along with the research and development of the conventional radio-based CDMA (RdCDMA) systems, there are various classes of spreading sequences facilitating operation in $\{+1, -1\}$ having been proposed [134], which include m-sequences or maximum-length sequences (MLS), Gold-sequences, Kasami sequences, etc. These classes of sequences have good correlation properties and are suitable for operation in both synchronous and asynchronous

communications scenarios. In our MoCDMA system, in order to implement the antipodal signaling, as in [61], two types of molecules assuming the same diffusion coefficient are introduced, one type (Type-A) is for sending $+1$ signed signals and one type (Type-B) is for sending -1 signed signals. At the receiver, we assume a passive observer, which is capable of counting the numbers of molecules of both Type-A and Type-B within a detection space at chip level. We examine in detail the observations and show that the received signals in our MoCDMA can be represented in the forms fully equivalent to that in the conventional RdCDMA systems with binary phase shift keying (BPSK) modulation [126]. Then, we derive the representations for the observations at both symbol level and block level. Furthermore, we derive a block-based representation that has the same structure as that in the orthogonal frequency-division multiplexing (OFDM) systems with zero-padding [126], which hence facilitates frequency(F)-domain signal processing.

We will show that due to the slow propagation of molecules, MoCDMA signals experience various types of interference, including ISI, inter-chip interference (ICI) and multiple-access interference (MAI), in addition to the counting noise, which increases with the number of NUs. Therefore, in MoCDMA systems, it is desirable that the receiver is capable of mitigating the above-mentioned interference to the lowest level possible. However, the transceivers in DMC are usually limited by their computation capability. Hence, in this chapter, we only consider those linear detection schemes of relatively low-complexity. Specifically, we introduce the matched-filtering (MF), zero-forcing (ZF) and minimum mean-square error (MMSE) detectors, which are operated at symbol-level, block-level or in the F-domain. We analyze their complexity, as well as investigate and compare their achievable performance. Our studies will clearly demonstrate the potentials and performance-complexity trade-off of the MoCDMA systems with different detection schemes.

To summary, the novelties of this chapter are as follows:

- A MoCDMA system fully equivalent to the conventional RdCDMA system with BPSK modulation is proposed, which is hence facilitated to employ nearly any desirable signal detection techniques developed with the conventional BPSK-assisted RdCDMA systems.
- A range of relatively low-complexity linear detection schemes operated at symbol-level, block-level, or at the block-level in F-domain are developed and studied.
- The complexity of different detection schemes is analyzed, and the performance of the MoCDMA systems with various detection schemes is investigated and compared.

The rest of chapter is structured as follows. First, the system model, including transmitter, channel model and receiver, as well as the main assumptions are detailed in Section 5.2. The representations of the received signals at symbol and block levels are addressed in Section 5.3. In Section 5.4, the various signal detection schemes at both symbol level and block level are derived. Furthermore, the complexity analysis of the different detection schemes is provided in this section. In Section 5.5, based on numerical simulations, we present and compare the bit error rate (BER)

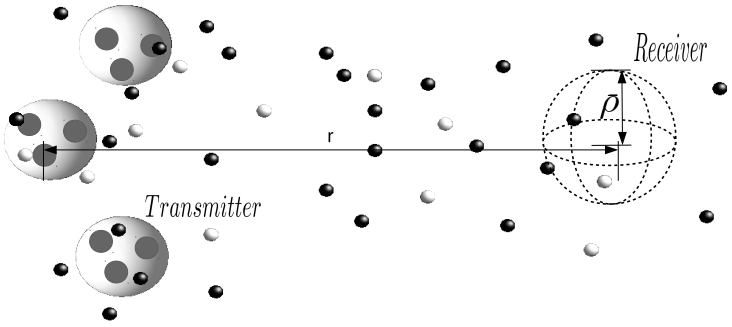

Figure 5.1: System model for MoCDMA DMC systems.

performance of the MoCDMA systems with various detection schemes. Finally, our concluding summary is provided in Section 5.6.

5.2 System Model

Assume that a DMC system is composed of K point-source NUs (transmitters) communicating with one spherical molecular receiver having a radius ρ. The locations of receiver and of all NUs are fixed. Furthermore, to focus our attention on the principles, we assume the same distance r between any of the NUs and the receiver[1], as shown in Fig. 5.1. At a NU transmitter, information is transmitted via emitting an impulse of $Q_c = Q/N$ molecules at the beginning of each of the N chips having a fixed chip-duration of T_c. Here, N is the spreading factor, and $T_s = NT_c$ is symbol-duration, or bit duration if binary modulation is employed. Below we analyze the transmitter, channel model and the receiver of MoCDMA systems in detail.

5.2.1 Transmitter

Let us assume that in the MoCDMA system, the kth NU's information to be transmitted is expressed as $\boldsymbol{B}_k = \{b_{k,0}, b_{k,1}, \ldots, b_{k,j}, \ldots\}$, where $b_{k,j} \in \{1, -1\}$. In the principle of MoCDMA, the uth bit of NU k is spread by a N length spreading sequence [135] expressed as $\boldsymbol{s}_k = [s_{k,0}, s_{k,1}, \ldots, s_{k,N-1}]^T$, where $s_{k,n} \in \{1, -1\}$, and $N = T_s/T_c$. Then, when assuming that BMoSK modulation is employed, and that Q_t molecules per pulse are emitted for the activated type (Type-A or Type-B) of molecules, the transmitted signal for the uth bit of NU k can be expressed as

$$s_k(t) = \sum_{q=0}^{N-1} \left[\frac{1 + b_{k,u}s_{k,q}}{2} Q_t \delta_A(t - uT_s - qT_c) + \frac{1 - b_{k,u}s_{k,q}}{2} Q_t \delta_B(t - uT_s - qT_c) \right], \quad k = 1, 2, \ldots, k, u = 0, 1, \ldots \tag{5.1}$$

[1] Asynchronous MoCDMA with different distances from receiver will be investigated in our future research.

where $\delta_A(t)$ and $\delta_B(t)$ represent the impulses of Type-A and Type-B molecules, respectively, which are defined as $\delta_A(0) = 1$ ($\delta_B(0) = 1$), and $\delta_A(t) = 0$ ($\delta_B(t) = 0$) for all $t \neq 0$. In (5.1), we assume that the number of molecules Q_t emitted per pulse obeys the Poisson distribution with an average of $\lambda_s = Q_c$.

5.2.2 Channel Model

We assume that molecules diffuse in a fluid medium without any flow, and that the fluid environment is stable. Hence, fluid medium's diffusion coefficient D is constant during transmission. On the other side, we assume that receiver is able to measure the concentration of molecules inside the spherical detection space. We assume that synchronization can be achieved between transmitters and receiver. Based on these assumptions, and considering that an impulse of Q_t molecules is released by a NU at $t = 0$, the concentration measured by the receiver at $t > 0$ follows Fick's diffusion Law, having the expression of [38]

$$c(t) = \frac{Q_t}{(4\pi Dt)^{\frac{3}{2}}} \exp\left(-\frac{r^2}{4Dt}\right),\ t > 0 \tag{5.2}$$

As shown in [38], $c(t)$ is a T-domain pulse function, the shape of which is dependent on the distance r between receiver and transmitter. For a given distance r, the maximum concentration can be obtained at $t_d = r^2/6D$, and is $c_{\max} = \left(\frac{3}{2\pi e}\right)^{\frac{3}{2}} \frac{Q_t}{r^3}$. As $c_{\max}$ decreases with r^3, DMCs are conceived to be only suitable for information transmission across very short distance in the fluid environments without flow.

5.2.3 Receiver

We assume that receiver is capable of identifying the two types, namely Type-A and Type-B, of molecules. Then, when assuming that there are K NUs sending signals in the form of (5.1) to receiver, the concentration difference between Type-A and Type-B molecules corresponding to the nth chip, $n = 0, 1, \ldots N-1$, of the uth bit can be expressed as

$$\begin{aligned} z(t) =& z_A(t) - z_B(t) \\ =& \sum_{k=1}^{K} \sum_{j=0}^{uN+n} \frac{1 + b_{k,[j/N]} s_{k,[j\%N]}}{2} \left[c_{A,k}((t-j)T_c) + n_{A,k,j}(t)\right] \\ & - \sum_{k=1}^{K} \sum_{j=0}^{uN+n} \frac{1 - b_{k,[j/N]} s_{k,[j\%N]}}{2} \left[c_{B,k}((t-j)T_c) + n_{B,k,j}(t)\right], \\ & (uN+n)T_c \leq t < (uN+n+1)T_c \end{aligned} \tag{5.3}$$

where $[j/N]$ is the integer part of j/N, $[j\,\%\,N]$ is the reminder of j/N, $n_{A,k,m}(t)$ and $n_{B,k,m}(t)$ are the particle counting noise caused by the corresponding types of molecules emitted by the kth NU sending the mth impulse of molecules [16]. Specifically for one particular type of

molecules, according to references [16, 74], when the average number of molecules Q_c per chip or $Q = NQ_c$ per symbol is sufficiently large, both $n_{A,k,j}(t)$ and $n_{B,k,j}(t)$ can be approximated as the Gaussian noise with zero mean and the variances of $\sigma^2_{A,k,j}(t) = \frac{1+b_{k,[j/N]}s_{k,[j\%N]}}{2V_R}c_{A,k}((t-j)T_c$ and $\sigma^2_{B,k,j}(t) = \frac{1-b_{k,[j/N]}s_{k,[j\%N]}}{2V_R}c_{B,k}((t-j)T_c)$, respectively, where $V_R = \frac{4}{3}\pi\rho^3$ is the volume of the spherical detector with a radius of ρ. For convenience, their distributions are expressed as $n_{A,k,j}(t) \sim \mathcal{N}\left(0, \sigma^2_{A,k,m}(t)\right)$ and $n_{B,k,j}(t) \sim \mathcal{N}\left(0, \sigma^2_{B,k,m}(t)\right)$, respectively.

According to the properties of $c(t)$ of (5.2), after an impulse of molecules is released by a NU at $t = 0$, the expected concentration at receiver reaches maximum at $t = t_d$. Therefore, for detection of the uth bits of K NUs, the receiver samples for the concentrations at $t = (uN+n)T_c + \hat{t}_d$ for $n = 0, 1, \ldots, N-1$, where $\hat{t}_d$ is the estimated t_d. Correspondingly, the concentration difference between Type-A and Type-B molecules at the sampling times can be expressed as

$$\begin{aligned}
Z_{u,n} &= z_A(t = (uN+n)T_c + \hat{t}_d) - z_B(t = (uN+n)T_c + \hat{t}_d) \\
&= \sum_{k=1}^{K}\sum_{j=0}^{uN+n} \frac{1 + b_{k,[j/N]}s_{k,[j\%N]}}{2}\Big[c_{A,k}\Big((uN+n-j)T_c + \hat{t}_d\Big) \\
&\qquad + n_{A,k,j}\Big((uN+n)T_c + \hat{t}_d\Big)\Big] \\
&\quad - \sum_{k=1}^{K}\sum_{j=0}^{uN+n} \frac{1 - b_{k,[j/N]}s_{k,[j\%N]}}{2}\Big[c_{B,k}\Big((uN+n-j)T_c + \hat{t}_d\Big) \\
&\qquad + n_{B,k,j}\Big((uN+n)T_c + \hat{t}_d\Big)\Big], \\
&\quad u = 0, 1, \ldots;\ n = 0, 1, \ldots, N-1
\end{aligned} \tag{5.4}$$

From the above equation we can conceive that even when there is just one NU, the detection of bit u experiences ISI from the bits sent in the front of bit u, via the index of j. Furthermore, due to multiple pulses are transmitted for each bit, there is also inter-chip interference (ICI) imposed by the chips sent with the same bit. However, from the properties of the impulse $c(t)$ we can readily observe that both ISI and ICI reduce significantly with time. Hence, our analysis below assumes that the maximum length of ISI/ICI is L chips. In this case, $Z_{u,n}$ in (5.4) can be represented in the form of

$$\begin{aligned}
Z_{u,n} &= \sum_{k=1}^{K}\sum_{j=\max\{0,uN+n-L\}}^{uN+n} \frac{1 + b_{k,[j/N]}s_{k,[j\%N]}}{2}\left[c_{A,k}(uN+n-j) + n_{A,k,j}(uN+n)\right] \\
&\quad - \sum_{k=1}^{K}\sum_{j=\max\{0,uN+n-L\}}^{uN+n} \frac{1 - b_{k,[j/N]}s_{k,[j\%N]}}{2}\left[c_{B,k}(uN+n-j) + n_{B,k,j}(uN+n)\right], \\
&\quad u = 0, 1, \ldots;\ n = 0, 1, \ldots, N-1
\end{aligned} \tag{5.5}$$

where $c_{X,k}(uN+n-j) = c_{X,k}\left((uN+n-j)T_c + \hat{t}_d\right)$ and $n_{X,k,j}(uN+n) = n_{X,k,j}\left((uN+n)T_c + \hat{t}_d\right)$, X is for A or B.

After carefully examining (5.5), we can see that, for given indices of k and j, we have either $1 + b_{k,[j/N]}s_{k,[j\%N]}/2 = 1$ and $1 - b_{k,[j/N]}s_{k,[j\%N]}/2 = 0$ when $b_{k,[j/N]}s_{k,[j\%N]} = 1$, or

$1 + b_{k,[j/N]}s_{k,[j\%N]}/2 = 0$ and $1 - b_{k,[j/N]}s_{k,[j\%N]}/2 = 1$ when $b_{k,[j/N]}s_{k,[j\%N]} = -1$. These observations infer that, at the right-hand side of (5.5), either the first term related to Type-A molecules or the second term relying on Type-B molecules appears, they never appear simultaneously for the given indices of k and j. Furthermore, in (5.5), $c_{A,k}(uN + n - j)$ and $c_{B,k}(uN + n - j)$ have the same statistical properties, the same are $n_{A,k,j}(uN + n)$ and $n_{B,k,j}(uN + n)$. Therefore, we can represent (5.5) by an equivalent form of

$$Z_{u,n} = \sum_{k=1}^{K} \sum_{j=\max\{0,uN+n-L\}}^{uN+n} b_{k,[j/N]}s_{k,[j\%N]} \left[c_k(uN + n - j) + n_{k,j}(uN + n)\right],$$
$$u = 0, 1, \ldots;\ n = 0, 1, \ldots, N - 1 \tag{5.6}$$

where $c_k(uN + n - j)$ is a sample obtained either from $c_{A,k}(t)$ or from $c_{B,k}(t)$, while $n_{k,j}(uN + n)$ has the distribution of $\mathcal{N}\left(0, \sigma^2_{k,j}(u, n)\right)$ with $\sigma^2_{k,j}(u, n) = V_R^{-1}c_k(uN + n - j)$.

Let $i = uN + n - j$. Then, (5.6) can be written as a more convenient form as

$$\begin{aligned} Z_{u,n} &= \sum_{k=1}^{K} \sum_{i=0}^{\min\{L,uN+n\}} b_{k,[(uN+n-i)/N]}s_{k,[(n-i)\%N]} \left[c_k(i) + n_{k,uN+n-i}(uN + n)\right] \\ &= \sum_{k=1}^{K} \sum_{i=0}^{\min\{L,uN+n\}} c_k(i)s_{k,[(n-i)\%N]}b_{k,[(uN+n-i)/N]} + N_{u,n}, \\ &\quad u = 0, 1, \ldots;\ n = 0, 1, \ldots, N - 1 \end{aligned} \tag{5.7}$$

where $N_{u,n} = \sum_{k=1}^{K} \sum_{i=0}^{\min\{L,uN+n\}} b_{k,[uN+n-i/N]}s_{k,[n-i\%N]}n_{k,uN+n-i}(uN + n)$, which can be well approximated by a Gaussian noise with the distribution of $\mathcal{N}\left(0, \sigma^2\right)$, where $\sigma^2 = V_R^{-1} \sum_{k=1}^{K} \sum_{i=0}^{\min\{L,uN+n\}} c_k(i) = KV_R^{-1} \sum_{i=0}^{\min\{L,uN+n\}} c_1(i)$. Note here that we have the last equation, due to the fact that $\sum_{i=0}^{\min\{L,uN+n\}} c_k(i)$ is the same for any index of k.

Equation (5.7) shows that in MoCDMA systems, there exist ISI, ICI as well as the MAI between NUs, which the receiver should handle properly in order to achieve desirable performance. Furthermore, we should draw reader attention that as shown in the previous formulas for $Z_{u,n}$, noise power in DMC is related to the transmitted signals, and any a transmitted molecule simultaneously contributes to the increase of noise power, in addition to its role for conveying information. This is because noise, referred to as *counting noise*, in DMC is the result of molecule's (random) Brownian motions, which cause an unwanted perturbation to the concentration (or number of molecules) predicted from the Fick's diffusion law [16]. Therefore, in our MoCDMA system, noise power increases with the number of NUs supported by the system, and also increases with the ISI/ICI and MAI. These effects are very different from that in the conventional RdCDMA systems, where environment noise, which is usually modeled as additive white Gaussian noise (AWGN), is independent of the transmitted signals, and hence of the number of users supported by a RdCDMA system. Furthermore, it is also independent of any other interfering signals, such as ISI, MAI, etc. In Section 5.5, we will discuss this issue further, when we study the error performance of MoCDMA systems.

Having obtained the equivalent formula, as shown in (5.7), for the observations, below we derive the representation of received signals in various forms.

5.3 Representation of Received Signals

For facilitating the detection, we assume that data are transmitted in blocks of length M bits per block, and that there is no inter-block interference. A data block transmitted by the kth NU is expressed as $\boldsymbol{b}_k = [b_{k,0}, b_{k,1}, \ldots, b_{k,M-1}]$. In this case, for a given block, the transmitted signals are spread over $MN + L$ observations, from $Z_{0,0}$ to $Z_{M-1,N-1}$ and also from $Z_{M-1,N}$ to $Z_{M-1,N+L-1}$. However, from the properties of $c(t)$ we know that, beyond its peak value, $c(t)$ decreases significantly with the increase of time, meaning that the interference generated by a transmitted pulse decreases significantly with the increase of time. Therefore, for simplicity, we assume that $L \leq N$. However, if in practice or in study where $L > N$, we can absorb the interference generated by those pulses at time $t > NT_c$ into the Gaussian noise, and assume that the Gaussian noise's variance is $\sigma^2 = KV_R^{-1} \sum_{i=0}^{\min\{L,uN+n\}} c_1(i) + \sigma_0^2$, where σ_0^2 is contributed by the above-mentioned interference.

Let

$$\begin{aligned} \boldsymbol{z} &= [Z_{0,0}, \ldots, Z_{0,N-1}; \ldots, Z_{M-1,0}, \ldots, Z_{M-1,N-1}; Z_{M-1,N}, \ldots, Z_{M-1,N+L-1}]^T, \\ \boldsymbol{n} &= [N_{0,0}, \ldots, N_{0,N-1}; \ldots, N_{M-1,0}, \ldots, N_{M-1,N-1}; N_{M-1,N}, \ldots, N_{M-1,N+L-1}]^T \end{aligned} \tag{5.8}$$

Then, it can be shown that we can write all the observations corresponding to the M data bits as

$$\boldsymbol{z} = \sum_{k=1}^{K} \boldsymbol{C}\boldsymbol{S}_k \boldsymbol{b}_k + \boldsymbol{n} \tag{5.9}$$

where $\boldsymbol{C}$ is a $([MN + L] \times MN)$ matrix, each column of which is constructed by zeros and the vector $\boldsymbol{c} = [c(0), c(1), \ldots, c(L)]^T$, and the vector continuously occupies $(L + 1)$ positions starting from the ith position in the ith column. Note that, the matrix $\boldsymbol{C}$ is the same for all NUs, and hence the index k is removed. In (5.9), $\boldsymbol{S}_k = \boldsymbol{I}_M \otimes \boldsymbol{s}_k$, where $\otimes$ denotes the Kronecker product operation. Hence, $\boldsymbol{S}_k$ is a $(MN \times M)$ matrix. Additionally, $\boldsymbol{n}$ is Gaussian distributed with zero mean and a covariance matrix of $\sigma^2 \boldsymbol{I}_{MN+L}$.

Below we consider the variants or approximated versions of (5.9), in order to facilitate different detection schemes.

First, if we cut the last L terms of $\boldsymbol{z}$ and add them correspondingly to the first L terms, we can obtain a representation of

$$\tilde{\boldsymbol{z}} = \sum_{k=1}^{K} \tilde{\boldsymbol{C}}\boldsymbol{S}_k \boldsymbol{b}_k + \tilde{\boldsymbol{n}} \tag{5.10}$$

where both $\tilde{\boldsymbol{z}}$ and $\tilde{\boldsymbol{n}}$ are MN-length, and we can still approximate $\tilde{\boldsymbol{n}}$ by the Gaussian distribution with zero mean but a covariance matrix of $\sigma^2 \boldsymbol{I}_{MN}$, $\tilde{\boldsymbol{C}}$ is now a $(MN \times MN)$ circulant matrix [136] having the diagonal elements being $c(0)$.

Second, if we only consider the observations corresponding to one bit, such as bit $u > 1$, then the observation vector has the form of

$$\begin{aligned} \boldsymbol{z}_u &= \sum_{k=1}^{K} \boldsymbol{C}_2 \boldsymbol{S}_{k2} \boldsymbol{b}_{k2} + \boldsymbol{n}_u \\ &= \sum_{k=1}^{K} \left(\boldsymbol{C}_0 \boldsymbol{s}_k b_{k,u} + \boldsymbol{C}_{-1} \boldsymbol{s}_k b_{k,u-1} \right) + \boldsymbol{n}_u \end{aligned} \tag{5.11}$$

where $\boldsymbol{z}_u = [Z_{u,0}, Z_{u,1}, \ldots, Z_{u,N-1}]^T$, $\boldsymbol{n}_u = [N_{u,0}, N_{u,1}, \ldots, N_{u,N-1}]^T$, $\boldsymbol{C}_2$ is a $(N \times 2N)$ matrix, with the last row structured by zeros and $\text{Rev}(\boldsymbol{c}^T) = [c(L), c(L-1), \ldots, c(0)]$, and $c(0)$ is positioned at the location of $(N-1, 2N-1)$. For the other rows, the non-zero elements are just the shifts of these $(L+1)$ elements, and the shift for the ith row is $(N-1-i)$ for $i = 0, 1, \ldots, N-2$. In (5.11), $\boldsymbol{S}_{k2} = \boldsymbol{I}_2 \otimes \boldsymbol{s}_k$ and $\boldsymbol{b}_{k2} = [b_{k,u-1}, b_{k,u}]^T$. According to the system model, bit u experiences interference from bit $(u-1)$. Hence, we can explicitly represent this as the second equation in (5.11), where $\boldsymbol{C}_{-1}$ is constituted by the first N columns of $\boldsymbol{C}_2$, while $\boldsymbol{C}_0$ is constituted by the other N columns of $\boldsymbol{C}_2$.

It can be shown that the second equation in (5.11) can also be expressed as

$$\boldsymbol{z}_u = \sum_{k=1}^{K} \left(\tilde{\boldsymbol{S}}_{k,0} \boldsymbol{c} b_{k,u} + \tilde{\boldsymbol{S}}_{k,-1} \boldsymbol{c} b_{k,u-1} \right) + \boldsymbol{n}_u \tag{5.12}$$

where $\boldsymbol{c} = [c_0, c_1, \ldots, c_L]^T$, $\tilde{\boldsymbol{S}}_{k,0}$ is a $N \times (L+1)$ lower diagonal matrix constructed as: a) $s_{k,0}$ is on diagonal; b) the first column is given by $\boldsymbol{s}_k$; and c) the other columns are obtained from the shifts of the first column after deleting those elements outside the matrix. $\tilde{\boldsymbol{S}}_{k,-1}$ is also a $N \times (L+1)$, which has only L none-zero rows starting from the bottom (row $(N-1)$) of the matrix. These none-zero rows can be constructed as follows: a) $s_{k,N-1}$ is on diagonal; b) from left to right, the first none-zero row has the non-zero elements of $s_{k,N-1}, s_{k,N-2}, \ldots, s_{k,N-L}$; and c) the other rows are obtained from the shifts of this first none-zero row after deleting those elements outside the matrix.

Additionally, when writing in more compact forms, (5.9) can be expressed as

$$\boldsymbol{z} = \boldsymbol{C}\boldsymbol{S}\boldsymbol{b} + \boldsymbol{n} \tag{5.13}$$

where $\boldsymbol{S} = [\boldsymbol{S}_1, \boldsymbol{S}_2, \ldots, \boldsymbol{S}_K]$ and $\boldsymbol{b} = \left[\boldsymbol{b}_1^T, \boldsymbol{b}_2^T, \ldots, \boldsymbol{b}_K^T\right]^T$. The presentation of (5.10) can be equivalently represented as

$$\tilde{\boldsymbol{z}} = \tilde{\boldsymbol{C}}\boldsymbol{S}\boldsymbol{b} + \tilde{\boldsymbol{n}} \tag{5.14}$$

where $\boldsymbol{S}$ and $\boldsymbol{b}$ have the same forms as that in (5.13). Correspondingly, (5.11) can be written as

$$\begin{aligned} \boldsymbol{z}_u =& \boldsymbol{C}_2 \boldsymbol{S}_2 \boldsymbol{b}_2 + \boldsymbol{n}_u \\ =& \boldsymbol{C}_0 \tilde{\boldsymbol{S}}_2 \boldsymbol{b}_u + \boldsymbol{C}_{-1} \tilde{\boldsymbol{S}}_2 \boldsymbol{b}_{u-1} + \boldsymbol{n}_u \end{aligned} \tag{5.15}$$

where $\boldsymbol{S}_2 = [\boldsymbol{S}_{12}, \boldsymbol{S}_{22}, \ldots, \boldsymbol{S}_{K2}]$, $\boldsymbol{b}_2 = [\boldsymbol{b}_{12}, \boldsymbol{b}_{22}, \ldots, \boldsymbol{b}_{K2}]^T$, $\tilde{\boldsymbol{S}}_2 = [\boldsymbol{s}_1, \boldsymbol{s}_2, \ldots, \boldsymbol{s}_K]$, $\boldsymbol{b}_u = \left[b_{1,u}^T, b_{2,u}^T, \ldots, b_{K,u}^T\right]^T$, and $\boldsymbol{b}_{u-1} = [b_{1,u-1}, b_{2,u-1}, \ldots, b_{K,u-1}]^T$. Finally, corresponding to (5.12), we have

$$\boldsymbol{z}_u = \tilde{\boldsymbol{S}}_0 \tilde{\boldsymbol{C}} \boldsymbol{b}_u + \tilde{\boldsymbol{S}}_{-1} \tilde{\boldsymbol{C}} \boldsymbol{b}_{u-1} + \boldsymbol{n}_u \tag{5.16}$$

where $\tilde{\boldsymbol{S}}_0 = \left[\tilde{\boldsymbol{S}}_{1,0}, \tilde{\boldsymbol{S}}_{2,0}, \ldots, \tilde{\boldsymbol{S}}_{K,0}\right]$, $\tilde{\boldsymbol{S}}_{-1} = \left[\tilde{\boldsymbol{S}}_{1,-1}, \tilde{\boldsymbol{S}}_{2,-1}, \ldots, \tilde{\boldsymbol{S}}_{K,-1}\right]$, $\tilde{\boldsymbol{C}} = \boldsymbol{I}_K \otimes \boldsymbol{c}$, and $\boldsymbol{b}_u, \boldsymbol{b}_{u-1}$ are the same as that in (5.15).

Having the observations represented in different forms, as shown in (5.9) - (5.16), let us consider the signal detection in the next section.

5.4 Signal Detection

In this section, we consider a range of detection algorithms. Considering that in DMC, communications terminals are usually simple devices and hard to implement high-complexity non-linear computation relied detection schemes, we consider only the linear detection schemes, which have relatively low complexity and facilitate the implementation in DMC systems. Specifically, we consider the matched-filtering (MF) detection, which is sometimes called as correlation detection, zero-forcing (ZF) detection, and minimum mean-square error (MMSE) detection.

For linear detection schemes, the decision variable for the uth bit of the kth NU can in general be expressed as

$$d_{k,u} = \boldsymbol{w}_{k,u}^T \boldsymbol{z}, \; u = 0, 1, \ldots, M-1; \; k = 1, 2, \ldots, K \tag{5.17}$$

where $\boldsymbol{w}_{k,u}$ is a weight vector, or called as receiver processing or post-processing vector, to be derived in the following subsections in different situations, $\boldsymbol{z}$ can be $\boldsymbol{z}$, $\tilde{\boldsymbol{z}}$, or $\boldsymbol{z}_u$, as shown in the Section 5.3.

Based on the decision variable $d_{k,u}$, the decision for the uth bit of the kth NU is simply made as

$$\hat{b}_{k,u} = \begin{cases} 1, & \text{if } d_{k,u} > 0 \\ 0 \text{ (or } -1), & \text{else} \end{cases} \tag{5.18}$$

for $u = 0, 1, \ldots, M-1$ and $k = 1, 2, \ldots, K$.

Let us now consider in detail the various detection schemes for deriving $\boldsymbol{w}_{k,u}$ by first addressing the symbol-based detection.

5.4.1 Symbol-Based Signal Detection

5.4.1.1 Matched-Filtering Detection

The MF-detector is derived based on (5.12). When MF detection is considered, the receiver does not attempt to suppress any interference, but with the objective to maximize the received energy by exploiting the knowledge about the transmitted signals as well as the channels. Let us assume that the receiver attempts to detect $b_{k,u}$ sent by the kth NU, whose spreading code $\boldsymbol{s}_k$ is known to the receiver. Furthermore, if the receiver knows $\boldsymbol{c}$, which contains the expected densities at different times, then the receiver can form the weight vector as

$$\boldsymbol{w}_{k,u} = \tilde{\boldsymbol{S}}_{k,0}\boldsymbol{c} \tag{5.19}$$

Upon substituting it into (5.17) associated with replacing $\boldsymbol{z}$ by $\boldsymbol{z}_u$ given by (5.12), we have

$$\begin{aligned} d_{k,u} =& \boldsymbol{w}_{k,u}^T \boldsymbol{z}_u \\ =& \|\tilde{\boldsymbol{S}}_{k,0}\boldsymbol{c}\|^2 b_{k,u} + \sum_{l\neq k}^{K} \boldsymbol{c}^T \tilde{\boldsymbol{S}}_{k,0}^T \tilde{\boldsymbol{S}}_{l,0}\boldsymbol{c} b_{l,u} + \sum_{l=1}^{K} \boldsymbol{c}^T \tilde{\boldsymbol{S}}_{k,0}^T \tilde{\boldsymbol{S}}_{l,-1}\boldsymbol{c} b_{l,u-1} + \boldsymbol{c}^T \tilde{\boldsymbol{S}}_{k,0}^T \boldsymbol{n}_u \end{aligned} \tag{5.20}$$

At the right-hand side of (5.20), the first term is the desired term, the second term is the MAI from the $(K-1)$ interfering NUs, the third term is the ISI from the $(u-1)$th bits sent by the K NUs, while the final term is noise.

In the case that the receiver does not know $\boldsymbol{c}$, we can set $\boldsymbol{c}$ in (5.19) as a $(L+1)$-length all-one vector expressed as $\mathbf{1}$, yielding

$$\boldsymbol{w}_{k,u} = \tilde{\boldsymbol{S}}_{k,0}\mathbf{1} \tag{5.21}$$

Correspondingly, we have

$$d_{k,u} = \mathbf{1}^T \tilde{\boldsymbol{S}}_{k,0}^T \tilde{\boldsymbol{S}}_{k,0}\boldsymbol{c} b_{k,u} + \sum_{l\neq k}^{K} \mathbf{1}^T \tilde{\boldsymbol{S}}_{k,0}^T \tilde{\boldsymbol{S}}_{l,0}\boldsymbol{c} b_{l,u} + \sum_{l=1}^{K} \mathbf{1}^T \tilde{\boldsymbol{S}}_{k,0}^T \tilde{\boldsymbol{S}}_{l,-1}\boldsymbol{c} b_{l,u-1} + \mathbf{1}^T \tilde{\boldsymbol{S}}_{k,0}^T \boldsymbol{n}_u \tag{5.22}$$

Following the tradition in wireless communications [80], the detector of (5.20) carries out maximal ratio combining (MRC), which is referred to as the MRC-detector, while (5.22) carries out equal-gain combining (EGC), which is referred to as the EGC-detector.

The MRC-detector is capable of maximizing the signal-to-noise ratio (SNR), when all the interference is approximated as Gaussian noise, as shown below. Upon substituting $\boldsymbol{z}_u$ from (5.12) into (5.17), we obtain

$$\begin{aligned} d_{k,u} =& \boldsymbol{w}_{k,u}^T \left(\sum_{k=1}^{K} \left(\tilde{\boldsymbol{S}}_{k,0}\boldsymbol{c} b_{k,u} + \tilde{\boldsymbol{S}}_{k,-1}\boldsymbol{c} b_{k,u-1} \right) + \boldsymbol{n}_u \right) \\ =& \boldsymbol{w}_{k,u}^T \tilde{\boldsymbol{S}}_{k,0}\boldsymbol{c} b_{k,u} + n_{k,u} \end{aligned} \tag{5.23}$$

where $n_{k,u} = \boldsymbol{w}_{k,u}^T \left(\sum_{l\neq k}^{K} \tilde{\boldsymbol{S}}_{l,0}\boldsymbol{c} b_{l,u} + \sum_{l=1}^{K} \tilde{\boldsymbol{S}}_{l,-1}\boldsymbol{c} b_{l,u-1} + \boldsymbol{n}_u \right)$, which is the processed interference plus noise. When we approximate this interference plus noise as a Gaussian random variable with

zero mean and power of $P_n = \boldsymbol{w}_{k,u}^T \boldsymbol{R}_I \boldsymbol{w}_{k,u}$, where $\boldsymbol{R}_I$ is the autocorrelation matrix of interference-plus-noise, i.e., of $\boldsymbol{I}_n = \sum_{l\neq k}^{K} \tilde{\boldsymbol{S}}_{l,0}\boldsymbol{c}b_{l,u} + \sum_{l=1}^{K} \tilde{\boldsymbol{S}}_{l,-1}\boldsymbol{c}b_{l,u-1} + \boldsymbol{n}_u$, the SNR for detection of $b_{k,u}$ can be expressed as

$$\begin{aligned}\gamma_{k,u} &= \frac{\|\boldsymbol{w}_{k,u}^T \tilde{\boldsymbol{S}}_{k,0}\boldsymbol{c}\|^2}{\boldsymbol{w}_{k,u}^T \boldsymbol{R}_I \boldsymbol{w}_{k,u}} \\ &= \frac{\|(\boldsymbol{R}_I^{1/2}\boldsymbol{w}_{k,u})^T (\boldsymbol{R}_I^{-1/2}\tilde{\boldsymbol{S}}_{k,0}\boldsymbol{c})\|^2}{\boldsymbol{w}_{k,u}^T \boldsymbol{R}_I \boldsymbol{w}_{k,u}} \\ &\leq \frac{\|(\boldsymbol{R}_I^{1/2}\boldsymbol{w}_{k,u})^T\|^2 \|(\boldsymbol{R}_I^{-1/2}\tilde{\boldsymbol{S}}_{k,0}\boldsymbol{c})\|^2}{\boldsymbol{w}_{k,u}^T \boldsymbol{R}_I \boldsymbol{w}_{k,u}}\end{aligned} \tag{5.24}$$

where we have the '$\leq$' relationship due to the Cauchy-Schwartz inequality [88, 136]. It is well-known that in (5.24), the equality is attained, if and only if

$$\boldsymbol{R}_I^{1/2}\boldsymbol{w}_{k,u} = a\boldsymbol{R}_I^{-1/2}\tilde{\boldsymbol{S}}_{k,0}\boldsymbol{c} \tag{5.25}$$

where a is a constant. Therefore,

$$\boldsymbol{w}_{k,u} = a\boldsymbol{R}_I^{-1}\tilde{\boldsymbol{S}}_{k,0}\boldsymbol{c},\ u = 0,1,\ldots,M-1;\ k = 1,2,\ldots,K \tag{5.26}$$

The detector with the weight vector of (5.26) is capable of maximizing the signal to interference-plus-noise ratio (SINR), after mitigating the interference in $\boldsymbol{I}_n$ [126]. However, computing (5.26) requires the knowledge about the spreading sequences used by all NUs, as well as the discrete channel impulse response of $\boldsymbol{c}$. If the receiver only has the knowledge about the NU being detected, i.e., $\boldsymbol{s}_k$ (or $\tilde{\boldsymbol{S}}_{k,0}$) and $\boldsymbol{c}$, the receiver is reduced to a MRC-detector. In this case, the receiver has to approximate $\boldsymbol{I}_n$ as a Gaussian noise vector, which has a covariance matrix of $\sigma_I^2\boldsymbol{I}_N$. Consequently, (5.26) is reduced to

$$\boldsymbol{w}_{k,u} = \frac{a}{\sigma_I^2}\tilde{\boldsymbol{S}}_{k,0}\boldsymbol{c} \equiv \tilde{\boldsymbol{S}}_{k,0}\boldsymbol{c} \tag{5.27}$$

which is (5.19). Therefore, MRC-detector maximizes SNR, after approximating all interference as Gaussian noise.

5.4.1.2 Zero-Forcing Detection

It is convenient to derive the symbol-based ZF-detector using either (5.15) or (5.16). The requirement for implementation of ZF detection is that the receiver employs the knowledge about the spreading sequences used by all NUs and their channel impulse responses to the receiver, so that the receiver can construct $\boldsymbol{C}_0$ and $\bar{\boldsymbol{S}}_2$ as seen in (5.15), or $\bar{\boldsymbol{C}}$ and $\tilde{\boldsymbol{S}}_0$ seen in (5.16). If this is the case, and if the ZF-detector is based on (5.15), the decision variables for the K NUs can be obtained as

$$\begin{aligned}\boldsymbol{d}_u &= \left(\boldsymbol{C}_0\bar{\boldsymbol{S}}_2\right)^{\dagger}\boldsymbol{z}_u \\ &= \left(\bar{\boldsymbol{S}}_2^T\boldsymbol{C}_0^T\boldsymbol{C}_0\bar{\boldsymbol{S}}_2\right)^{-1}\bar{\boldsymbol{S}}_2^T\boldsymbol{C}_0^T\boldsymbol{z}_u,\ u = 0,1,\ldots,M-1\end{aligned} \tag{5.28}$$

where $\boldsymbol{A}^{\dagger}$ denotes the pseudo-inverse of $\boldsymbol{A}$ [136]. Upon substituting $\boldsymbol{z}_u$ from (5.15) into (5.28), we have

$$\boldsymbol{d}_u = \boldsymbol{b}_u + \underbrace{\left(\bar{\boldsymbol{S}}_2^T \boldsymbol{C}_0^T \boldsymbol{C}_0 \bar{\boldsymbol{S}}_2\right)^{-1} \bar{\boldsymbol{S}}_2^T \boldsymbol{C}_0^T \left(\boldsymbol{C}_{-1} \bar{\boldsymbol{S}}_2 \boldsymbol{b}_{u-1} + \boldsymbol{n}_u\right)}_{\text{ISI and noise}} \tag{5.29}$$

From (5.29) we can see that the MAI is fully removed. However, there is still ISI.

Similarly, if the ZF-detector is derived based on (5.16), the decision variables for the K NUs can be obtained as

$$\begin{aligned} \boldsymbol{d}_u &= \left(\tilde{\boldsymbol{S}}_0 \tilde{\boldsymbol{C}}\right)^{\dagger} \boldsymbol{z}_u \\ &= \left(\tilde{\boldsymbol{C}}^T \tilde{\boldsymbol{S}}_0^T \tilde{\boldsymbol{S}}_0 \tilde{\boldsymbol{C}}\right)^{-1} \tilde{\boldsymbol{C}}^T \tilde{\boldsymbol{S}}_0^T \boldsymbol{z}_u,\ u = 0, 1, \ldots, M-1 \end{aligned} \tag{5.30}$$

which can also fully remove the MAI.

Specifically, the weight vector for detecting the uth bit of the kth NU is given by the kth column of $\left(\boldsymbol{C}_0 \bar{\boldsymbol{S}}_2\right)^{\dagger}$ in (5.28) or of $\left(\tilde{\boldsymbol{S}}_0 \tilde{\boldsymbol{C}}\right)^{\dagger}$ in (5.30), which can be expressed in detail as

$$\boldsymbol{w}_{k,u} = \left(\boldsymbol{C}_0 \bar{\boldsymbol{S}}_2 \left(\bar{\boldsymbol{S}}_2^T \boldsymbol{C}_0^T \boldsymbol{C}_0 \bar{\boldsymbol{S}}_2\right)^{-1}\right)(\ : k),\ k = 1, 2, \ldots, K \tag{5.31}$$

or

$$\boldsymbol{w}_{k,u} = \left(\tilde{\boldsymbol{S}}_0 \tilde{\boldsymbol{C}} \left(\tilde{\boldsymbol{C}}^T \tilde{\boldsymbol{S}}_0^T \tilde{\boldsymbol{S}}_0 \tilde{\boldsymbol{C}}\right)^{-1}\right)(\ : k),\ k = 1, 2, \ldots, K \tag{5.32}$$

In the above two equations, $\boldsymbol{A}(\ : k)$ denotes the kth column of $\boldsymbol{A}$.

5.4.1.3 Minimum Mean-Square Error Detection

We derive the MMSE-detector based on (5.12). A similar one can be derived from (5.11).

The MMSE-detector is derived based on minimizing the mean-square error (MSE) between the estimated data and the actual data, which can be obtained from the optimization problem of

$$\begin{aligned} \boldsymbol{w}_{k,u} &= \arg\min_{\boldsymbol{w}} \left\{E\left[\|b_{k,u} - d_{k,u}\|^2\right]\right\} \\ &= \arg\min_{\boldsymbol{w}} \left\{E\left[\|b_{k,u} - \boldsymbol{w}^T \boldsymbol{z}_u\|^2\right]\right\} \end{aligned} \tag{5.33}$$

Let us define the cost function as

$$\begin{aligned} J_{k,u}(\boldsymbol{w}) &= E\left[\|b_{k,u} - \boldsymbol{w}^T \boldsymbol{z}_u\|^2\right] \\ &= 1 - 2\boldsymbol{r}_{ku}^T \boldsymbol{w} + \boldsymbol{w}^T \boldsymbol{R}_u \boldsymbol{w} \end{aligned} \tag{5.34}$$

where $\boldsymbol{R}_u$ is the auto-correlation matrix of $\boldsymbol{z}_u$, which can be derived from (5.12) and expressed as

$$\boldsymbol{R}_u = \sum_{k=1}^{K} \left(\tilde{\boldsymbol{S}}_{k,0} + \tilde{\boldsymbol{S}}_{k,-1}\right) \boldsymbol{c}\boldsymbol{c}^T \left(\tilde{\boldsymbol{S}}_{k,0} + \tilde{\boldsymbol{S}}_{k,-1}\right)^T + \sigma^2 \boldsymbol{I}_N \tag{5.35}$$

In (5.34), $\boldsymbol{r}_{ku}$ is the cross-correlation between $\boldsymbol{z}_u$ and $b_{k,u}$, which is

$$\boldsymbol{r}_{k,u} = \tilde{\boldsymbol{S}}_{k,0}\boldsymbol{c} \tag{5.36}$$

Upon taking the derivatives of $J_{k,u}(\boldsymbol{w})$ with respect to $\boldsymbol{w}$ and equating the result to zero, we obtain

$$\frac{\partial J_{k,u}(\boldsymbol{w})}{\partial(\boldsymbol{w})} = -2\boldsymbol{r}_{k,u} + 2\boldsymbol{R}_u\boldsymbol{w} = 0 \tag{5.37}$$

from which we obtain the optimum weight vector implementing MMSE-detector as

$$\begin{aligned}\boldsymbol{w}_{k,u} =& \boldsymbol{R}_u^{-1}\boldsymbol{r}_{k,u} \\ =& \left(\sum_{k=1}^{K}\left(\tilde{\boldsymbol{S}}_{k,0}+\tilde{\boldsymbol{S}}_{k,-1}\right)\boldsymbol{c}\boldsymbol{c}^T\left(\tilde{\boldsymbol{S}}_{k,0}+\tilde{\boldsymbol{S}}_{k,-1}\right)^T + \sigma^2\boldsymbol{I}_N\right)^{-1}\tilde{\boldsymbol{S}}_{k,0}\boldsymbol{c}, \\ & u = 0,1,\ldots,M-1;\ k = 1,2,\ldots,K\end{aligned} \tag{5.38}$$

From (5.38) we are inferred that for implementing the MMSE-detector, the receiver needs the knowledge about the spreading sequences used by all NUs and the channel impulse responses to the receiver, so that the receiver can construct the matrices/vectors as seen in the formula. Furthermore, the receiver requires the noise power expressed as σ^2. In this case, the MMSE-detector is capable of achieving a best trade-off between interference (including both MAI and ISI) suppression and noise suppression. In practice, if accurate noise power is not available, we may set it as an approximated non-zero value, which should not result in a big performance loss, provided that the approximated value is not too different from the real noise power.

Additionally, when the receiver does not have the knowledge of the spreading sequences of the K NUs, but that of the desired NU, the receiver has to approximate $\boldsymbol{R}_u$ as a constant diagonal matrix, making (5.38) be reduced to the weight vector of the MRC-detector.

Having considered the symbol-based detection, below we derive the block-based detector. It is known that in the conventional RdCDMA systems, symbol-based detectors have lower detection complexity, the block-based detectors are able to achieve better error performance. In Section 5.5, we will compare the two classes of detectors in the context of the MoCDMA.

5.4.2 Block-Based Signal Detection

In this section we derive the block-based detection schemes, which detect the information bits sent by a NU simultaneously based on the block-based observations, as shown in (5.9) or (5.13).

5.4.2.1 Matched-Filtering Detection

Again, let us first consider the MF-based detection of the data bits sent by the kth NU. From (5.9) we can readily know that the weight matrix for simultaneously detecting the block of M bits sent

by the kth NU is

$$\boldsymbol{W}_k = \boldsymbol{C}\boldsymbol{S}_k,\ k = 1, 2, \ldots, K \tag{5.39}$$

Correspondingly, the decision variables for the M bits sent by the kth NU is

$$\begin{aligned}\boldsymbol{d}_k =& \boldsymbol{W}_k^T \boldsymbol{z} \\ =& \boldsymbol{S}_k^T \boldsymbol{R}_C \boldsymbol{S}_k \boldsymbol{b}_k + \sum_{l \neq k}^{K} \boldsymbol{S}_k^T \boldsymbol{R}_C \boldsymbol{S}_l \boldsymbol{b}_l + \boldsymbol{n}'\end{aligned} \tag{5.40}$$

where $\boldsymbol{n}' = \boldsymbol{S}_k^T \boldsymbol{C}^T \boldsymbol{n}$, $\boldsymbol{R}_C = \boldsymbol{C}^T \boldsymbol{C}$ is the auto-correlation matrix of $\boldsymbol{C}$.

From (5.39) we can conceive that the weight vector $\boldsymbol{w}_{k,u}$ for detecting the uth bit sent by the kth NU is

$$\boldsymbol{w}_{k,u} = (\boldsymbol{C}\boldsymbol{S}_k)(\ : u),\ u = 0, 1, \ldots, M-1 \tag{5.41}$$

Equation (5.40) infers that the detection of a bit of NU k experiences both MAI and ISI/ICI. The MAI is characterized by the second term at the right-hand side, while ISI/ICI is given via the non-diagonal non-zero entries in $\boldsymbol{S}_k^T \boldsymbol{R}_C \boldsymbol{S}_k$. The merit with the detection is that, when given the spreading codes of NUs as well as their locations, $\boldsymbol{W}_k$ and hence $\boldsymbol{w}_{k,u}$ are fixed. Therefore, they can be repeatedly used without requiring re-computation.

5.4.2.2 Zero-Forcing Detection

For the ZF-detector, it is convenient to start with (5.13), from which we can find that the weight matrix achieving zero-forcing in terms of the KM bits sent by K NUs is

$$\boldsymbol{W} = (\boldsymbol{C}\boldsymbol{S})^{\dagger} \tag{5.42}$$

Assume that $K \leq N$, making $\boldsymbol{C}\boldsymbol{S}$ be column rank full. In this case, we have

$$\boldsymbol{W} = \boldsymbol{C}\boldsymbol{S}(\boldsymbol{S}^T \boldsymbol{R}_C \boldsymbol{S})^{-1} \tag{5.43}$$

which includes inverting a $(MK \times MK)$ matrix. Fortunately, when the receiver has the knowledge of the spreading sequences and the positions of NUs, all the matrices are fixed. Hence, $\boldsymbol{W}$ is also fixed. Upon substituting (5.42) into (5.13), it can be shown that the decision variables for the KM bits sent by the K NUs are given by

$$\boldsymbol{d} = \boldsymbol{W}^T \boldsymbol{z} = \boldsymbol{b} + \boldsymbol{n}' \tag{5.44}$$

where $\boldsymbol{n}' = (\boldsymbol{S}^T \boldsymbol{R}_C \boldsymbol{S})^{-1} \boldsymbol{S}^T \boldsymbol{C}^T \boldsymbol{n}$. Explicitly, (5.44) shows that both the MAI and ISI/ICI are fully suppressed.

If we concern the weight matrix for detection one NU or that for detecting one bit, we can obtain them from (5.43), and for the kth NU we have

$$\begin{aligned}\boldsymbol{W}_k =& \boldsymbol{W}(\ :(k-1)M \rightarrow kM)\\ \boldsymbol{w}_{k,u} =& \boldsymbol{W}(\ :(k-1)M+u)\end{aligned} \tag{5.45}$$

where $\boldsymbol{W}(\ :(k-1)M \rightarrow kM)$ means selecting the columns from the $(k-1)M$-th to the kM-th columns of $\boldsymbol{W}$.

As above-mentioned, ZF-detector has the capability to fully remove MAI and ISI/ICI, but it conventionally has the disadvantages of noise amplification [126]. Below we derive the block-based MMSE-detector for MoCDMA.

5.4.2.3 Minimum Mean-Square Error Detection

Let us derive the block-based MMSE-detector based on (5.9), to directly derive the weight matrix for detecting the M bits sent by NU k. Then, the optimization problem for finding the MMSE solution to detect NU k is given by

$$\boldsymbol{W}_k = \arg\min_{\boldsymbol{W}} \left\{ E\left[\|\boldsymbol{d}_k - \boldsymbol{W}^T\boldsymbol{z}\|^2 \right] \right\} \tag{5.46}$$

Let us define the cost function as

$$J_k(\boldsymbol{W}) = E\left[\|\boldsymbol{d}_k - \boldsymbol{W}^T\boldsymbol{z}\|^2 \right] \tag{5.47}$$

Upon assuming that data bits are uniform random variables, we can obtain the covariance matrix of $\boldsymbol{d}_k - \boldsymbol{W}^T\boldsymbol{z}$ as

$$\boldsymbol{J}_k(\boldsymbol{W}) = \boldsymbol{I}_M - \boldsymbol{R}_{\boldsymbol{z}\boldsymbol{b}_k}^T\boldsymbol{W} - \boldsymbol{W}^T\boldsymbol{R}_{\boldsymbol{z}\boldsymbol{b}_k} + \boldsymbol{W}^T\boldsymbol{R}_{\boldsymbol{z}}\boldsymbol{W} \tag{5.48}$$

where $\boldsymbol{R}_z = E[\boldsymbol{z}\boldsymbol{z}^T]$ and $\boldsymbol{R}_{\boldsymbol{z}\boldsymbol{b}_k} = E[\boldsymbol{z}\boldsymbol{b}_k]$, which are given by

$$\begin{aligned}\boldsymbol{R}_{\boldsymbol{z}} =& \sum_{k=1}^{K} \boldsymbol{C}\boldsymbol{S}_k\boldsymbol{S}_k^T\boldsymbol{C}^T + \sigma^2\boldsymbol{I}_{MN+L},\\ \boldsymbol{R}_{\boldsymbol{z}\boldsymbol{b}_k} =& \boldsymbol{C}\boldsymbol{S}_k\end{aligned} \tag{5.49}$$

The optimum weight matrix $\boldsymbol{W}_k$ can be obtained by differentiating the trace of $\boldsymbol{J}_k(\boldsymbol{W})$ with respect to $\boldsymbol{W}$ and equating the result to zero, i.e.,

$$\frac{\partial \mathrm{Tr}\left(\boldsymbol{J}_k(\boldsymbol{W})\right)}{\partial \boldsymbol{W}} = -2\boldsymbol{R}_{\boldsymbol{z}\boldsymbol{b}_k} + 2\boldsymbol{R}_{\boldsymbol{z}}\boldsymbol{W} = \boldsymbol{0} \tag{5.50}$$

the solution of which is the optimal solution, given as

$$\boldsymbol{W}_k = \boldsymbol{R}_{\boldsymbol{z}}^{-1}\boldsymbol{R}_{\boldsymbol{z}\boldsymbol{b}_k},\ k = 1, 2, \ldots, K \tag{5.51}$$

Upon substituting the results in (5.49) into (5.50), we obtain

$$\begin{aligned}\boldsymbol{W}_k &= \left(\sum_{k=1}^{K} \boldsymbol{C}\boldsymbol{S}_k\boldsymbol{S}_k^T\boldsymbol{C}^T + \sigma^2\boldsymbol{I}_{MN+L}\right)^{-1}\boldsymbol{C}\boldsymbol{S}_k \\ &= \left(\boldsymbol{C}\boldsymbol{S}\boldsymbol{S}^T\boldsymbol{C}^T + \sigma^2\boldsymbol{I}_{MN+L}\right)^{-1}\boldsymbol{C}\boldsymbol{S}_k \end{aligned} \tag{5.52}$$

Furthermore, if we record the uth column of $\boldsymbol{S}_k$ as $\boldsymbol{s}_{k,u} = \boldsymbol{S}_k(\ :u)$, the weight vector for detecting the uth bit of the kth NU is

$$\boldsymbol{w}_{k,u} = \left(\boldsymbol{C}\boldsymbol{S}\boldsymbol{S}^T\boldsymbol{C}^T + \sigma^2\boldsymbol{I}_{MN+L}\right)^{-1}\boldsymbol{C}\boldsymbol{s}_{k,u},\ u = 0,1,\ldots,M-1 \tag{5.53}$$

Note that, from (5.52) and (5.53) we can conceive that the weight matrix for detecting all the KM bits of the K NUs is

$$\boldsymbol{W} = \left(\boldsymbol{C}\boldsymbol{S}\boldsymbol{S}^T\boldsymbol{C}^T + \sigma^2\boldsymbol{I}_{MN+L}\right)^{-1}\boldsymbol{C}\boldsymbol{S} \tag{5.54}$$

$$= \boldsymbol{C}\boldsymbol{S}\left(\boldsymbol{S}^T\boldsymbol{R}_C\boldsymbol{S} + \sigma^2\boldsymbol{I}_{MK}\right)^{-1} \tag{5.55}$$

where (5.55) is obtained from (5.54) upon applying the matrix inverse lemma.

As shown in (5.52) and (5.53), the matrices are fixed, provided that the spreading codes are given and that the positions of NUs are fixed, making the concentrations presenting at receiver constants. In this case, the matrix inverse in the above formulas is only required to be computed once during a communication session, which hence does not generate significant increase of complexity, in comparison to the MF-detector. Furthermore, although it may not fully suppress the MAI and ISI/ICI, as the ZF-detector does, the MMSE-detector is capable of seeking a best trade-off between interference suppression and noise suppression. Hence, in general, the MMSE-detector outperforms the corresponding ZF-detector in terms of the achievable error performance.

5.4.3 Frequency-Domain Detection

The F-domain detectors can be derived based on (5.10), where $\tilde{\boldsymbol{C}}$ is a circulant matrix that can be diagonalized using fast Fourier transform (FFT). Let the FFT matrix be $\boldsymbol{F}$, which satisfies $\boldsymbol{F}\boldsymbol{F}^H = \boldsymbol{F}^H\boldsymbol{F} = \boldsymbol{I}$ [126]. Then, the observation equation of (5.10) can be written as

$$\tilde{\boldsymbol{z}} = \sum_{k=1}^{K} \boldsymbol{F}^H\boldsymbol{\Lambda}\boldsymbol{F}\boldsymbol{S}_k\boldsymbol{b}_k + \tilde{\boldsymbol{n}} \tag{5.56}$$

after applying $\tilde{\boldsymbol{C}} = \boldsymbol{F}^H\boldsymbol{\Lambda}\boldsymbol{F}$, where $\boldsymbol{\Lambda} = \text{diag}\{\lambda_0, \lambda_1, \ldots, \lambda_{MN-1}\}$ is a diagonal matrix. Therefore, upon executing the FFT operation to transform (5.10) to the F-domain, we obtain

$$\boldsymbol{y} = \boldsymbol{F}\tilde{\boldsymbol{z}} = \sum_{k=1}^{K} \boldsymbol{\Lambda}\boldsymbol{F}\boldsymbol{S}_k\boldsymbol{b}_k + \boldsymbol{n}' \tag{5.57}$$

where $\boldsymbol{n}' = \boldsymbol{F}\tilde{\boldsymbol{n}}$. Note that in principle, $\boldsymbol{y}$ gives the observations of MN subcarriers [126], and hence in the F-domain.

Consequently, by following the principles of F-domain equalization (FDE) [97, 126, 137, 138], the decision variables derived from (5.57) for detecting $\boldsymbol{b}_k$ of NU k can be formed as

$$\begin{aligned}\boldsymbol{d}_k =& \boldsymbol{S}_k^T \boldsymbol{F}^H \boldsymbol{W}_k^H \boldsymbol{y} \\ =& \boldsymbol{S}_k^T \boldsymbol{F}^H \boldsymbol{W}_k^H \boldsymbol{F}\tilde{\boldsymbol{z}} \\ =& \boldsymbol{S}_k^T \boldsymbol{F}^H \boldsymbol{W}_k^H \boldsymbol{\Lambda} \boldsymbol{F} \boldsymbol{S}_k \boldsymbol{b}_k + \sum_{l \neq k}^{K} \boldsymbol{S}_k^T \boldsymbol{F}^H \boldsymbol{W}_k^H \boldsymbol{\Lambda} \boldsymbol{F} \boldsymbol{S}_l \boldsymbol{b}_l + \bar{\boldsymbol{n}}'\end{aligned} \tag{5.58}$$

where $\bar{\boldsymbol{n}}' = \boldsymbol{S}_k^T \boldsymbol{F}^H \boldsymbol{W}_k^H \boldsymbol{n}'$. The above operations on $\boldsymbol{y}$ are as follows. First, the FDE is operated by multiplying $\boldsymbol{W}_k^H$ on $\boldsymbol{y}$. Then, multiplying $\boldsymbol{F}^H$ on the FDE results transforms signals from F-domain to time (T)-domain. Finally, despreading is achieved by multiplying $\boldsymbol{S}_k^T$, yielding the decision variables for detecting the M bits of the kth NU.

There are various FDE schemes available in conventional wireless communications [97, 126, 137, 138]. As in the previous sections, we consider the low-complexity MF-, ZF- and MMSE-detectors. Correspondingly, we have the weight matrices as below [126]:

$$\begin{aligned}&\text{MF: } \boldsymbol{W}_k = \text{diag}\{\lambda_0, \lambda_1, \ldots, \lambda_{MN-1}\} \\ &\text{ZF: } \boldsymbol{W}_k = \text{diag}\left\{\frac{1}{\lambda_0^*}, \frac{1}{\lambda_1^*}, \ldots, \frac{1}{\lambda_{MN-1}^*}\right\} \\ &\text{MMSE: } \boldsymbol{W}_k = \text{diag}\left\{\frac{\lambda_0}{|\lambda_0|^2 + \sigma^2}, \frac{\lambda_1}{|\lambda_1|^2 + \sigma^2}, \ldots, \frac{\lambda_{MN-1}}{|\lambda_{MN-1}|^2 + \sigma^2}\right\}\end{aligned} \tag{5.59}$$

It can be shown that, when orthogonal spreading codes are assigned to different NUs, and when ZF-FDE is used, we have

$$\boldsymbol{d}_k = \mu \boldsymbol{b}_k + \bar{\boldsymbol{n}}' \tag{5.60}$$

where μ is a constant. Hence, there is no ISI and MAI.

Additionally, when we express the uth column of $\boldsymbol{S}_k$ as $\boldsymbol{s}_{k,u}$, the weight vector for detecting $b_{k,u}$ is

$$\boldsymbol{w}_{k,u} = \boldsymbol{F}^H \boldsymbol{W}_k^H \boldsymbol{F} \boldsymbol{s}_{k,u} \tag{5.61}$$

which can be directly applied to (5.17) associated with replacing $\boldsymbol{z}$ in (5.17) by $\tilde{\boldsymbol{z}}$, for obtaining the decision variable of $d_{k,u}$ under the principle of FDE.

5.4.4 Complexity of Detection Schemes

In this section, we analyze the complexity of the detection schemes described above. Considering that the weight vector $\boldsymbol{w}_{k,u}$ in symbol-based detection and $\boldsymbol{W}_k$ in block-based detection are fixed in

one session of detection, we consider the complexity for preparing $\boldsymbol{w}_{k,u}$ or $\boldsymbol{W}_k$ and the complexity for detection separately. Furthermore, in order to describe the complexity of the different cases, we assume that the arithmetic operation of individual elements in a vector or matrix has the complexity of $\mathcal{O}(1)$. Additionally, the complexity is expressed in terms of one bit and one NU.

Let us first consider the symbol-based detection. As shown in Section 5.4.1, all the detection schemes considered have the decision variable for detecting one bit formed by (5.17). Hence, once the N-length weight vector is prepared, the detection complexity of all the detectors, namely, the MF- (MRC, EGC), ZF- and MMSE-detectors, is the same and is $\mathcal{O}(N)$ per bit per NU. By contrast, the complexity for preparation of the weight vectors of different detection schemes may be different. First, for the MF-detector, $\boldsymbol{w}_{k,u}$ is given by (5.19) for the MRC-detector, and by (5.21) for the EGC-detector, both of which have the complexity of $\mathcal{O}(N(L+1))$. For the ZF-detector, corresponding to (5.15) and (5.16), the weight vectors are given by (5.31) and (5.32), respectively. It is known that the complexity for inverting a $(K \times K)$ dimensional matrix is $\mathcal{O}(K^3)$ [139]. Hence, we can readily derive that the complexity for preparing the weight vector for the ZF-detector based on (5.31) is $\mathcal{O}((N+K)^2)$, while for that based on (5.32) is $\mathcal{O}(N(L+1)+2NK+K^2)$. Since we assumed that $N \geq L+1$, the complexity for preparation of the ZF-detector is $\mathcal{O}((N+K)^2)$ per bit per NU. Finally, the complexity for preparing the weight vector based on (5.38) for the symbol-based MMSE-detector can be similarly analyzed, which is $\mathcal{O}(N^3/K + 2N^2 + 3N(L+1) + N/K)$.

For the block-based detectors, first, the MF-detector computes (5.39) for the weight matrix to detect the M bits of a NU. Considering that $\boldsymbol{C}$ has at most $(L+1)$ non-zero elements per row, and $\boldsymbol{S}_k$ has exactly N non-zero elements per column, and that the positions of all these non-zero elements are known, we can find that the complexity to compute (5.39) is $\mathcal{O}(M(MN+L)\min\{N, L+1\})$. Dividing it by M gives the complexity of $\mathcal{O}((MN+L)\min\{N, L+1\})$ per bit per NU. Similarly, the MF-detector detects M bits simultaneously based on (5.40), which has the complexity of $\mathcal{O}(M(MN+L))$ for detecting M bits. Hence, the complexity per bit per NU is $\mathcal{O}(MN+L)$. Note that, this complexity is the upper-bound. This is because in the block-based MF-detector (the same are the ZF- and MMSE-detectors), there should be many zero elements in the weight matrix $\boldsymbol{W}$, the corresponding computations of which are not needed.

The block-based ZF-detector computes the weight matrix based on (5.43). In detail, computing $\boldsymbol{CS}$ needs $\mathcal{O}((MN+L)MK \times \min\{L+1, N\})$, computing $\boldsymbol{S}^T\boldsymbol{C}^T\boldsymbol{CS}$ needs $\mathcal{O}(M^2K^2(MN+L))$, computing the inverse of $(\boldsymbol{S}^T\boldsymbol{C}^T\boldsymbol{CS})$ has the complexity of $\mathcal{O}(M^3K^3)$, Finally, computing $\boldsymbol{CS}(\boldsymbol{S}^T\boldsymbol{C}^T\boldsymbol{CS})^{-1}$ needs the complexity of $\mathcal{O}(M^2K^2(MN+L))$. In total, computing $\boldsymbol{W}$ in (5.43) has the complexity of $\mathcal{O}((MN+L)MK \times \min\{L+1, N\} + 2M^2K^2(MN+L) + M^3K^3)$. Considering this complexity is for detecting MK bits, the per bit per NU complexity for preparation of ZF detection is then $\mathcal{O}((MN+L) \times \min\{L+1, N\} + 2MK(MN+L) + M^2K^2)$. After $\boldsymbol{W}$, which is of size $(MK \times (MN+L))$, is prepared, the detection complexity of the block-based ZF-detector can be found to be $\mathcal{O}(MN+L)$ per bit per NU.

Table 5.1: Complexity of preparation and that of detection for various detection schemes.

Symbol-based	Preparation	Detection
MF	$\mathcal{O}(N(L+1))$	$\mathcal{O}(N)$
ZF	$\mathcal{O}((N+K)^2)$	$\mathcal{O}(N)$
MMSE	$\mathcal{O}(N^3/K + 2N^2 + 3N(L+1) + N/K)$	$\mathcal{O}(N)$
Block-based		
MF	$\mathcal{O}((MN+L)\min\{N, L+1\})$	$\mathcal{O}(MN+L)$
ZF	$\mathcal{O}((MN+L)\times\min\{L+1, N\} + 2MK(MN+L) + M^2K^2)$	$\mathcal{O}(MN+L)$
MMSE	$\mathcal{O}((MN+L)\times\min\{L+1, N\} + 2MK(MN+L) + M^2K^2)$	$\mathcal{O}(MN+L)$
Frequency-domain		
MF	$\mathcal{O}(MN^2\times\min\{L+1, \log(MN)\} + MN^2\log(MN))$	$\mathcal{O}(2N(\log(MN)+1))$
ZF	$\mathcal{O}(MN^2\times\min\{L+1, \log(MN)\} + MN^2\log(MN))$	$\mathcal{O}(2N(\log(MN)+1))$
MMSE	$\mathcal{O}(MN^2\times\min\{L+1, \log(MN)\} + MN^2\log(MN))$	$\mathcal{O}(2N(\log(MN)+1))$

For the block-based MMSE-detector, upon comparing (5.43) for the block-based ZF-detector with (5.54) for the MMSE-detector, we can readily figure out the complexity for preparing $\boldsymbol{W}$ for the MMSE-detector, which is the same as that for the block-based ZF-detector, after ignoring the MK additions related to $\sigma^2\boldsymbol{I}_{MK}$. Furthermore, the detection complexity of the block-based MMSE-detector is also the same as that of the block-based ZF-detector.

Finally, for the F-domain detectors, if we ignore the slight differences among the $\boldsymbol{W}_k$'s seen in (5.59), all the three detectors have the same complexity for both preparation and detection. Specifically for preparation, the receiver needs to compute $\boldsymbol{\Lambda} = \boldsymbol{F}\tilde{\boldsymbol{C}}\boldsymbol{F}^H$. It is known that the FFT (IFFT) on a MN-length vector has the complexity of $\mathcal{O}(MN\log(MN))$. We also know that each row of $\tilde{\boldsymbol{C}}$ has only $(L+1)$ non-zero elements. Hence, it can be readily analyze that the complexity for preparation of $\boldsymbol{W}_k$ is $\mathcal{O}(MN^2\times\min\{L+1, \log(MN)\} + MN^2\log(MN))$. For detection, according to (5.58), it includes the operations of FFT, F-domain processing, IFFT and despread. In addition to the FFT (IFFT), multiplying a diagonal matrix of $(MN\times MN)$ dimensional on a vector of length-MN has the complexity of $\mathcal{O}(MN)$. Furthermore, remembering that $\boldsymbol{s}_{k,u}$ has only N non-zero elements, multiplying $\boldsymbol{S}_k^T$ with a MN-length vector has the complexity of $\mathcal{O}(MN)$. Therefore, the total computation for detection has a complexity of $\mathcal{O}(2MN(\log(MN)+1))$, which is for detection M bits. Hence, the detection complexity is $\mathcal{O}(2N(\log(MN)+1))$ per bit per NU. Note that, this complexity is also an upper-bound, as $\boldsymbol{W}_k$ in (5.59) may not need to be updated for detecting every block, and there are also some matrix operations do not need to be repeatedly computed.

The complexity related to the different detection schemes is summarized in Table 5.1. The block-based detectors in general have higher complexity than the corresponding symbol-based detectors and F-domain detectors, if long blocks are detected. Furthermore, the complexity for preparing the block-based ZF- and MMSE-detectors increases with M^2. Therefore, in practice, it is not desirable to detect long blocks, unless significant performance gain is attainable.

5.5 Performance Results and Discussion

In this section, we demonstrate and compare the BER performance of the MoCDMA systems with different detection schemes and different parameters. In our simulations, unless specifically notified, the default assumptions and parameters are as follows: maximum length sequences (MLS) with $N = 16$, data block length of $M = 100$, ISI length of $L = 10$, number of NUs of $K = 4$, SNR of $SNR = 20$ dB, symbol duration of $T = 5 \times 10^{-4}$ s, diffusion coefficient of $D = 2.2 \times 10^{-9}$ nm/s, and the radius of receiver of $\rho = 15$ nm. Following [110], the SNR is defined as

$$\gamma_b = \frac{c_0^2}{E[\sigma_0^2]} = \frac{c_0^2}{\frac{1}{V_R}c_0} = V_R c_0 \tag{5.62}$$

which is the ratio between the power received from a single pulse of molecules and the corresponding noise power generated by this pulse.

In addition to MLS, in our studies we also compare the performance of the MoCDMA systems with respectively the gold sequences and orthogonal Walsh codes as spreading sequences [135]. However, we should note that MLS are periodic sequences, one of which can be obtained from another one with a certain number of shifts [135]. On the other side, MoCDMA conflicts severe ISI and ICI. In this case, if the period of MLS is N, meaning that each symbol duration is spread by a whole sequence, the ICI in the current symbol duration and the ISI in the following symbol durations will be fully despread by another sequence assigned to another NU, generating high MAI. Based on the above observation and in order to reduce interference, in our studies, the spreading sequences are generated as follows. First, we generate a MLS with its period larger than $K * N$. Then, this sequence is divided into K sections, from each of which one spreading sequence of length N is obtained. When the spreading sequences are designed in this way, the sequences assigned to the K NUs are randomized. Furthermore, they can guarantee that no sequence is despread by another sequence in the current and also in the following K symbol durations, which hence allows MAI mitigation.

Let us first compare the different detection schemes considered in this chapter in Fig. 5.2, where all the detection schemes described in Section 5.4 are respectively considered. Explicitly, due to the severe interference, which includes ISI/ICI and MAI, the MF-based detectors can hardly provide reasonable performance. Specifically, when the symbol-based detector is considered, the MRC-detector is able to support $K = 2$ or even $K = 4$ NUs, but at the cost of significantly increased SNR, inferring an enormously increase of the number of molecules emitted per molecular pulse by the transmitter. By contrast, the EGC-detector does not work, even when the number of NUs supported is as low as $K = 2$. Similar observations are also obtained for the MF-detector operated with both the block-based detection and the F-domain detection. When comparing the MF-detector with the EGC-detector, as shown in Fig. 5.2(a), the EGC-detector is about 5 dB worse than the MF-detector, when $K = 1$ and at the BER of 10^{-2}. This observation implies that using the amplitude information in molecular detection is critical.

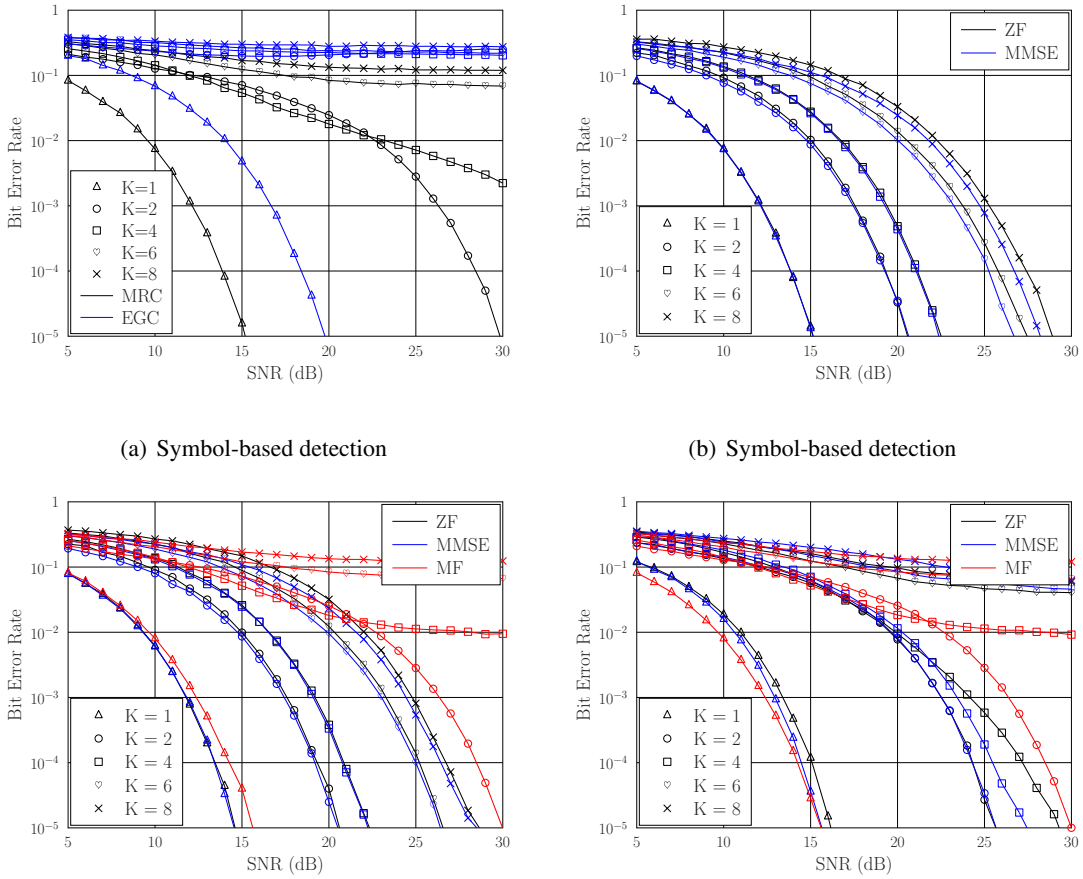

(a) Symbol-based detection

(b) Symbol-based detection

(c) Block-based detection

(d) Frequency-domain detection

Figure 5.2: Comparison of BER performance of the MoCDMA systems with various detection schemes, when $T = 5 \times 10^{-4}s$, $r = 380nm$, $L = 10$, $N = 16$ and $M = 100$, supporting $K = 1, 2, 4, 6$, or 8 NUs.

Compared to the MF-detector, both the ZF-detector and MMSE-detector are highly efficient, when they are operated with both the symbol- and block-based detection. As shown in Fig. 5.2(b) and Fig. 5.2(c), even when the number of NUs supported is as high as $K = 8$, the BER curves appear in the water-falling form, and a low BER can be attainable, provided that the SNR is sufficiently high. When comparing the ZF-detector with the MMSE-detector, we can see that the MMSE-detector slightly outperforms the ZF-detector. This observation becomes clearer, as K increases or/and when SNR is low.

Fig. 5.2(b) and Fig. 5.2(c) show that when K increases, the BER performance degrades significantly. In the conventional RdCDMA systems with ZF- or MMSE-detector, it is well-known that when the number of users supported is smaller than the spreading factor by several numbers, which is the case considered with Fig. 5.2 where $K \leq N/2$, the BER performance should be close to the single-user BER bound[2] [126]. However, this does not happen with the MoCDMA systems

[2]Single-user BER bound is the BER of the system supporting single user.

with ZF- or MMSE-detector. This phenomena can be explained in detail as follows with the aid of (5.7). As we discussed at the end of Section 5.2, in the conventional communications systems, background noise has nothing to do with the transmitted signals. Hence, the power of background noise maintains unchanged, no matter how many users are simultaneously supported. By contrast, in DMC systems, noise (more accurately counting noise) is directly generated by the transmitted signals, and noise power is linearly proportional to the number of molecules emitted from the transmitters. Hence, in our MoCDMA systems, the noise power increases linearly with the number of NUs supported by the system. In this case, for a given SNR γ_b as defined in (5.62), which is also the SNR depicted in the figures, the effective SNR is in fact decreases significantly with the increase of K of the number of NUs supported. From the discussion in Section 5.2 and (5.7), we can know that increasing the value of K results in the increase of ISI/ICI and MAI, all of which in return result in the increase of noise power, making the effective SNR significantly reduce. Therefore, as seen in Fig. 5.2(b) and Fig. 5.2(c), in order to maintain the same BER, such as 10^{-4}, significant increase of SNR is required, when the number of NUs is increased.

When the symbol-based detection (Fig. 5.2(b)) is replaced by the block-based detection (Fig. 5.2(c)), we can see only slight performance improvement for either ZF- or MMSE-detector. Therefore, the dominant interference in MoCDMA systems can usually be effectively suppressed by the symbol-based ZF- or MMSE-detectors.

Finally, when comparing the F-domain detection (Fig. 5.2(d)) with the block-based detection (Fig. 5.2(c)), we can observe explicit performance degradation of the F-domain detectors. As shown in Fig. 5.2(d), even when the ZF- or MMSE-detector is employed, the MoCDMA system is unable to support $K = 6$ or more NUs. However, we should note that when the channel is time-variant, a F-domain detection scheme has lower complexity than the corresponding block-based detection scheme. As seen in Sections 5.4.2.2 and 5.4.2.3, both the block-based ZF- and MMSE-detectors need to invert a big-sized matrix. By contrast, as shown in Section 5.4.3, all the F-domain detection schemes, which include the ZF- and MMSE-detectors, are free from the matrix inversion.

In the second set of figures shown in Fig. 5.3, we depict the BER performance of the MoCDMA systems versus the transmission distance r, when the symbol-based detection (Fig. 5.3(a)), block-based detection (Fig. 5.3(b)) and the F-domain detection (Fig. 5.3(c)) are respectively employed, and when the MoCDMA systems use a spreading factor of $N = 16$ to support $K = 4$ NUs. From the results we have the following observations. First, as the transmission distance increases, the BER performance achieved by all the detectors becomes worse. This is because as the distance increases, the received molecular density pulse becomes wider, resulting in that the peak value of the pulse becomes smaller, and hence stronger interference as well as higher noise power. Second, due to the MAI, the EGC detector in general performs poorly, even when the transmission distance is as low as 200 nm. The MF-detector and the F-domain detector perform reasonably, if the transmission distance is relatively short, such as less than 350 nm. By contrast, the symbol- and block-based ZF- and MMSE-detectors are capable of providing promising BER performance, even when the trans-

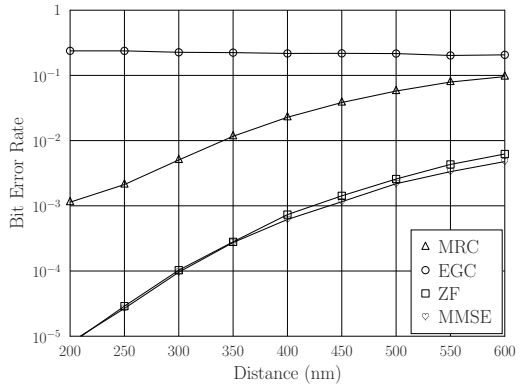

(a) Symbol-Based detection

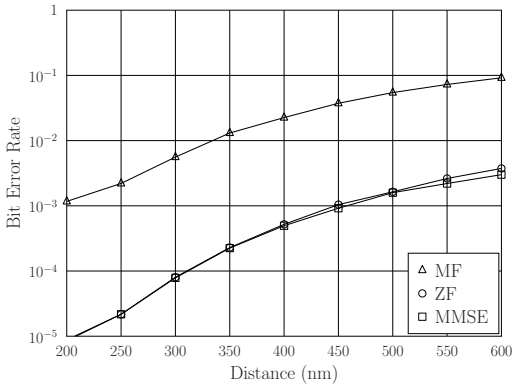

(b) Block-based detection

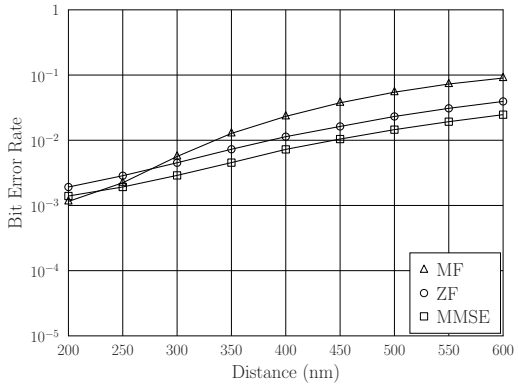

(c) Frequency-domain detection

Figure 5.3: BER performance versus transmission distance of the MoCDMA systems with symbol-based, block-based and F-domain detection, respectively, when SNR= 20dB, $T = 5 \times 10^{-4}s$, L=10, $M = 10$, N=16 and $K = 4$.

mission distance is as high as 600 nm, the maximum distance considered. Finally, from Fig. 5.3(a) and Fig. 5.3(b), we observe that the MMSE-detector performs slightly better than the ZF-detector, when $r > 400$ nm. By contrast, Fig. 5.3(c) shows that the F-domain MMSE-detector always outperforms the F-domain ZF-detector over the distance range as considered.

In Fig. 5.4, we demonstrate the impact of the ISI length exploited by the receiver on the BER performance of the MoCDMA systems with symbol-based (Fig. 5.4(a)) and block-based (Fig. 5.4(b)) detectors, respectively, in the principles of both ZF- and MMSE-detectors. Note that for the F-domain detectors, all the ISI is always invoked due to the FFT operation. In our investigation, we assume that the total ISI length is $L = 10$, and the ISI length exploited by the receiver is $L_{Rx} = 1, 2, 4, 6$ or 10. The results of Fig. 5.4 show that for both the symbol- and block-based detection with either ZF- or MMSE-detector, the BER performance in general improves as more ISI is exploited by the receiver. However, provided $L_{Rx} \geq 6$, the BER performance achieved by both the ZF- and MMSE-detectors in the two cases is nearly the same. This observation infers that although there is still ISI beyond $L_{Rx} = 6$, the ISI is in general ignorable, as the result that the

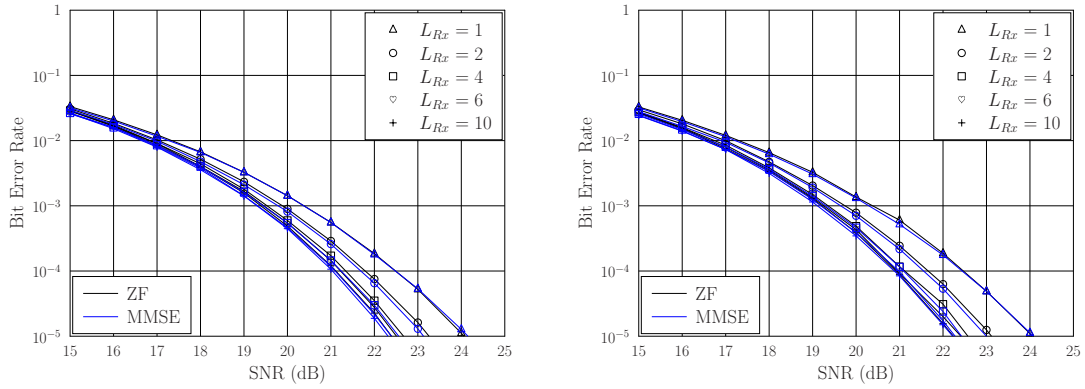

(a) Symbol-based detection

(b) Block-based detection

Figure 5.4: Impact of the ISI length exploited by the receiver on the BER performance of MoCDMA systems with symbol-based and block-based detectors, respectively, when $K = 4$, $T = 5 \times 10^{-4}s$, $r = 380nm$, $L = 10$, $M = 100$, $N = 16$ and $K = 4$.

molecular density is reduced to a very low level after about 6 chip durations.

In Fig. 5.5, the impact of different spreading sequences on the BER performance of the MoCDMA systems with ZF- and MMSE-detectors is investigated. Specifically, MLS, Gold-sequences, and (orthogonal) Walsh codes are considered. Here, it is worth noting that even though for a single carrier, the MMSE-equalizer outperforms both the MF- and ZF-equalizers. However, this is not necessary the case when all the subcarriers are considered, as the result that the spreading sequences are not exploited by the equalizers operated with individual subcarriers. As shown in Fig. 5.5, explicitly, due to the different types of interference existing in MoCDMA, different sequences may yield different performance. In more detail, for all the three cases and two detectors, Gold sequences result in the best BER performance, owing to the merit that Gold sequences belong to a class of near-orthogonal sequences. When the symbol-based or block-based MMSE-detector is considered, or for the block-based ZF-detector, the MLS outperforms the Walsh codes. By contrast, for the symbol-based ZF-detector, which type of sequences should be chosen from the MLS and Walsh codes is depended on the SNR that the system is operated with. Specifically, when the SNR is relatively low, MLS is preferred. Otherwise, when the SNR is sufficiently high, Walsh codes is preferred. Finally, for the F-domain detector, Walsh codes outperform MLS, due to the MLS used are near-random sequences, as mentioned at the beginning of this section. Furthermore, when Walsh codes are employed, the ZF-detector surprisingly outperforms the MMSE-detector. This is because the above mentioned that spreading sequences are not involved in the equalization of individual subcarriers. Therefore, while the despreading of the ZF-processed signals yields zero ISI/ICI and zero MAI, the despreading of the MMSE-processed signals returns significant interference. Consequently, the MMSE-detector is outperformed by the ZF-detector. Overall, Gold sequences are seems a class of promising sequences for application in MoCDMA systems.

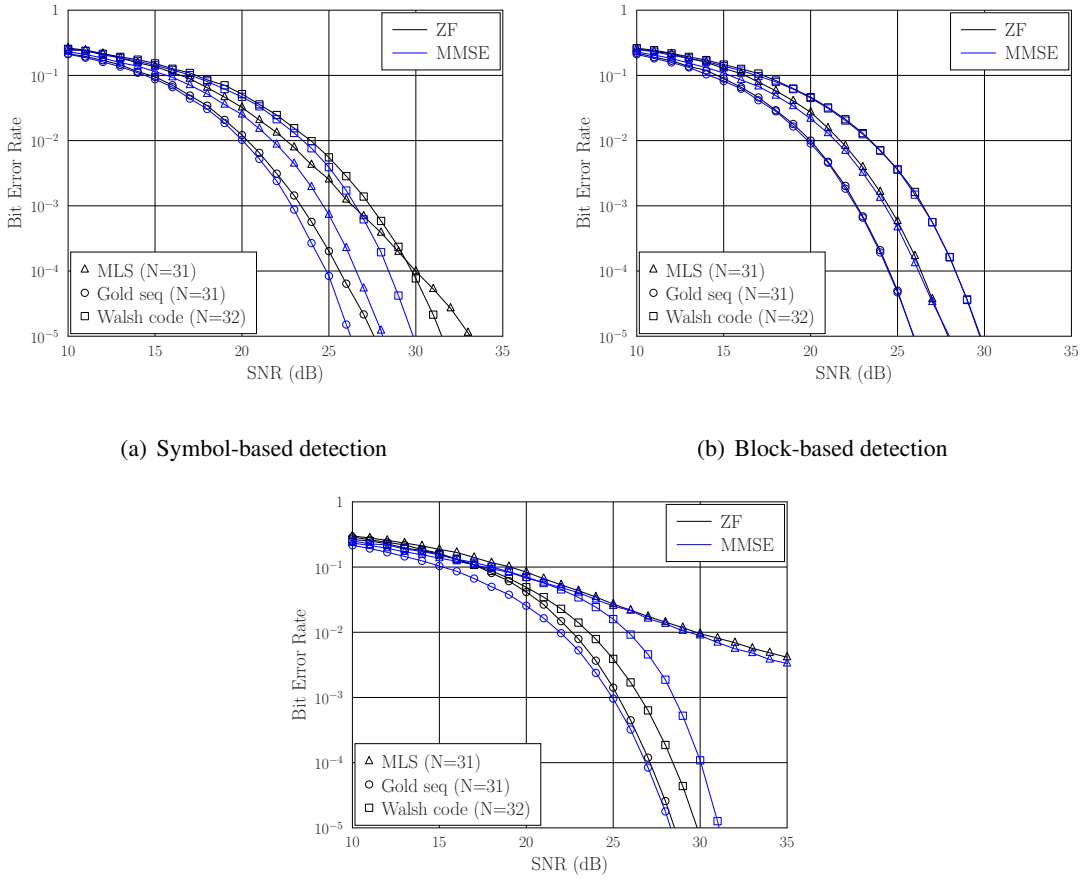

(a) Symbol-based detection

(b) Block-based detection

(c) Frequency-domain detection

Figure 5.5: Impact of different spreading sequences on the BER performance of the MoCDMA systems with the parameters of $T = 5 \times 10^{-4}s$, $r = 380nm$, N=31 for MLS and Gold sequences and 32 for Walsh codes, $L = 10$, $M = 100$, and $K = 8$.

Finally, in Fig. 5.6 we investigate the impact of spreading factor on the BER performance of the MoCDMA systems employing the MMSE-detector, as an example. More specifically, we aim to find out the impact of K/N on the BER performance of MoCDMA systems. It is known that in the conventional RdCDMA systems, the BER performance of multiuser detectors usually slightly improves, as K/N is kept a constant, while K and N simultaneously increase. However, as shown in Fig. 5.6 for all the three types of detection schemes, the BER performance is more dependent on the number of NUs supported by the MoCDMA systems. Specifically, as shown in Fig. 5.6(a) and Fig. 5.6(b), the BER performance of $N = 16,\ K = 8$ having a K/N ratio of 0.5 is similar as that of $N = 31,\ K = 8$ having a K/N ratio of about 0.25. The performance of $N = 31,\ K = 8$ is much worse than that of $N = 16,\ K = 4$, both of which have a K/N ratio 0.25. By contrast, for the F-domain MMSE-detector, although the BER performance of $N = 31,\ K = 8$ is better than that of $N = 16,\ K = 8$, it is much worse than that of $N = 16,\ K = 4$, which again have a similar K/N ratio of about 0.25. The reason behind this observation, which is distinctively different from that in the conventional RdCDMA, is that in MoCDMA, the noise power is coupled with the number

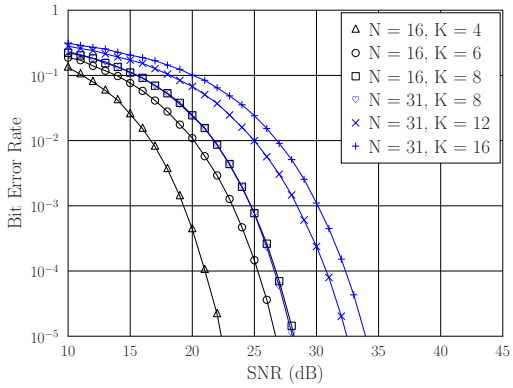

(a) Symbol-based MMSE-detector

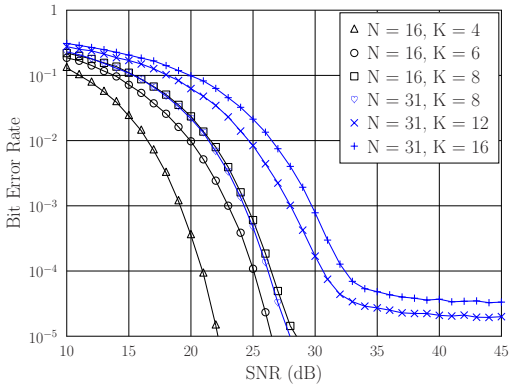

(b) Block-based MMSE-detector

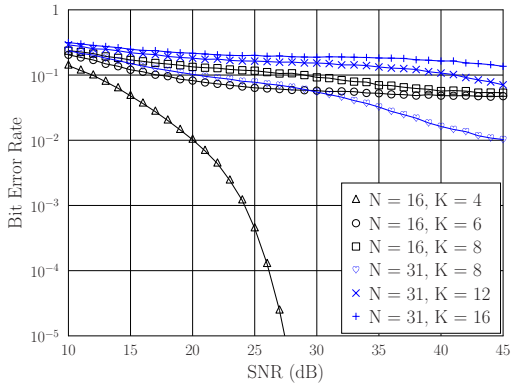

(c) Frequency-domain MMSE-detector

Figure 5.6: Impact of different spreading factors and different number of NUs on the BER performance of the MoCDMA systems using MLS and with MMSE-detector, when assuming the other parameters of $T = 5 \times 10^{-4}s$, $r = 380nm$, $L = 10$, $M = 100$.

of NUs as well as with the different types of interferences generated by all the NUs. Therefore, regardless of what spreading factor is used, the noise power increases with the increase of the number of NUs, and furthermore, the noise power is unable to be reduced by the spreading and de-spreading operations in the MoCDMA systems. Note that, the error-floors seen in Fig. 5.6(b) are due to the special spreading sequences derived from MLS-based sequences, which result in that some interference is unable to be fully suppressed by the MMSE-detector.

5.6 Conclusion

In this chapter, we introduced a MoCDMA system designed based on two types of molecules. We demonstrated that this MoCDMA scheme mirrors to the conventional RdCDMA with BPSK modulation. Straightforwardly, the rich of signal processing schemes developed for the conventional RdCDMA with BPSK modulation can be adopted/extended for the MoCDMA systems. In this

chapter, we derived the various expressions for representing the received signals. Based on these expressions, we introduced both symbol-based and block-based detection schemes that are operated in the principles of MF, ZF and MMSE. Furthermore, we developed the F-domain block-based detectors also in the principles of MF, ZF and MMSE. Our studies in this chapter explained that all the detectors introduced have relatively low complexity, suitable for operation in DMC systems, and different detectors may make different trade-off between complexity and reliability. We revealed and also justified that the counting noise in DMC is different from the background noise in the conventional radio-based communication systems. As a consequence, a MoCDMA system supporting multiple NUs is incapable of achieving the near single-user performance as done in a conventional RdCDMA system supporting multiple users, even when the number of NUs simultaneously supported is as low as 2.

Chapter 6

Conclusions and Future Work

6.1 Conclusions

In this thesis, we have first provided a background review for MC. Different channel models and modulation schemes in MC have been discussed. Furthermore, the challenges in the research and development of DMC have been addressed. In DMC , CSK modulation has been regarded as the simplest modulation scheme, which encodes information with the aid of the number of molecules released by the transmitter. On the other side, MoSK encodes message into different types of molecules. Both of them have some advantages and disadvantages.

In Chapter 2, we have proposed a range of approaches for analyzing and computing the BER of the DMC systems without or with ISIC, based on which exact and approximate BER expressions have respectively been derived. Our studies and comparison show that both the Gaussian- and Gamma-approximation are capable of providing near-accurate BER estimation, provided that the respective optimum thresholds are applied in detection. However, the optimum detection threshold estimated by the Gaussian- or Gamma-approximation is explicitly different from that given by the Poisson modeling, and hence it is practically not optimum. The BER performance of the OOK-modulated DMC systems without ISIC is very sensitive to the change of detection threshold, whereas, the ISIC is able to mitigate the sensitivity to the variation of detection threshold. Furthermore, the employment of ISIC is able to improve the BER performance of the OOK-modulated DMC systems, especially in the scenarios where transmission distance is relatively long or/and transmission rate is high, both resulting in long ISI. However, ISIC amplifies the counting noise, which may result in performance degradation in the case of short ISI. We have shown that, when ISI is long, the Monte-Carlo approach or the different types of simplified approaches may be employed for evaluating the BER of the DMC systems without or with ISIC. The studies and performance results show that all these approaches are effective approaches, and are capable of providing near-accurate BER estimation.

In Chapter 3, different approaches have been introduced for analyzing and evaluating the BER performance of the BMoSK-modulated DMC systems without or with ISIC. Correspondingly, a range of BER expressions have been obtained, which have also been validated using simulations and analysis. Based on our studies and performance results, we can conclude that the Poisson modelling is in general near-accurate. By contrast, the Gaussian-approximation is not very accurate, if the average number of molecules presenting within the detection space is insufficient to apply the Gaussian approximation, which may be due to the insufficient number of molecules transmitted and/or insufficient residue molecules resulted from ISI. Our studies also show that, when ISI is very long, the Monte-Carlo approach or the simplified Poisson approach allows to attain near-accurate BER with relatively low computation complexity. With respect to detection, the studies show that, if an increased computation complexity and extra storage of detected information are available, an improved detection threshold may be employed by DMC systems to achieve significantly improved BER performance, especially, when the DMC systems without ISIC is considered. By contrast, when the DMC systems use ISIC, the BER performance improvement resulted from applying the improved threshold becomes moderate. This implies that the ISIC operation makes the distributions of the decision variables conditioned on $b_u = 1$ and 0 more symmetric with respect to zero, making the decision threshold $C_T = 0$ closer to optimum. Furthermore, our studies demonstrate that the threshold relied by the OOK scheme is highly sensitive to the environment changes, and hence difficult to manage in practice, while the threshold in the BMoSK is always near zero, which is feasible for practical implementation.

In Chapter 4, we have investigated the receiving equalization techniques for the ISI mitigation and signal detection in BMoSK-DMC systems. Three types of LEQs have been considered, namely the MF-LEQ, ZF-LEQ and MMSE-LEQ. We have examined the effects of the different parameters defining transmit signals and characterizing DMC channels on the error performance of the BMoSK-DMC systems. Our studies and performance results show that to achieve the best possible performance, the MF-LEQ is reduced to a symbol-based detector, which detects individual bits independently under the ISI. In BMoSK-DMC systems, the channel matrix is diagonal dominant, which makes the ZF-LEQ highly efficient, achieving nearly the same performance as the MMSE-LEQ, although MMSE-LEQ has a slightly higher complexity than the ZF-LEQ. Both the ZF-LEQ and MMSE-LEQ are capable of effectively suppressing the ISI, yielding significantly improved detection reliability beyond the MF-LEQ. Nevertheless, both the ZF-LEQ and MMSE-LEQ are still low-complexity equalizers that are feasible for implementation, although their complexity is slightly higher than that of the MF-LEQ.

In Chapter 5, we have introduced a MoCDMA system designed based on two types of molecules, and demonstrated that this MoCDMA scheme mirrors to the conventional RdCDMA with BPSK modulation. Straightforwardly, the rich of signal processing schemes developed for the conventional RdCDMA with BPSK modulation can be adopted/extended for the MoCDMA systems. In this chapter, we have derived the various expressions for representing the received

signals. Based on these expressions, we have introduced both symbol-based and block-based detection schemes that are operated in the principles of MF, ZF and MMSE. Furthermore, we have developed the F-domain block-based detectors also in the principles of MF, ZF and MMSE. Our studies in this chapter explain that all the detectors introduced have relatively low complexity, suitable for operation in DMC systems, and different detectors may make different trade-off between complexity and reliability. We have revealed and also justified that the counting noise in DMC is different from the background noise in the conventional radio-based communication systems. As a consequence, a MoCDMA system supporting multiple NUs is incapable of achieving the near single-user performance as done in a conventional RdCDMA system supporting multiple users, even when the number of NUs simultaneously supported is as low as 2.

6.2 Future Work

Molecular Communications is a typical cross-discipline research area. The research in this area is just at its start, there are a lot of research issues. Specifically, following this thesis, there are several open issues, which are listed as follows.

1. Performance of molecular communications in time-variant diffusion channels:
   In most references, the diffusion coefficient of a liquid is assumed to be constant during information transmission. However, the temperature, concentration and pressure of molecules in a liquid medium always change over time. Therefore, the diffusion coefficient in particle is time-variant due to its dependence on the above mentioned factors. Consequently, the system performance of the modulation and interference cancellation schemes considered in Chapter 2 and 3 may not be attained in practice. Therefore, it is important to investigate the achievable performance of the molecular communication schemes by considering the effect from these time-variant factors.

2. Differential detection:
   Amplitude detection has been widely used for pulse-based modulation operated in diffusion-based channels. However, the performance of amplitude detection is seriously affected by the noise and observation time. In order to improve the performance, strictly synchronised systems with low noise are required. It seems that more stable observations for concentration can be obtained, if we take the differentiation with time. This detection technique may improve the systems detection performance, but require further investigation.

3. Asynchronous MoCDMA with Mobility:
   The MoCDMA studied in Chapter 5 assumes synchronous transmission. Furthermore, our studies in Chapter 5 assumes static terminals. However, in practical DMC systems, it is hard to position all the transmission terminals so that they have the same distance from the receiver. Therefore, implementing synchronous MoCDMA is highly challenging. In addition,

in DMC, most terminals might be in move, which makes it is very difficult to implement synchronous MoCDMA. Based on the above arguments, it is very important to investigate the asynchronous MoCDMA with/without mobility, and design the high-efficiency transmission and detection schemes. Furthermore, it is highly important and also challenging to analyze the performance of the asynchronous MoCDMA systems with various modulation and detection schemes.

4. Relay-assisted DMC:

   In previous chapter, it is shown that the BER of the DMC systems with ISIC, BMoSK modulation or liner equalizer becomes relatively high, when transmission distance is longer than about 300nm. In order to provide reliable transmission for relatively long distance, the relay system has been investigated in some literature [49, 50]. On the other hand, transmission power can be saved when relay is employed. In [48], authors have discussed the probability to capture and reuse the received molecules. Moreover, an optical-to-chemical signal conversion interface has been proposed in [104], which can link macroworld with microworld. Therefore, there is a huge potential for relay system to be used in DMC systems. Correspondingly, the performance analysis approaches and the transceiver schemes studied in this thesis may be extended and improved for the relay-assisted of DMC systems.

Bibliography

[1] L. Parcerisa Giné and I. F. Akyildiz, "Molecular communication options for long range nanonetworks," *Comput. Netw.*, vol. 53, pp. 2753–2766, Nov. 2009.

[2] T. Suda, M. Moore, T. Nakano, R. Egashira, and A. Enomoto, "Exploratory research on molecular communication between nanomachines," in *in: Conference on Genetic and Evolutionary Computation (GECCO 2005), ACM*, 2005.

[3] B. Atakan, O. B. Akan, and S. Balasubramaniam, "Body area nanonetworks with molecular communications in nanomedicine," *IEEE Communications Magazine*, vol. 50, pp. 28–34, January 2012.

[4] I. Llatser, C. Kremers, D. N. Chigrin, J. M. Jornet, M. C. Lemme, A. Cabellos-Aparicio, and E. Alarcón, "Characterization of graphene-based nano-antennas in the terahertz band," in *2012 6th European Conference on Antennas and Propagation (EUCAP)*, pp. 194–198, March 2012.

[5] T. Nakano, T. Suda, Y. Okaie, M. J. Moore, and A. V. Vasilakos, "Molecular communication among biological nanomachines: A layered architecture and research issues," *IEEE Transactions on NanoBioscience*, vol. 13, pp. 169–197, Sept 2014.

[6] T. Nakano, M. J. Moore, F. Wei, A. V. Vasilakos, and J. Shuai, "Molecular communication and networking: Opportunities and challenges," *IEEE Transactions on NanoBioscience*, vol. 11, pp. 135–148, June 2012.

[7] I. F. Akyildiz, F. Brunetti, and C. Blázquez, "Nanonetworks: A new communication paradigm," *Comput. Netw.*, vol. 52, pp. 2260–2279, Aug. 2008.

[8] T. Nakano, A. W. Eckford, and T. Haraguchi, *Molecular Communication*. Cambridge University Press, 2013. Cambridge Books Online.

[9] T. Nakano, M. Moore, A. Enomoto, and T. Suda, *Molecular Communication Technology as a Biological ICT*, pp. 49–86. Berlin, Heidelberg: Springer Berlin Heidelberg, 2011.

[10] L. C. Cobo and I. F. Akyildiz, "Bacteria-based communication in nanonetworks," *Nano Communication Networks*, vol. 1, no. 4, pp. 244 – 256, 2010.

[11] M. Gregori and I. F. Akyildiz, "A new nanonetwork architecture using flagellated bacteria and catalytic nanomotors," *IEEE Journal on Selected Areas in Communications*, vol. 28, pp. 612–619, May 2010.

[12] A. Guney, B. Atakan, and O. B. Akan, "Mobile ad hoc nanonetworks with collision-based molecular communication," *IEEE Transactions on Mobile Computing*, vol. 11, pp. 353–366, March 2012.

[13] H. B. Yilmaz, A. C. Heren, T. Tugcu, and C. B. Chae, "Three-dimensional channel characteristics for molecular communications with an absorbing receiver," *IEEE Communications Letters*, vol. 18, pp. 929–932, June 2014.

[14] M. Pierobon and I. F. Akyildiz, "Noise analysis in ligand-binding reception for molecular communication in nanonetworks," *IEEE Transactions on Signal Processing*, vol. 59, pp. 4168–4182, Sept 2011.

[15] M. Pierobon and I. F. Akyildiz, "A physical end-to-end model for molecular communication in nanonetworks," *IEEE Journal on Selected Areas in Communications*, vol. 28, pp. 602–611, May 2010.

[16] M. Pierobon and I. F. Akyildiz, "Diffusion-based noise analysis for molecular communication in nanonetworks," *IEEE Transactions on Signal Processing*, vol. 59, pp. 2532–2547, June 2011.

[17] N. Farsad, W. Guo, and A. W. Eckford, "Table-top molecular communication: Text messages through chemical signals," *CoRR*, vol. abs/1310.0070, 2013.

[18] N. Farsad, N. R. Kim, A. W. Eckford, and C. B. Chae, "Channel and noise models for nonlinear molecular communication systems," *IEEE Journal on Selected Areas in Communications*, vol. 32, pp. 2392–2401, Dec 2014.

[19] W. Guo, T. Asyhari, N. Farsad, H. B. Yilmaz, B. Li, A. Eckford, and C. B. Chae, "Molecular communications: channel model and physical layer techniques," *IEEE Wireless Communications*, vol. 23, pp. 120–127, August 2016.

[20] A. Noel, K. C. Cheung, and R. Schober, "Optimal receiver design for diffusive molecular communication with flow and additive noise," *IEEE Transactions on NanoBioscience*, vol. 13, pp. 350–362, Sept 2014.

[21] M. U. Mahfuz, D. Makrakis, and H. T. Mouftah, "A comprehensive study of sampling-based optimum signal detection in concentration-encoded molecular communication," *IEEE Transactions on NanoBioscience*, vol. 13, pp. 208–222, Sept 2014.

[22] D. Kilinc and O. B. Akan, "Receiver design for molecular communication," *IEEE Journal on Selected Areas in Communications*, vol. 31, pp. 705–714, December 2013.

[23] C. T. Chou, "Impact of receiver reaction mechanisms on the performance of molecular communication networks," *IEEE Transactions on Nanotechnology*, vol. 14, pp. 304–317, March 2015.

[24] H. ShahMohammadian, G. G. Messier, and S. Magierowski, "Modelling the reception process in diffusion-based molecular communication channels," in *2013 IEEE International Conference on Communications Workshops (ICC)*, pp. 782–786, June 2013.

[25] A. Akkaya, H. B. Yilmaz, C. B. Chae, and T. Tugcu, "Effect of receptor density and size on signal reception in molecular communication via diffusion with an absorbing receiver," *IEEE Communications Letters*, vol. 19, pp. 155–158, Feb 2015.

[26] Y. Deng, A. Noel, M. Elkashlan, A. Nallanathan, and K. C. Cheung, "Modeling and simulation of molecular communication systems with a reversible adsorption receiver," *IEEE Transactions on Molecular, Biological and Multi-Scale Communications*, vol. 1, pp. 347–362, Dec 2015.

[27] A. Ahmadzadeh, H. Arjmandi, A. Burkovski, and R. Schober, "Comprehensive reactive receiver modeling for diffusive molecular communication systems: Reversible binding, molecule degradation, and finite number of receptors," *IEEE Transactions on NanoBioscience*, vol. 15, pp. 713–727, Oct 2016.

[28] M. Al-Zu'bi and A. Sanagavarapu Mohan, "Modeling of ligand-receptor protein interaction in biodegradable spherical bounded biological micro-environments," *IEEE Access*, vol. PP, pp. 1–1, 04 2018.

[29] A. C. Heren, H. B. Yilmaz, C. B. Chae, and T. Tugcu, "Effect of degradation in molecular communication: Impairment or enhancement?," *IEEE Transactions on Molecular, Biological and Multi-Scale Communications*, vol. 1, pp. 217–229, June 2015.

[30] H. ShahMohammadian, G. G. Messier, and S. Magierowski, "Optimum receiver for molecule shift keying modulation in diffusion-based molecular communication channels," *Nano Communication Networks*, vol. 3, no. 3, pp. 183 – 195, 2012.

[31] A. Ahmadzadeh, H. Arjmandi, A. Burkovski, and R. Schober, "Reactive receiver modeling for diffusive molecular communication systems with molecule degradation," in *2016 IEEE International Conference on Communications (ICC)*, pp. 1–7, May 2016.

[32] S. Qiu, T. Asyhari, W. Guo, S. Wang, B. Li, C. Zhao, and M. Leeson, "Molecular channel fading due to diffusivity fluctuations," *IEEE Communications Letters*, vol. 21, pp. 676–679, March 2017.

[33] S. Huang, L. Lin, H. Yan, J. Xu, and F. Liu, "Statistical analysis of received signal and error performance for mobile molecular communication," *IEEE Transactions on NanoBioscience*, vol. 18, pp. 415–427, July 2019.

[34] G. Chang, L. Lin, and H. Yan, "Adaptive detection and isi mitigation for mobile molecular communication," *IEEE Transactions on NanoBioscience*, vol. PP, pp. 1–1, 12 2017.

[35] A. Ahmadzadeh, V. Jamali, A. Noel, and R. Schober, "Diffusive mobile molecular communications over time-variant channels," *IEEE Communications Letters*, vol. 21, pp. 1265–1268, June 2017.

[36] M. U. Mahfuz, D. Makrakis, and H. T. Mouftah, "Concentration-encoded subdiffusive molecular communication: Theory, channel characteristics, and optimum signal detection," *IEEE Transactions on NanoBioscience*, vol. 15, pp. 533–548, Sept 2016.

[37] M. U. Mahfuz, D. Makrakis, and H. Mouftah, "Spatiotemporal distribution and modulation schemes for concentration-encoded medium-to-long range molecular communication," in *2010 25th Biennial Symposium on Communications*, pp. 100–105, May 2010.

[38] I. Llatser, A. Cabellos-Aparicio, M. Pierobon, and E. Alarcon, "Detection techniques for diffusion-based molecular communication," *IEEE Journal on Selected Areas in Communications*, vol. 31, pp. 726–734, December 2013.

[39] N. R. Kim and C. B. Chae, "Novel modulation techniques using isomers as messenger molecules for nano communication networks via diffusion," *IEEE Journal on Selected Areas in Communications*, vol. 31, pp. 847–856, December 2013.

[40] M. S. Kuran, H. B. Yilmaz, T. Tugcu, and I. F. Akyildiz, "Modulation techniques for communication via diffusion in nanonetworks," in *Communications (ICC), 2011 IEEE International Conference on*, pp. 1–5, June 2011.

[41] M. U. Mahfuz, "Achievable strength-based signal detection in quantity-constrained PAM OOK concentration-encoded molecular communication," *IEEE Transactions on NanoBioscience*, vol. 15, pp. 619–626, Oct 2016.

[42] S. Kadloor, R. S. Adve, and A. W. Eckford, "Molecular communication using Brownian motion with drift," *IEEE Transactions on NanoBioscience*, vol. 11, pp. 89–99, June 2012.

[43] N. Farsad, Y. Murin, W. Guo, C. Chae, A. W. Eckford, and A. Goldsmith, "Communication system design and analysis for asynchronous molecular timing channels," *IEEE Transactions on Molecular, Biological and Multi-Scale Communications*, vol. 3, pp. 239–253, Dec 2017.

[44] H. Awan and C. T. Chou, "Generalized solution for the demodulation of reaction shift keying signals in molecular communication networks," *IEEE Transactions on Communications*, vol. 65, pp. 715–727, Feb 2017.

[45] T. Nakano and T. Suda, "Molecular communication using dynamic properties of oscillating and propagating patterns in concentration of information molecules," *IEEE Transactions on Communications*, vol. 65, pp. 3386–3398, Aug 2017.

[46] H. Arjmandi, A. Gohari, M. N. Kenari, and F. Bateni, "Diffusion-based nanonetworking: A new modulation technique and performance analysis," *IEEE Communications Letters*, vol. 17, pp. 645–648, April 2013.

[47] M. H. Kabir, S. M. R. Islam, and K. S. Kwak*, "D-MoSK modulation in molecular communications," *IEEE Transactions on NanoBioscience*, vol. 14, pp. 680–683, Sept 2015.

[48] W. Guo, Y. Deng, H. B. Yilmaz, N. Farsad, M. Elkashlan, A. Eckford, A. Nallanathan, and C. Chae, "Smiet: Simultaneous molecular information and energy transfer," *IEEE Wireless Communications*, vol. 25, pp. 106–113, February 2018.

[49] N. Tavakkoli, P. Azmi, and N. Mokari, "Optimal positioning of relay node in cooperative molecular communication networks," *IEEE Transactions on Communications*, vol. 65, pp. 5293–5304, Dec 2017.

[50] S. K. Tiwari, T. R. T. Reddy, and P. K. Upadhyay, "Error performance optimization using logarithmic barrier function in molecular nanonetworks," *IEEE Communications Letters*, vol. 21, pp. 2408–2411, Nov 2017.

[51] T. Nakano and J. Q. Liu, "Design and analysis of molecular relay channels: An information theoretic approach," *IEEE Transactions on NanoBioscience*, vol. 9, pp. 213–221, Sept 2010.

[52] A. Aijaz, A. H. Aghvami, and M. R. Nakhai, "On error performance of network coding in diffusion-based molecular nanonetworks," *IEEE Transactions on Nanotechnology*, vol. 13, pp. 871–874, Sept 2014.

[53] B. C. Akdeniz, B. Tepekule, A. E. Pusane, and T. Tuğcu, "Network coding applications in molecular communication," in *2015 23nd Signal Processing and Communications Applications Conference (SIU)*, pp. 1212–1215, May 2015.

[54] M. F. Ghazani, G. Aminian, M. Mirmohseni, A. Gohari, and M. N. Kenari, "Physical layer network coding in molecular two-way relay networks," in *2016 Iran Workshop on Communication and Information Theory (IWCIT)*, pp. 1–6, May 2016.

[55] B. Atakan and Ö. B. Akan, "On molecular multiple-access, broadcast, and relay channels in nanonetworks," in *BIONETICS*, 2008.

[56] Y. Zamiri-Jafarian, S. Gazor, and H. Zamiri-Jafarian, "Molecular code division multiple access in nano communication systems," in *2016 IEEE Wireless Communications and Networking Conference*, pp. 1–6, April 2016.

[57] J. Suzuki, S. Balasubramaniam, and A. Prina-Mello, "Multi-objective TDMA optimization for neuron-based molecular communication," in *BODYNETS*, 2012.

[58] Q. Liu and K. Yang, "Multiple-access channel capacity of diffusion and ligand-based molecular communication," in *Proceedings of the 16th ACM International Conference on Modeling, Analysis & Simulation of Wireless and Mobile Systems*, MSWiM '13, (New York, NY, USA), pp. 151–158, ACM, 2013.

[59] G. Aminian, M. Farahnak-Ghazani, M. Mirmohseni, M. Nasiri-Kenari, and F. Fekri, "On the capacity of point-to-point and multiple-access molecular communications with ligand-receptors," *IEEE Transactions on Molecular, Biological and Multi-Scale Communications*, vol. 1, pp. 331–346, Dec 2015.

[60] M. J. Moore, Y. Okaie, and T. Nakano, "Diffusion-based multiple access by nano-transmitters to a micro-receiver," *IEEE Communications Letters*, vol. 18, pp. 385–388, March 2014.

[61] S. Korte, M. Damrath, M. Damrath, and P. A. Hoeher, "Multiple channel access techniques for diffusion-based molecular communications," in *SCC 2017; 11th International ITG Conference on Systems, Communications and Coding*, pp. 1–6, Feb 2017.

[62] M. U. Mahfuz, D. Makrakis, and H. T. Mouftah, "A comprehensive analysis of strength-based optimum signal detection in concentration-encoded molecular communication with spike transmission," *IEEE Transactions on NanoBioscience*, vol. 14, pp. 67–83, Jan 2015.

[63] A. Aijaz and A. H. Aghvami, "Error performance of diffusion-based molecular communication using pulse-based modulation," *IEEE Transactions on NanoBioscience*, vol. 14, pp. 146–151, Jan 2015.

[64] A. Singhal, R. Mallik, and B. Lall, "Performance analysis of amplitude modulation schemes for diffusion-based molecular communication," *IEEE Transactions on Wireless Communications*, vol. 14, pp. 5681–5691, Oct 2015.

[65] S. Galmés and B. Atakan, "Performance analysis of diffusion-based molecular communications with memory," *IEEE Transactions on Communications*, vol. 64, pp. 3786–3793, Sept 2016.

[66] P. C. Yeh, K. C. Chen, Y. C. Lee, L. S. Meng, P. J. Shih, P. Y. Ko, W. A. Lin, and C. H. Lee, "A new frontier of wireless communication theory: diffusion-based molecular communications," *IEEE Wireless Communications*, vol. 19, pp. 28–35, Oct 2012.

[67] I. F. Akyildiz, F. Fekri, R. Sivakumar, C. R. Forest, and B. K. Hammer, "Monaco: fundamentals of molecular nano-communication networks," *IEEE Wireless Communications*, vol. 19, pp. 12–18, Oct 2012.

[68] N. Farsad, H. B. Yilmaz, A. Eckford, C. B. Chae, and W. Guo, "A comprehensive survey of recent advancements in molecular communication," *IEEE Communications Surveys Tutorials*, vol. 18, pp. 1887–1919, thirdquarter 2016.

[69] I. Llatser, A. Cabellos-Aparicio, and E. Alarcon, "Networking challenges and principles in diffusion-based molecular communication," *IEEE Wireless Communications*, vol. 19, pp. 36–41, Oct 2012.

[70] B. Atakan and O. B. Akan, "On channel capacity and error compensation in molecular communication," *Transactions on Computational Systems Biology X*, vol. 10, pp. 59–80, 2008.

[71] B. Atakan and O. B. Akan, "Deterministic capacity of information flow in molecular nanonetworks," *Nano Communication Networks*, vol. 1, no. 1, pp. 31 – 42, 2010.

[72] A. W. Eckford, "Achievable information rates for molecular communication with distinct molecules," in *Bio-Inspired Models of Network, Information and Computing Systems, 2007. Bionetics 2007. 2nd*, pp. 313–315, Dec 2007.

[73] Y. K. Lin, W. A. Lin, C. H. Lee, and P. C. Yeh, "Asynchronous threshold-based detection for quantity-type-modulated molecular communication systems," *IEEE Transactions on Molecular, Biological and Multi-Scale Communications*, vol. 1, pp. 37–49, March 2015.

[74] L. S. Meng, P. C. Yeh, K. C. Chen, and I. F. Akyildiz, "On receiver design for diffusion-based molecular communication," *IEEE Transactions on Signal Processing*, vol. 62, pp. 6032–6044, Nov 2014.

[75] C. T. Chou, "A markovian approach to the optimal demodulation of diffusion-based molecular communication networks," *IEEE Transactions on Communications*, vol. 63, pp. 3728–3743, Oct 2015.

[76] R. Mosayebi, H. Arjmandi, A. Gohari, M. Nasiri-Kenari, and U. Mitra, "Receivers for diffusion-based molecular communication: Exploiting memory and sampling rate," *IEEE Journal on Selected Areas in Communications*, vol. 32, pp. 2368–2380, Dec 2014.

[77] L. Shi and L. L. Yang, "Diffusion-based molecular communications: Inter-symbol interference cancellation and system performance," in *2016 IEEE/CIC International Conference on Communications in China (ICCC)*, pp. 1–6, July 2016.

[78] A. Ahmadzadeh, A. Noel, and R. Schober, "Analysis and design of multi-hop diffusion-based molecular communication networks," *IEEE Transactions on Molecular, Biological and Multi-Scale Communications*, vol. 1, pp. 144–157, June 2015.

[79] A. Papoulis, *Probability, Random Variables, and Stochastic Processes*. New York: McGraw-Hill, Inc, 3 ed., 1991.

[80] J. G. Proakis, *Digital Communications*. McGraw Hill, 5 ed., 2007.

[81] J. Shi, C. Dong, and L.-L. Yang, "Performance comparison of cooperative relay links with different relay processing strategies: Nakagami/Gamma approximation approaches," *EURASIP Journal on Wireless Communications and Networking*, vol. 2014, no. 1, p. 53, 2014.

[82] M. K. Simon and M.-S. Alouini, *Digital Communication over Fading Channels*. New York: John Wiley & Sons, 2 ed., 2005.

[83] N. Nakagami, "The m-distribution, a general formula for intensity distribution of rapid fading," in *Statistical Methods in Radio Wave Propagation* (W. G. Hoffman, ed.), Oxford, England: Pergamon, 1960.

[84] A. F. Molisch, J. R. Foerster, and M. Pendergrass, "Channel models for ultrawideband personal area networks," *IEEE Wireless Communications*, vol. 10, pp. 14–21, December 2003.

[85] A. F. Molisch, "Ultrawideband propagation channels-theory, measurement, and modeling," *IEEE Transactions on Vehicular Technology*, vol. 54, pp. 1528 – 1545, November 2005.

[86] T. S. Rappaport, R. W. H. Jr., R. C. Daniels, and J. N. Murdock, *Millimeter Wave Wireless Communications: Systems and Circuits*. USA: Prentice Hall, 2015.

[87] I. Gradshteyn and I. Ryzhik, *Table of Integrals, Series, and Products*. New York, London: Academic Press, Inc, 7 ed., 2007.

[88] X. Wang and H. V. Poor, *Wireless Communication Systems - Advanced Techniques for Signal Reception*. Prentice Hall, 2003.

[89] H. Holm and M. S. Alouini, "Sum and difference of two squared correlated Nakagami variates in connection with the McKay distribution," *IEEE Transactions on Communications*, vol. 52, pp. 1367–1376, Aug 2004.

[90] J. G. Skellam, "The frequency distribution of the difference between two poisson variates belonging to different populations," *Journal of the Royal Statistical Society*, vol. 109, no. 3, pp. 296–296, 1946.

[91] D. Karlis and I. Ntzoufras, "Bayesian analysis of the difference of count data," *Statistics in Medicine*, vol. 25, pp. 1885–1905, June 2006.

[92] H. B. Yilmaz, N.-R. Kim, and C.-B. Chae, "Effect of ISI mitigation on modulation techniques in molecular communication via diffusion," in *Proceedings of ACM The First Annual International Conference on Nanoscale Computing and Communication*, NANOCOM' 14, (New York, NY, USA), pp. 3:1–3:9, ACM, 2007.

[93] Y. Deng, A. Noel, M. Elkashlan, A. Nallanathan, and K. C. Cheung, "Modeling and simulation of molecular communication systems with a reversible adsorption receiver," *IEEE Transactions on Molecular, Biological and Multi-Scale Communications*, vol. 1, pp. 347–362, Dec 2015.

[94] Y. Deng, A. Noel, W. Guo, A. Nallanathan, and M. Elkashlan, "Analyzing large-scale multiuser molecular communication via 3-D stochastic geometry," *IEEE Transactions on Molecular, Biological and Multi-Scale Communications*, vol. 3, pp. 118–133, June 2017.

[95] B. D. Unluturk and I. Akyildiz, "An end-to-end model of plant pheromone channel for long range molecular communications," *IEEE Transactions on NanoBioscience*, vol. PP, no. 99, pp. 1–1, 2016.

[96] U. A. K. Chude-Okonkwo, R. Malekian, and B. T. S. Maharaj, "Molecular communication model for targeted drug delivery in multiple disease sites with diversely expressed enzymes," *IEEE Transactions on NanoBioscience*, vol. 15, pp. 230–245, April 2016.

[97] K. Takeda and F. Adachi, "Joint transmit/receive one-tap minimum mean square error frequency-domain equalisation for broadband multicode direct-sequence code division multiple access," *IET Communications*, vol. 4, pp. 1752–1764, Sep. 2010.

[98] K. Aghababaiyan, V. Shah-Mansouri, and B. Maham, "Capacity bounds of neuro-spike communication by exploiting temporal modulations," in *2018 IEEE Wireless Communications and Networking Conference (WCNC)*, pp. 1–6, April 2018.

[99] K. Aghababaiyan and B. Maham, "Error probability analysis of neuro-spike communication channel," in *2017 IEEE Symposium on Computers and Communications (ISCC)*, pp. 932–937, July 2017.

[100] K. Aghababaiyan, V. Shah-Mansouri, and B. Maham, "Asynchronous neuro-spike array - based communication," in *2018 IEEE International Black Sea Conference on Communications and Networking (BlackSeaCom)*, pp. 1–5, June 2018.

[101] Ankit and M. R. Bhatnagar, "Boolean and and or logic for cell signalling gateways: a communication perspective," *IET Nanobiotechnology*, vol. 12, no. 8, pp. 1130–1139, 2018.

[102] M. S. Kuran, T. Tugcu, and B. O. Edis, "Calcium signaling: overview and research directions of a molecular communication paradigm," *IEEE Wireless Communications*, vol. 19, pp. 20–27, Oct 2012.

[103] T. Nakano, Y. Okaie, S. Kobayashi, T. Hara, Y. Hiraoka, and T. Haraguchi, "Methods and applications of mobile molecular communication," *Proceedings of the IEEE*, vol. 107, pp. 1442–1456, July 2019.

[104] L. Grebenstein, J. Kirchner, R. S. Peixoto, W. Zimmermann, F. Irnstorfer, W. Wicke, A. Ahmadzadeh, V. Jamali, G. Fischer, R. Weigel, A. Burkovski, and R. Schober, "Biological optical-to-chemical signal conversion interface: A small-scale modulator for molecular communications," *IEEE Transactions on NanoBioscience*, vol. 18, pp. 31–42, Jan 2019.

[105] L. Feng, A. Ali, M. Iqbal, A. K. Bashir, S. A. Hussain, and S. Pack, "Optimal haptic communications over nanonetworks for e-health systems," *IEEE Transactions on Industrial Informatics*, vol. 15, pp. 3016–3027, May 2019.

[106] S. Salehi, N. S. Moayedian, S. Haghjooy Javanmard, and E. Alarcón, "Lifetime improvement of a multiple transmitter local drug delivery system based on diffusive molecular communication," *IEEE Transactions on NanoBioscience*, vol. 17, pp. 352–360, July 2018.

[107] S. M. Mustam, S. K. Syed-Yusof, and S. Zubair, "Capacity and delay spread in multilayer diffusion-based molecular communication (dbmc) channel," *IEEE Transactions on NanoBioscience*, vol. 15, pp. 599–612, Oct 2016.

[108] G. Aminian, H. Arjmandi, A. Gohari, M. Nasiri-Kenari, and U. Mitra, "Capacity of diffusion-based molecular communication networks over LTI-poisson channels," *IEEE Transactions on Molecular, Biological and Multi-Scale Communications*, vol. 1, pp. 188–201, June 2015.

[109] M. Pierobon and I. F. Akyildiz, "Capacity of a diffusion-based molecular communication system with channel memory and molecular noise," *IEEE Transactions on Information Theory*, vol. 59, pp. 942–954, Feb 2013.

[110] L. Shi and L. Yang, "Error performance analysis of diffusive molecular communication systems with on-off keying modulation," *IEEE Transactions on Molecular, Biological and Multi-Scale Communications*, vol. 3, pp. 224–238, Dec 2017.

[111] A. Einolghozati and F. Fekri, "Analysis of error-detection schemes in diffusion-based molecular communication," *IEEE Journal on Selected Areas in Communications*, vol. 34, pp. 615–624, March 2016.

[112] P. J. Shih, C. H. Lee, P. C. Yeh, and K. C. Chen, "Channel codes for reliability enhancement in molecular communication," *IEEE Journal on Selected Areas in Communications*, vol. 31, pp. 857–867, December 2013.

[113] M. Movahednasab, M. Soleimanifar, A. Gohari, M. Nasiri-Kenari, and U. Mitra, "Adaptive transmission rate with a fixed threshold decoder for diffusion-based molecular communication," *IEEE Transactions on Communications*, vol. 64, pp. 236–248, Jan 2016.

[114] V. Loscrí, C. Marchal, N. Mitton, G. Fortino, and A. V. Vasilakos, "Security and privacy in molecular communication and networking: Opportunities and challenges," *IEEE Transactions on NanoBioscience*, vol. 13, pp. 198–207, Sept 2014.

[115] M. Kuscu and O. B. Akan, "The internet of molecular things based on FRET," *IEEE Internet of Things Journal*, vol. 3, pp. 4–17, Feb 2016.

[116] K. Aghababaiyan, R. G. Zefreh, and V. Shah-Mansouri, "Enhancing data rate of molecular communication system using brownian motion," *IET Nanobiotechnology*, vol. 13, no. 3, pp. 293–300, 2019.

[117] A. Einolghozati, M. Sardari, and F. Fekri, "Capacity of diffusion-based molecular communication with ligand receptors," in *Information Theory Workshop (ITW), 2011 IEEE*, pp. 85–89, Oct 2011.

[118] B. Tepekule, A. E. Pusane, H. B. Yilmaz, C. Chae, and T. Tugcu, "ISI mitigation techniques in molecular communication," *IEEE Transactions on Molecular, Biological and Multi-Scale Communications*, vol. 1, pp. 202–216, June 2015.

[119] H. Arjmandi, M. Movahednasab, A. Gohari, M. Mirmohseni, M. Nasiri-Kenari, and F. Fekri, "On ISI-avoiding modulations for diffusion-based molecular communication," *IEEE Transactions on Molecular, Biological and Multi-Scale Communications*, vol. PP, no. 99, pp. 1–1, 2016.

[120] B. Tepekule, A. E. Pusane, M. A. Kuran, and T. Tugcu, "A novel pre-equalization method for molecular communication via diffusion in nanonetworks," *IEEE Communications Letters*, vol. 19, pp. 1311–1314, Aug 2015.

[121] B. Li, M. Sun, S. Wang*, W. Guo, and C. Zhao, "Low-complexity noncoherent signal detection for nanoscale molecular communications," *IEEE Transactions on NanoBioscience*, vol. 15, pp. 3–10, Jan 2016.

[122] B. Li, M. Sun, S. Wang, W. Guo, and C. Zhao, "Local convexity inspired low-complexity noncoherent signal detector for nanoscale molecular communications," *IEEE Transactions on Communications*, vol. 64, pp. 2079–2091, May 2016.

[123] B. C. Akdeniz, A. E. Pusane, and T. Tugcu, "Optimal reception delay in diffusion-based molecular communication," *IEEE Communications Letters*, vol. 22, pp. 57–60, Jan 2018.

[124] B. Koo, H. B. Yilmaz, A. W. Eckford, and C.-B. Chae, "Detection algorithms for molecular MIMO," *2015 IEEE International Conference on Communications (ICC)*, pp. 1122–1127, 2015.

[125] B. H. Koo, C. Lee, H. B. Yilmaz, N. Farsad, A. Eckford, and C. B. Chae, "Molecular MIMO: From theory to prototype," *IEEE Journal on Selected Areas in Communications*, vol. 34, pp. 600–614, March 2016.

[126] L.-L. Yang, *Multicarrier Communications*. Chichester, United Kingdom: John Wiley, 2009.

[127] Y. Lu, M. D. Higgins, and M. S. Leeson, "Self-orthogonal convolutional codes (SOCCs) for diffusion-based molecular communication systems," in *2015 IEEE International Conference on Communications (ICC)*, pp. 1049–1053, June 2015.

[128] P.-Y. Ko, Y.-C. Lee, P. C. Yeh, C. han Lee, and K. C. Chen, "A new paradigm for channel coding in diffusion-based molecular communications: Molecular coding distance function," in *2012 IEEE Global Communications Conference (GLOBECOM)*, pp. 3748–3753, Dec 2012.

[129] L. Mu, X. Liu, and L. Yang, "Redundant residue number system coded diffusive molecular communications," in *2018 10th International Conference on Wireless Communications and Signal Processing (WCSP)*, pp. 1–6, Oct 2018.

[130] L. Meng, P. Yeh, K. Chen, and I. F. Akyildiz, "MIMO communications based on molecular diffusion," in *2012 IEEE Global Communications Conference (GLOBECOM)*, pp. 5380–5385, Dec 2012.

[131] Y. Huang, M. Wen, L. Yang, C. Chae, and F. Ji, "Spatial modulation for molecular communication," *IEEE Transactions on NanoBioscience*, vol. 18, pp. 381–395, July 2019.

[132] M. C. Gursoy, E. Basar, A. E. Pusane, and T. Tugcu, "Index modulation for molecular communication via diffusion systems," *IEEE Transactions on Communications*, vol. 67, pp. 3337–3350, May 2019.

[133] D. G. Brennan, "Linear diversity combining techniques," *Proceedings of the IRE*, vol. 47, pp. 1075–1102, June 1959.

[134] L. Hanzo, L.-L. Yang, E.-L. Kuan, and K. Yen, *Single- and Multi-carrier DS-CDMA*. Chichester, United Kingdom: John Wiley and IEEE Press, 2003.

[135] R. E. Ziemer and R. L. Peterson, *Digital Communications and Spread Spectrum Systems*. New York: Macmillan Publishing Company, 1985.

[136] H. L. V. Trees, *Optimum Array Processing*. Wiley Interscience, 2002.

[137] D. Garg and F. Adachi, "Packet access using DS-CDMA with frequency-domain equalization," *IEEE Journal on Selected Areas in Communications*, vol. 24, pp. 161–170, Jan 2006.

[138] F. Adachi, T. Sao, and T. Itagaki, "Performance of multicode DS-CDMA using frequency domain equalisation in frequency selective fading channel," *Electronics Letters*, vol. 39, pp. 239–241, Jan 2003.

[139] G. Golub and C. Loan, *Matrix Computations*. Baltimore and London: The Johns Hopkins University Press, 3 ed., 1996.